②

# NAVAL POSTGRADUATE SCHOOL
## Monterey, California

DTIC
SELECTED
MAR 1 7 1989
D

D

# THESIS

A COMPARISON OF TWO FREQUENCY DOMAIN
ADAPTIVE BEAMFORMING
ALGORITHMS FOR SONAR SIGNAL PROCESSING

by

Nikitas V. Nikitakos

December 1988

Thesis Advisor                    Lawrence J. Ziomek

13

## REPORT DOCUMENTATION PAGE

| 1a Report Security Classification Unclassified | | | 1b Restrictive Markings | | | |
|---|---|---|---|---|---|---|
| 2a Security Classification Authority | | | 3 Distribution Availability of Report | | | |
| 2b Declassification Downgrading Schedule | | | Approved for public release; distribution is unlimited. | | | |
| 4 Performing Organization Report Number(s) | | | 5 Monitoring Organization Report Number(s) | | | |
| 6a Name of Performing Organization Naval Postgraduate School | | 6b Office Symbol *(if applicable)* 62Zm | 7a Name of Monitoring Organization Naval Postgraduate School | | | |
| 6c Address *(city, state, and ZIP code)* Monterey, CA 93943-5000 | | | 7b Address *(city, state, and ZIP code)* Monterey, CA 93943-5000 | | | |
| 8a Name of Funding Sponsoring Organization | | 8b Office Symbol *(if applicable)* | 9 Procurement Instrument Identification Number | | | |
| 8c Address *(city, state, and ZIP code)* | | | 10 Source of Funding Numbers | | | |
| | | | Program Element No | Project No | Task No | Work Unit Accession No |

| 11 Title *(include security classification)* A COMPARISON OF TWO FREQUENCY DOMAIN ADAPTIVE BEAMFORMING ALGORITHMS FOR SONAR SIGNAL PROCESSING |
|---|

| 12 Personal Author(s) Nikitas V. Nikitakos | | | |
|---|---|---|---|
| 13a Type of Report Master's Thesis | 13b Time Covered From To | 14 Date of Report *(year, month, day)* December 1988 | 15 Page Count 121 |

16 Supplementary Notation The views expressed in this thesis are those of the author and do not reflect the official policy or position of the Department of Defense or the U.S. Government.

| 17 Cosati Codes | | | 18 Subject Terms *(continue on reverse if necessary and identify by block number)* |
|---|---|---|---|
| Field | Group | Subgroup | Frequency Domain Adaptive Beamforming Algorithms-Planar Arrays -Sonar signal processing |
| | | | |

19 Abstract *(continue on reverse if necessary and identify by block number)*

Computer simulation studies of two frequency domain adaptive beamforming algorithms are presented. The two algorithms are the frequency domain adaptive beamforming modified least-mean-square algorithm, and the proposed new frequency domain adaptive beamforming algorithm based on modified adaptive linear prediction-error filtering. The simulation studies were conducted to determine the multiple broadband target localization capability and the full angular coverage capability of the two algorithms. The number of iterations that the adaptive algorithms took to reach a minimum estimation error was determined. The algorithms were evaluated at several signal-to-noise ratios. Finally, using the results of the simulation studies a comparison between the two algorithms is performed.

| 20 Distribution Availability of Abstract ☒ unclassified unlimited ☐ same as report ☐ DTIC users | 21 Abstract Security Classification Unclassified | |
|---|---|---|
| 22a Name of Responsible Individual Lawrence J. Ziomek | 22b Telephone *(include Area code)* (408) 646-3206 | 22c Office Symbol 62Zm |

DD FORM 1473,84 MAR      83 APR edition may be used until exhausted      security classification of this page

All other editions are obsolete

A Comparison of Two Frequency Domain Adaptive Beamforming
Algorithms for Sonar Signal Processing

by

Nikitas V. Nikitakos
Lieutenant, Hellenic Navy
B.S., Hellenic Naval Academy, 1980
M.S. in Applied Mathematics, NPS, June 1988

Submitted in partial fulfillment of the
requirements for the degree of

MASTER OF SCIENCE IN ELECTRICAL ENGINEERING

from the

NAVAL POSTGRADUATE SCHOOL
December 1988

Author: _N. B. Nikntakos_____
Nikitas V. Nikitakos

Approved by: _Lawrence J. Ziomek_____
Lawrence J. Ziomek, Thesis Advisor

_____
Murali Tummala, Second Reader

_____
John P. Powers, Chairman,
Department of Electrical and Computer Engineering

_____
Gordon E. Schacher,
Dean of Science and Engineering

# ABSTRACT

Computer simulation studies of two frequency domain adaptive beamforming algorithms are presented. The two algorithms are the frequency domain adaptive beamforming modified least-mean-square algorithm, and the proposed new frequency domain adaptive beamforming algorithm based on modified adaptive linear prediction-error filtering. The simulation studies were conducted to determine the multiple broadband target localization capability and the full angular coverage capability of the two algorithms. The number of iterations that the adaptive algorithms took to reach a minimum estimation error was determined. The algorithms were evaluated at several signal-to-noise ratios. Finally, using the results of the simulation studies a comparison between the two algorithms is performed.

iii

# TABLE OF CONTENTS

## LIST OF TABLES

# LIST OF FIGURES

## ACKNOWLEDGEMENTS

x

# I. INTRODUCTION

One of the major research items in underwater acoustic signal processing is to develop new sonar signal processing algorithms capable of quickly and accurately solving target localization problems. Present technology dictates that several lines of bearing to a target must be obtained before a sonar fire control solution can be computed. Obtaining these lines of bearing is a time consuming and often dangerous task due to the increased probability of counterdetection and, as a result, evasive maneuvering and defensive action on the part of the target. A sonar system capable of providing timely, accurate target localization while minimizing own ship maneuvering would result in longer firing ranges and, therefore, a reduction of the threat to one's own ship.

Frequency domain beamforming is accomplished by applying appropriate phase shifts at the sensor outputs of an array to account for the relative propagation delays of a signal from a particular direction. The phase-shifted signals from all sensors are then added together coherently to realize the full array gain. Discrete Fourier Transform (DFT) beamforming is the usual method of determining the direction of arrival of a plane wave signal. A discrete number of direction cosine bins are formed and each bin corresponds to a discrete direction. If the number of direction cosine bins is large, very fine spatial resolution can be obtained. The phase shifts needed to cancel the relative propagation delays can be determined adaptively.

The research performed in this thesis is a continuation of the work of Ziomek and Behrle [Ref. 1] and fully evaluates the capabilities of the complex, modified least-mean square, frequency domain, adaptive beamforming algorithm that they developed via computer simulation studies. Also, a new frequency domain adaptive beamforming algorithm based on modified adaptive linear prediction-error filtering is proposed, which promises better resolution in low signal-to-noise ratio environments especially when multiple targets share common spectral lines [Ref. 2,3]. The computer simulation studies were designed to test the two algorithms specifically for their multiple broadband target localization capability, their full angular coverage capability, and their angular resolution as a function of the input signal-to-noise ratio (SNR) at a single element in the array. Using lower SNR values than those used by Ziomek and Behrle [Ref. 1] in the evaluation of the modified LMS algorithm, and changing some assumptions, such as the

1

number of array elements, sampling rate, and number of iterations, a comparison was performed between the two algorithms.

Each target was modeled as a broadband sound source. As a result, the frequency spectrum of the output signal from each element of the planar array contains several frequency components. An estimate of the bearing and depression angles associated with each frequency component is provided as a result of processing the output frequency spectrum from each element in the array through the frequency domain adaptive beamforming algorithms. Therefore, if each target exhibits at least one unique frequency component (or spectral line), then all targets can be located.

Full angular coverage is the ability to localize a target regardless of its relative position with respect to the array. The broadside case is the easiest since it is at this position that the far-field beam pattern beamwidth is its narrowest. The endfire case is the most difficult since the far-field beam pattern beamwidth is the broadest at this point. The full angular coverage and multiple broadband target capabilities were tested simultaneously.

Baseline results were the first assembled. They are defined as the bearing and depression angle estimation errors (measured in degrees) as a function of harmonic number, and the number of iterations of the two algorithms, for the "no noise" case. Identical cases were then run using additive, zero mean, white, gaussian noise to corrupt the output signal from each element of the planar array. Average bearing and depression angle estimation errors were plotted as a function of the input SNR at a single element of the planar array, and the harmonic number.

Chapter II describes the theory used in the development of the two frequency domain adaptive beamforming algorithms. First the already known modified complex least-mean-square (LMS) adaptive algorithm is summarized. Then the new algorithm which is based on modified complex adaptive linear prediction-error filtering is discussed. For both algorithms the construction of the direction cosine estimates, and the angle estimates will be presented in detail.

Chapter III contains computer simulation results and an explanation of these results. The results are presented as plots of the average estimation errors of the bearing and depression angles at three distinct signal-to-noise ratio levels (-3dB, -6dB, -9dB) for five different cases for each of the two algorithms. The different test cases include targets evaluated at broadside, endfire, random placement, and targets which share a spectral line. Conclusions concerning the effect of harmonic number, sampling rate, number of

2

array elements, number of iterations used in the two algorithms, and SNR are made. The Appendix contains tabular numerical data for all results.

Chapter IV will present final conclusions and recommendations for future research.

# II. ANALYSIS

This chapter will present a brief analysis of the two frequency domain adaptive beamforming algorithms for planar arrays which are evaluated in this thesis. The goal of both algorithms is to localize multiple broadband targets by processing the output electrical signals from a planar array of sensors to provide estimates of direction (both bearing and depression angles) and frequency content of the multiple acoustic fields incident upon the array. The development of the modified complex least-mean-square adaptive beamforming algorithm for planar arrays is a summary of the analysis section of a paper by Ziomek and Behrle [Ref. 1]. However the modified complex adaptive linear prediction-error filter beamforming algorithm for planar arrays is presented for the first time. As a theoretical background for both algorithms, the principles of adaptive beamforming for planar arrays in the frequency domain are presented in the next section.

## A. FREQUENCY DOMAIN ADAPTIVE BEAMFORMING FOR PLANAR ARRAYS

Consider a planar array of M x N (odd), equally spaced, point source elements lying in the XY plane where M and N are the total odd number of elements in the X and Y directions, respectively. Let the random output electrical signal received at time instant $l$ and element $(m,n)$ in the array be given by

$$r(l,m,n) = y(l,m,n) + n(l,m,n), \quad \begin{aligned} l &= -L',...,0,...,L' \\ m &= -M',...,0,...M' \\ n &= -N',...,0,...N' \end{aligned} \quad (2.1)$$

where $y(l,m,n)$ and $n(l,m,n)$ are the deterministic signal and random receiver noise, respectively,

$$L' = (L - 1)/2 \qquad (2.2)$$

4

$$M' = (M - 1)/2 \qquad (2.3)$$

$$N' = (N - 1)/2 \qquad (2.4)$$

and

$$L \geq 2K + 1 \qquad (2.5)$$

is the total number of time samples that must be taken per element in order to avoid aliasing when the signal $y(l,m,n)$ is composed of K harmonics [Ref. 4]. If we designate the length of the data record (i.e., the fundamental period ) recorded at each element in the array as $T_0$ seconds, then the fundamental frequency (i.e., the FFT bin spacing ) is $f_0 = \dfrac{1}{T_0}$ Hz, the highest frequency component that can be calculated in $y(l,m,n)$ is $Kf_0$ Hz, and the output received signals $r(l,m,n)$ must be sampled at a rate of

$$f_s = L/T_0 \text{ samples/sec,} \qquad (2.6)$$

where L is given by Eq. (2.5) [Ref. 4]. Taking the DFT of Eq. (2.1) with respect to the time index $l$ yields the complex frequency domain samples.

$$
\begin{aligned}
R(q,m,n) = Y(q,m,n) + N(q,m,n), \quad & q = -L',...,0,...,L' \\
& m = -M',...,0,...,M' \\
& n = -N',...,0,...,N' ,
\end{aligned}
\qquad (2.7)
$$

where the index q represents the harmonic number. If the acoustic field incident upon the planar arrray is a single general plane wave $g(t \mp \dfrac{r \cdot \hat{n}_0}{c})$ propagating in the $\pm \hat{n}_0$ direction (see Fig. 1), where $\hat{n}_0$ is a unit vector and g(t) is an arbitrary baseband function, then it can be shown that the output electrical signal at time instant $l$ and element (m,n) in the array is given by [Ref. 4 p. 160]:

$$y(l,m,n) = g(lT_s \mp \frac{u_0 m d_x + v_0 n d_y}{c}) . \qquad (2.8)$$
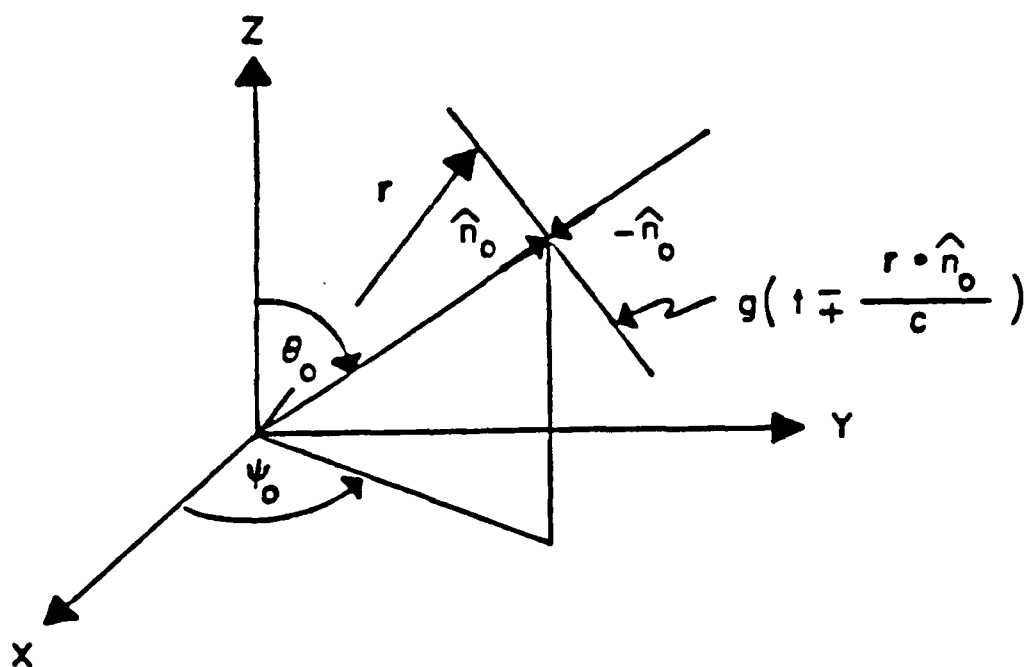
Figure 1. General plane-wave field g $(t \mp \frac{r \cdot \hat{n}_0}{c})$ propagating in the $\pm \hat{n}_0$ direction

The corresponding frequency spectrum is given by [Ref. 2]

$$Y(q,m,n) = Lc_q \exp( \mp \frac{j2\pi q f_0 u_0 m d_x}{c} ) \exp( \mp \frac{j2\pi q f_0 v_0 n d_y}{c} ) \qquad (2.9)$$

where

$$c_q = Y(q,0,0)/L, \quad q = -L',...,0,...,L' \qquad (2.10)$$

are the complex Fourier series coefficients that can be used to represent g(t) by a finite Fourier series with K harmonics during the time interval $|t| \leq \frac{T_0}{2}, f_0 = \frac{1}{T_0}$ ,

$$u_0 = \sin \theta_0 \cos \psi_0 \qquad (2.11)$$

and

$$v_0 = \sin \theta_0 \sin \psi_0 \qquad (2.12)$$

are the dimensionless direction cosines with respect to the X and Y axes, respectively; $\theta_0$ and $\psi_0$ are the depression and bearing angles, respectively; $d_x$ and $d_y$ are the interelement spacings in meters in the X and Y directions, respectively; and c is the speed of sound in meters per second.

Equation (2.9) is the basis for the frequency domain adaptive beamforming algorithms to be presented in this thesis. The algorithms presented use a planar array to estimate both $\theta_0$ and $\psi_0$ for each harmonic q present in the multiple incident plane-wave fields via frequency domain adaptive beamforming. Therefore, we shall use the following generalized version of Eq. (2.8)

$$y(l,m,n) = \sum_k g_k(lT_s \mp \frac{u_{0k}md_x + v_{0k}nd_y}{c} ) \qquad (2.13)$$

which represents the output electrical signal at time instant $l$ and element (m,n) in the planar array due to several incident plane-wave fields, where $g_k(t)$, $u_{0k}$, and $v_{0k}$ are the arbitrary time function and direction cosines associated with the kth sound source (target), respectively.

7

## B. FREQUENCY DOMAIN MODIFIED COMPLEX LMS ADAPTIVE BEAMFORMING ALGORITHM

The frequency domain adaptive beamforming algorithm to be discussed is based on processing the output complex frequency domain data R(q,m,n) from all $M \times N$ elements in the planar array. We begin by defining the complex estimation error as

$$e(q) \equiv s(q) - \hat{s}(q) \qquad (2.14)$$

where

$$s(q) = \frac{1}{LMN} \sum_{m=-M'}^{M'} \sum_{n=-N'}^{N'} |R(q,m,n)| \; \exp[\,+j\angle R(q,0,0)] \qquad (2.15)$$

is the reference signal;

$$\begin{aligned}
\hat{s}(q) &= \frac{1}{LMN} \sum_{m=-M'}^{M'} \sum_{n=-N'}^{N'} c(q,m)d(q,n)R(q,m,n) \\
&= \frac{\underline{c}^T(q)\underline{R}(q)\underline{d}(q)}{LMN}
\end{aligned} \qquad (2.16)$$

is the estimate of s(q); c(q,m) and d(q,n) are the unit magnitude complex weights in the X and Y directions, respectively; $\underline{c}(q)$ and $\underline{d}(q)$ are the $M \times 1$ and $N \times 1$ complex weight vectors in the X and Y directions, respectively; given by

$$\underline{c}(q) = [c(q,-M'),...,c(q,0),...,c(q,M')]^T \qquad (2.17)$$

and

$$\underline{d}(q) = [d(q,-N'),...,d(q,0),...,d(q,N')]^T \qquad (2.18)$$

8

respectively; and

$$\underline{R}(q) = \begin{bmatrix} R(q, -M', -N')...R(q, -M',0)...R(q, -M',N') \\ R(q,0, -N') \quad ... \quad R(q,0,0) \quad ... \quad R(q,0,N') \\ R(q,M', -N') \quad ... \quad R(q,M',0) \quad ... \quad R(q,M',N') \end{bmatrix} \qquad (2.19)$$

is the M x N complex data matrix. Next, define the $(M+N)$ x 1 complex weight vector $\underline{w}(q)$ as follows:

$$\underline{w}(q) \equiv \begin{bmatrix} \underline{c}(q) \\ \hline \underline{d}(q) \end{bmatrix} \qquad (2.20)$$

Therefore,

$$\underline{c}(q) = \underline{A} \ \underline{w}(q) \qquad (2.21)$$

where

$$\underline{A} = \begin{bmatrix} I & | & 0 \\ MxM & & MxN \end{bmatrix} \qquad (2.22)$$

is a M x $(M+N)$ matrix, $\underline{I}$ is a M x M identity matrix, and $\underline{0}$ is a M x N null matrix as indicated; and

$$\underline{d}(q) = \underline{B} \ \underline{w}(q) \qquad (2.23)$$

where

$$\underline{B} = \begin{bmatrix} 0 & | & I \\ NxM & & NxN \end{bmatrix} \qquad (2.24)$$

is a N x $(M+N)$ matrix, $\underline{0}$ is a N x M null matrix, and $\underline{I}$ is a N x N identity matrix as indicated. Substituting Eqs. (2.21) and (2.23) into Eq. (2.16) yields

9

$$\hat{s}(q) = \frac{\underline{w}^T(q)Z(q)\underline{w}(q)}{LMN} \qquad (2.25)$$

where

$$Z(q) = A^T R(q) B \qquad (2.26)$$

is a $(M+N)$ x $(M+N)$ complex matrix. The complex weight vector that minimizes the mean-square error $E\{|e(q)|^2\}$ is given by [Ref. 1]

$$\underline{w}_{i+1}(q) = \underline{w}_i(q) + 2\mu_i e_i(q)[Z(q) + Z^T(q)]^* \underline{w}_i^*, \quad i = 0,1,2,\dots \qquad (2.27)$$

where

$$e_i(q) = s(q) - \hat{s}_i(q) \qquad (2.28)$$

is the estimation error after the ith iteration,

$$\hat{s}_i(q) = \frac{\underline{w}_i^T(q)Z(q)\underline{w}_i(q)}{LMN} \qquad (2.29)$$

is the estimate of s(q) after the ith iteration, and, the step-size parameter $\mu_i$ is given by

$$\mu_i = \mu_0 = (\sigma_y^2 + \sigma_n^2)^{-1}, \quad i = 0,1,2,\dots \qquad (2.30)$$

where $\mu_0$ is constant and $\sigma_y^2$ and $\sigma_n^2$ are the signal and noise power, respectively, at the center element in the array. After each iteration, each component of the complex weight vector $\underline{w}_{i-1}(q)$ is normalized by its respective magnitude in order to maintain unit magnitude.

Once the complex weight vector $\underline{w}_{i-1}(q)$ converges to a steady-state value $\underline{w}_{ss}(q)$, the steady-state complex weight vectors $\underline{c}_{ss}(q)$ and $\underline{d}_{ss}(q)$ can be obtained from Eqs. (2.21) and (2.23), respectively. The estimates of $\theta_0(q)$ and $\psi_0(q)$ at each harmonic q are given by [Ref. 3]

$$\hat{\theta}_0(q) = \sin^{-1}\left[\{[\hat{u}_0^{LS}(q)]^2 + [\hat{v}_0^{LS}(q)]^2\}^{1/2}\right], \quad q \neq 0 \tag{2.31}$$

and

$$\hat{\psi}_0(q) = \tan^{-1}\left[\frac{\hat{v}_0^{LS}(q)}{\hat{u}_0^{LS}(q)}\right], \quad q \neq 0 \tag{2.32}$$

where $\hat{u}_0^{LS}(q)$ and $\hat{v}_0^{LS}(q)$ represent estimates of the direction cosines obtained by using a least-squares fit to the "unwrapped" steady-state phase weights $\theta_{SS}^{U}(q,m)$ and $\phi_{SS}^{U}(q,n)$, respectively. Note that in the absence of noise

$$\theta_{SS}^{U}(q,m) = \pm\frac{2\pi q f_0 u_0(q) m d_x}{c}, \qquad \begin{array}{l} q = -L',...,0,...,L' \\ m = -M',...,0,...,M' \end{array} \tag{2.33}$$

and

$$\phi_{SS}^{U}(q,n) = \pm\frac{2\pi q f_0 v_0(q) n d_x}{c}, \qquad \begin{array}{l} q = -L',...,0,...,L' \\ n = -N',...,0,...,N' \end{array} \tag{2.34}$$

The steady-state phase weights need to be "unwrapped", that is, allowed to take on values outside the closed interval $[-\pi, \pi]$, in order to ensure full angular coverage (i.e., $0 \leq \theta_0(q) \leq \frac{\pi}{2}$ and $0 \leq \psi_0(q) \leq 2\pi$) and correct depression and bearing angle estimates, $\hat{\theta}_0(q)$ and $\hat{\psi}_0(q)$, respectively. Finally, substituting Eqs. (2.15) and (2.16) into Eq. (2.14) yields the following expression for the steady-state estimation error:

$$e_{SS}(q) = \frac{1}{LMN}\sum_{m=-M'}^{M'}\sum_{n=-N'}^{N'}|R(q,m,n)|\exp[+j\angle R(q,0,0)] \tag{2.35}$$
$$- \exp\{+j[\theta_{SS}^{W}(q,m) + \phi_{SS}^{W}(q,n) + \angle R(q,m,n)]\}$$

where

11

$$R(q,m,n) = |R(q,m,n)| \exp[ +j\angle R(q,m,n)] \tag{2.36}$$

$$c_{SS}(q,m) = a_{SS}(q,m) \exp[ +j\theta_{SS}^{W}(q,m)] = \exp[ +j\theta_{SS}^{W}(q,m)] \tag{2.37}$$

and

$$d_{SS}(q,n) = b_{SS}(q,n) \exp[ +j\phi_{SS}^{W}(q,n)] = \exp[ +j\phi_{SS}^{W}(q,n)] \tag{2.38}$$

where $a_{SS}(q,m) = 1$ and $b_{SS}(q,n) = 1$ are real, unit magnitude, amplitude weights and $\theta_{SS}^{W}(q,m)$ and $\phi_{SS}^{W}(q,n)$ are real, "wrapped" phase weights. The procedure for the unwrapping of the steady-state phase weights in order to obtain least-squares estimates of the direction cosines at each harmonic is described by Behrle [Ref. 5].

## C. FREQUENCY DOMAIN MODIFIED COMPLEX ADAPTIVE LINEAR PREDICTION-ERRROR FILTER BEAMFORMING ALGORITHM

Consider a planar array of M x N (odd), equally spaced, point source elements lying in the XY plane where M and N are the total odd number of elements in the X and Y directions, respectively. Figure 2 shows a linear prediction-error filtering structure in the frequency domain (i.e., after the operation of a time domain DFT). The frequency domain adaptive algorithm to be presented is based on processing the output complex frequency domain data R(q,m,n) given by Eq. (2-7). Since the target localization problem requires only phase informations in our algorithm, we processes phase only data.

Let the one-step forward linear prediction errors for harmonic number q in the X and Y directions, be given by

$$F_{p_x}(q,i,n) = s_x(q,i,n) - \hat{s}_x(q,i,n), \qquad n = -N',...,0,...,N' \tag{2.39}$$

and

$$F_{p_y}(q,m,i) = s_y(q,m,i) - \hat{s}_y(q,m,i), \qquad m = -M',...,0,...,M' \tag{2.40}$$
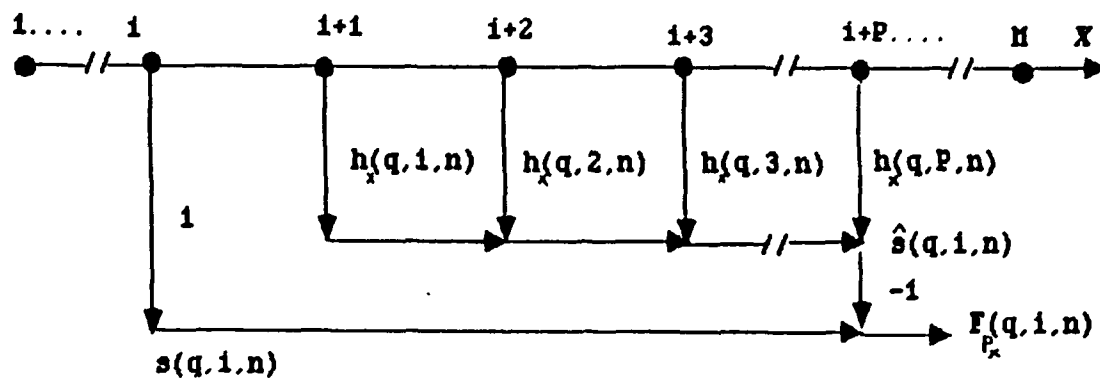
**Figure 2.** Frequency domain linear prediction-error filter structure

respectiv.ly, with

$$N' = \frac{N-1}{2} \qquad (2.41)$$

and

$$M' = \frac{M-1}{2}, \qquad (2.42)$$

where i is the number of the reference element in the direction of processing; $s_x(\cdot)$ and $\hat{s}_x(\cdot)$ are the reference signal and the estimate of the reference signal in the X direction, respectively; and $s_y(\cdot)$ and $\hat{s}_y(\cdot)$ are the reference signal and the estimate of the reference signal in the Y direction, respectively. Each one of the above signals is defined as follows:

$$s_x(q,i,n) = R(q,i,n), \qquad (2.43)$$

$$\hat{s}_x(q,i,n) = \frac{1}{P} \sum_{p=1}^{P} h_x(q,p,n) R(q,i+p,n) = \frac{1}{P} h_x^T(q,n) r(q,i,n), \qquad (2.44)$$

13

$$s_y(q,m,i) = R(q,m,i), \qquad (2.45)$$

and

$$\hat{s}_y(q,m,i) = \frac{1}{P}\sum_{p=1}^{P}h_y(q,m,p)R(q,m,i+p) = \frac{1}{P}\underline{h}_y^T(q,m)\underline{r}(q,m,i) \qquad (2.46)$$

where $\underline{h}_x(q,n)$ and $\underline{h}_y(q,m)$ are the P x 1 complex weight vectors in the X and Y directions, respectively , and $\underline{r}(q,i,n)$ and $\underline{r}(q,m,i)$ are the P x 1 complex frequency domain data vectors in the X and Y directions, respectively, given by

$$\underline{h}_x(q,n) = [h_x(q,1,n),\, h_x(q,2,n),\ldots\ldots,h_x(q,P,n)]^T, \qquad (2.47)$$

$$\underline{r}(q,i,n) = [R(q,i+1,n),R(q,i+2,n),\ldots\ldots,R(q,i+P,n)]^T, \qquad (2.48)$$

$$\underline{h}_y(q,m) = [h_y(q,m,1),\, h_y(q,m,2)\ldots\ldots,h_y(q,m,P)]^T, \qquad (2.49)$$

and

$$\underline{r}(q,m,i) = [R(q,m,i+1),R(q,m,i+2),\ldots\ldots,R(q,m,i+P)]^T \qquad (2.50)$$

where P is the order of the linear prediction-error filter.

Substituting Eqs. (2.43) and (2.44) into Eq. (2-39) and, substituting Eqs. (2.45) and (2.46) into Eq. (2.40) yields

$$F_{p_x}(q,i,n) = R(q,i,n) - \frac{1}{P}\sum_{p=1}^{P}h_x(q,p,n)R(q,i+p,n), \quad n = -N,\ldots,0,\ldots,N, \qquad (2.51)$$

and

14

$$F_{p_y}(q,m,i) = R(q,m,i) - \frac{1}{P}\sum_{p=1}^{P} h_y(q,m,p) R(q,m,i+p), \quad m = -M',...,0,...,M'. \quad (2.52)$$

Since we are working with phase only data, Eqs. (2.51) and (2.52) become:

$$F_{p_x}(q,i,n) = \exp[\,+j\angle R(q,i,n)]$$
$$-\frac{1}{P}\sum_{p=1}^{P} |h_x(q,p,n)| \exp[\,+j\angle h_x(q,p,n)] \exp[\,+j\angle R(q,i+p,n)], \quad (2.53)$$
$$n = -N',...,0,...,N'$$

and

$$F_{p_y}(q,m,i) = \exp[\,+j\angle R(q,m,i)]$$
$$-\frac{1}{P}\sum_{p=1}^{P} |h_y(q,m,p)| \exp[\,+j\angle h_y(q,m,p)] \exp[\,+j\angle R(q,m,i+p)], \quad (2.54)$$
$$m = -M',...,0,...,M'.$$

From Eqs. (2.53) and (2.54) it can be seen that if each component of the complex weight vectors have unit magnitude, then the forward linear prediction error become zero when

$$\exp[\,+j\angle R(q,i,n)] = \frac{1}{P}\sum_{p=1}^{P} \exp[\,+j\angle h_x(q,p,n)] \exp[\,+j\angle R(q,i+p,n)], \quad (2.55)$$
$$n = -N',...,0,...,N'$$

and

$$\exp[\,+j\angle R(q,m,i)] = \frac{1}{P}\sum_{p=1}^{P} \exp[\,+j\angle h_y(q,m,p)] \exp[\,+j\angle R(q,m,i+p)], \quad (2.56)$$
$$m = -M',...,0,...,M'.$$

15

Equations (2.55) and (2.56) will be valid only if the phase weights cophase the data at the output of each element in the prediction-error filters.

The algorithm used for the optimum estimation of the complex weight vectors is a modified, complex least mean-square (LMS) algorithm. The estimates of the complex weight vectors in the X and Y directions after the k-th iteration in X and Y directions is given by

$$[\underline{h}_x(q,n)]_{k+1} = [\underline{h}_x(q,n)]_k + 2\mu_k[F_{p_x}(q,i,n)]_k[\underline{r}^*(q,i,n)],$$
$$n = -N',...,0,...N'$$
$$k = 0,1,2,3,.... \qquad (2.57)$$

and

$$[\underline{h}_y(q,m)]_{k+1} = [\underline{h}_y(q,m)]_k + 2\mu_k[F_{p_y}(q,m,i)]_k[\underline{r}^*(q,m,i)],$$
$$m = -M',...,0,...,M'$$
$$k = 0,1,2,3,..... \qquad (2.58)$$

respectively, where the index k denotes the k-th step of iteration, $F_{r_x}(\cdot)$ and, $F_{r_y}(\cdot)_k$ are the forward linear prediction errors in the X and Y directions, respectively, after the k-th iteration: $\underline{r}^*(\cdot)$ is the complex conjugate of the data vector; and the step-size parameter $\mu_x$ is given by

$$\mu_k = \mu_0 = (\sigma_y^2 + \sigma_n^2)^{-1}, \quad k = 0,1,2,... \qquad (2.59)$$

where $\mu_0$ is a constant, and it is equal to the inverse of the sum of the signal and noise power, $\sigma_y^2$ and $\sigma_n^2$, respectively, at the center element of the array. After each iteration of the algorithm, each component of the complex weight vectors is normalized by its respective magnitude in order to maintain unit magnitude.

Since we are working with multiple linear arrays to obtain estimates of the targets' locations, we use average, steady-state, complex weight vectors in the X and Y directions, that is,

$$\underline{h}_{x_{avg}}(q) = \frac{1}{N} \sum_{n=-N'}^{N'} \underline{h}_x(q,n) \tag{2.60}$$

and

$$\underline{h}_{y_{avg}}(q) = \frac{1}{M} \sum_{m=-M'}^{M'} \underline{h}_y(q,m). \tag{2.61}$$

Note that each of the P x 1 average, steady-state, complex weight vectors in the X and Y directions is given by

$$\underline{h}_{x_{avg}}(q) = [h_{x_{avg}}(q,1), h_{x_{avg}}(q,2),........,h_{x_{avg}}(q,P)]^T \tag{2.62}$$

and

$$\underline{h}_{y_{avg}}(q) = [h_{y_{avg}}(q,1), h_{y_{avg}}(q,2),........,h_{y_{avg}}(q,P)]^T. \tag{2.63}$$

Next, if we now use the average, steady-state, complex weight vectors in the X and Y directions, then the one-step, steady-state, forward linear prediction errors for harmonic number q in the X and Y directions, are given by

$$F_{p_x}(q,i,n) = R(q,i,n) - \frac{1}{P} \sum_{p=1}^{P} h_{x_{avg}}(q,p)R(q,i+p,n), \quad n = -N',...,0,...,N', \tag{2.64}$$

and

$$F_{p_y}(q,m,i) = R(q,m,i) - \frac{1}{P} \sum_{p=1}^{P} h_{y_{avg}}(q,m,p)R(q,m,i+p), \quad m = -M',...,0,...,M'. \tag{2.65}$$

If we define the forward spatial Z-transform of g(i) as

$$G(z) = Z\{g(i)\} = \sum_{i=-\infty}^{\infty} g(i)z^i, \qquad (2.66)$$

then

$$Z\{g(i+p)\} = G(z)z^{-p}, \qquad (2.67)$$

and, upon taking the forward spatial Z-transform of Eqs. (2.64) and (2.65) with respect to i, we obtain

$$F_{P_x}(q,z_x,n) = R(q,z_x,n)[1 - \frac{1}{P}\sum_{p=1}^{P} h_{x_{cvg}}(q,p)z_x^{-p}], \quad n = -N',...,0,...,N', \qquad (2.68)$$

and

$$F_{P_y}(q,m,z_y) = R(q,m,z_y)[1 - \frac{1}{P}\sum_{p=1}^{P} h_{y_{cvg}}(q,p)z_y^{-p}], \quad m = -M',...,0,...,M'. \qquad (2.69)$$

From Eqs. (2.68) and (2.69), the transfer functions of the one-step forward linear prediction-error filters (analysis filters) in the X and Y directions are given by

$$H_{PE_x}(q,z_x,n) = \frac{F_{P_x}(q,z_x,n)}{R(q,z_x,n)} = 1 - \frac{1}{P}\sum_{p=1}^{P} h_{x_{cvg}}(q,p)z_x^{-p}, \quad n = -N',...,0,...,N', \qquad (2.70)$$

and

$$H_{PE_y}(q,m,z_y) = \frac{F_{P_y}(q,m,z_y)}{R(q,m,z_y)} = 1 - \frac{1}{P}\sum_{p=1}^{P} h_{y_{cvg}}(q,p)z_y^{-p}, \quad m = -M',...,0,...,M'. \qquad (2.71)$$

Since the average complex weights in the X and Y directions are independent of the indices n and m, the transfer functions are also independent of n and m, that is,

18

$$H_{PE_x}(c, z_x) = 1 - \frac{1}{P} \sum_{p=1}^{P} h_{x_{avg}}(q,p) z_x^{-p}, \qquad (2.72)$$

and

$$H_{PE_y}(q, z_y) = 1 - \frac{1}{P} \sum_{p=1}^{P} h_{y_{avg}}(q,p) z_y^{-p}. \qquad (2.73)$$

Therefore the transfer functions of the inverse filters (synthesis filters) in the X and Y directions are given by

$$H_{PE_x}^{-1}(q, z_x) = \frac{1}{1 - \frac{1}{P} \sum_{p=1}^{P} h_{x_{avg}}(q,p) z_x^{-p}} \qquad (2.74)$$

and

$$H_{PE_y}^{-1}(q, z_y) = \frac{1}{1 - \frac{1}{P} \sum_{p=1}^{P} h_{y_{avg}}(q,p) z_y^{-p}}. \qquad (2.75)$$

In order to obtain the spatial-frequency response (angular response) of the filter described by Eq. (2.74), let

$$z_x = \exp(+j2\pi f_x d_x) = \exp(\frac{+j2\pi u d_x}{\lambda}). \qquad (2.76)$$

Substituting Eq.(2.76) into Eq.(2.74) yields

$$H_{PE_x}^{-1}(q, u) = \frac{1}{1 - \frac{1}{P} \sum_{p=1}^{P} h_{x_{avg}}(q,p) \exp(\frac{-j2\pi p u d_x}{\lambda})}. \qquad (2.77)$$

19

Similarly, if we let

$$z_y = \exp(+j2\pi f_y d_y) = \exp(\frac{+j2\pi v d_y}{\lambda}) \qquad (2.78)$$

in Eq. (2.75), we obtain

$$H_{PE_y}^{-1}(q,v) = \frac{1}{1 - \frac{1}{P}\sum_{p=1}^{P} h_{y_{avg}}(q,p) \exp(\frac{-j2\pi p v d_y}{\lambda})} . \qquad (2.79)$$

Equations (2-77) and (2-79) are then evaluated as functions of the direction cosines u and v, respectively, for a given harmonic q. The values of u and v that maximize Eqs. (2-77) and (2-79), respectively, then become the linear prediction-error estimates $\hat{u}_0^{PE}(q)$ and $\hat{v}_0^{PE}(q)$ of $u_0(q)$ and $v_0(q)$ . The estimates of $\theta_0(q)$ and $\psi_0(q)$ at each harmonic q are given by [Ref. 3]

$$\hat{\theta}_0(q) = \sin^{-1}\left[\{[\hat{u}_0^{PE}(q)]^2 + [\hat{v}_0^{PE}(q)]^2\}^{1/2}\right], \quad q \neq 0 \qquad (2.80)$$

and

$$\hat{\psi}_0(q) = \tan^{-1}\left[\frac{\hat{v}_0^{PE}(q)}{\hat{u}_0^{PE}(q)}\right], \qquad q \neq 0 \qquad (2.81)$$

where $\hat{u}_0^{PE}(q)$ and $\hat{v}_0^{PE}(q)$ are the estimates of the direction cosines obtained by using the adaptive linear prediction-error algorithm.

# III. SIMULATION RESULTS

Computer simulation results for five test cases are presented in this chapter. The test cases were designed to test both of the algorithms multiple broadband target localization capability, full angular coverage capabilities, and their angular resolution as a function of the input SNR at a single element in the array, harmonic number, and the number of iterations.

For simplification purposes, in all of the simulation results we use the following notation:

- LMS: When the frequency domain modified complex Least-Mean-Square adaptive beamforming algorithm is used.

- ALP: When the frequency domain modified complex adaptive linear prediction-error filtering beamforming algorithm is used.

The test cases are described below:

1. Case 1 - A single broadband target radiating six harmonics, located at broadside relative to the planar array;

2. Case 2 - Three broadband targets, each radiating two unique harmonics, located at random positions;

3. Case 3 - A single broadband target radiating six harmonics, located at endfire relative to the planar array;

4. Case 4 - Three broadband targets. Two targets are located in the same plane and have a common harmonic. Three subcases were examined. Each subcase used a different harmonic as the common spectral line.

5. Case 5 - Three broadband targets, located at random positions. Two targets have a common harmonic. Three subcases were examined. Each subcase used a different harmonic as the common spectral line.

The simulation results of these five cases are based upon processing the output electrical signals from a 11 x 11 planar array of equally spaced hydrophones. The acoustic field incident upon the planar array was, in general, the sum of several plane-wave fields travelling in different directions. Each plane-wave field consisted of an arbitrary number of harmonics (spectral lines) emanating from one of the broadband sound

sources. As a result, the output electrical signal at each element of the planar array was composed of an arbitrary number K of harmonics, all with identical amplitudes of unity.

The fundamental frequency for all test cases was chosen to be $f_0 = 1000$ Hz. Via Eq. (2-6), the fundamental period at each element of the array was 1 millisecond. The sampling parameter, S, was set equal to 10. The number of time samples taken per element of the array is given by

$$L = SK + 5 \tag{3.1}$$

where L is the total number of samples taken per element, K is the total number of harmonics present in the signal, and S is the sampling parameter. With $S = 10$ and $K = 6$, $L = 65$ time samples per element.

In the computer simulations presented in this thesis, the interelement spacing is

$$d_x = d_y = \frac{\lambda_{min}}{2}, \tag{3.2}$$

where the minimum wavelength is

$$\lambda_{min} = \frac{c}{f_{max}}, \tag{3.3}$$

and

$$f_{max} = Kf_0 \quad \text{Hz} \tag{3.4}$$

Substituting Eqs. (3.3) and (3.4) into Eq. (3.2) yields

$$d_x = d_y = \frac{c}{(2Kf_0)}. \tag{3.5}$$

For the ALP algorithm, the order of the forward prediction-error filter was 10. The reference element was the first element of each linear array and the number of linear arrays that have been processed in both directions was 11. Initial simulation tests indi-

cated that the number of iterations required for the LMS algorithm to approach a steady-state error was 100, while for the ALP algorithm 1000 iterations were required.

Baseline, or "no noise" test case results were the first generated to ensure that both algorithms were working properly in a noise-free environment. Figure 3 depicts the noise-free, time domain, received signal at element (1,1) for Case 2. For each baseline test case, bearing and depression angle estimation errors (measured in degrees) were obtained by running the computer simulation once allowing 100 iterations for the LMS algorithm and 1000 iterations for the ALP algorithm.

Following compilation of the baseline results for the first three cases, identical test cases were run using additive, wide-sense stationary, zero mean, white, gaussian noise samples to corrupt the time samples of the received signal. Figure 4 depicts the time domain, received signal at element (1,1) for case 2 for a SNR = -9dB. For each test case, and for a given input SNR at a single element of the array, average bearing and depression angle estimation errors were obtained by running the computer simulation 10 times. During each run, the LMS algorithm was allowed 100 iterations whereas the ALP algorithm was allowed 1000 iterations.
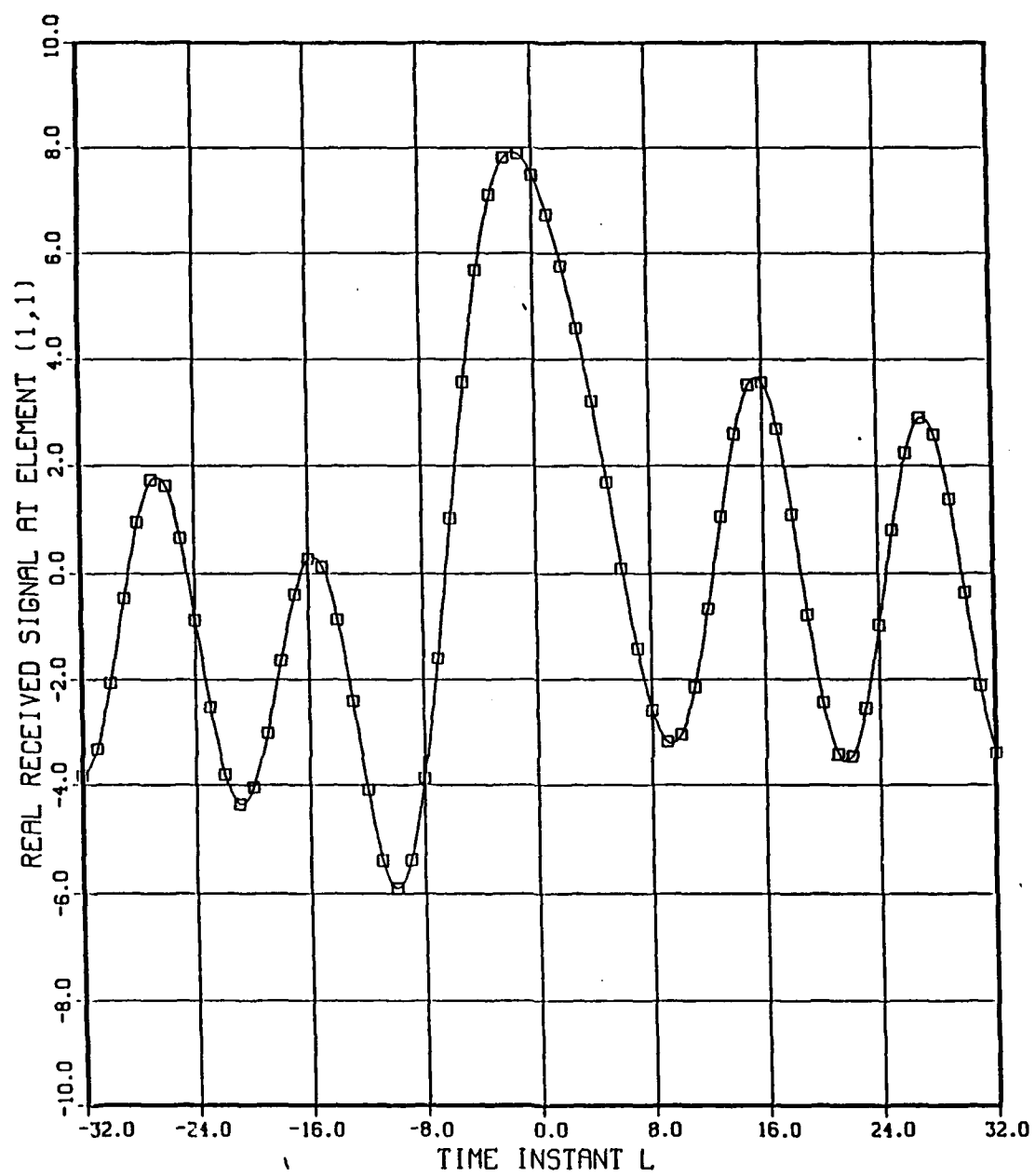
Figure 3.    Real Received Signal at Element (1,1), for Case LMS2 : No Noise

24
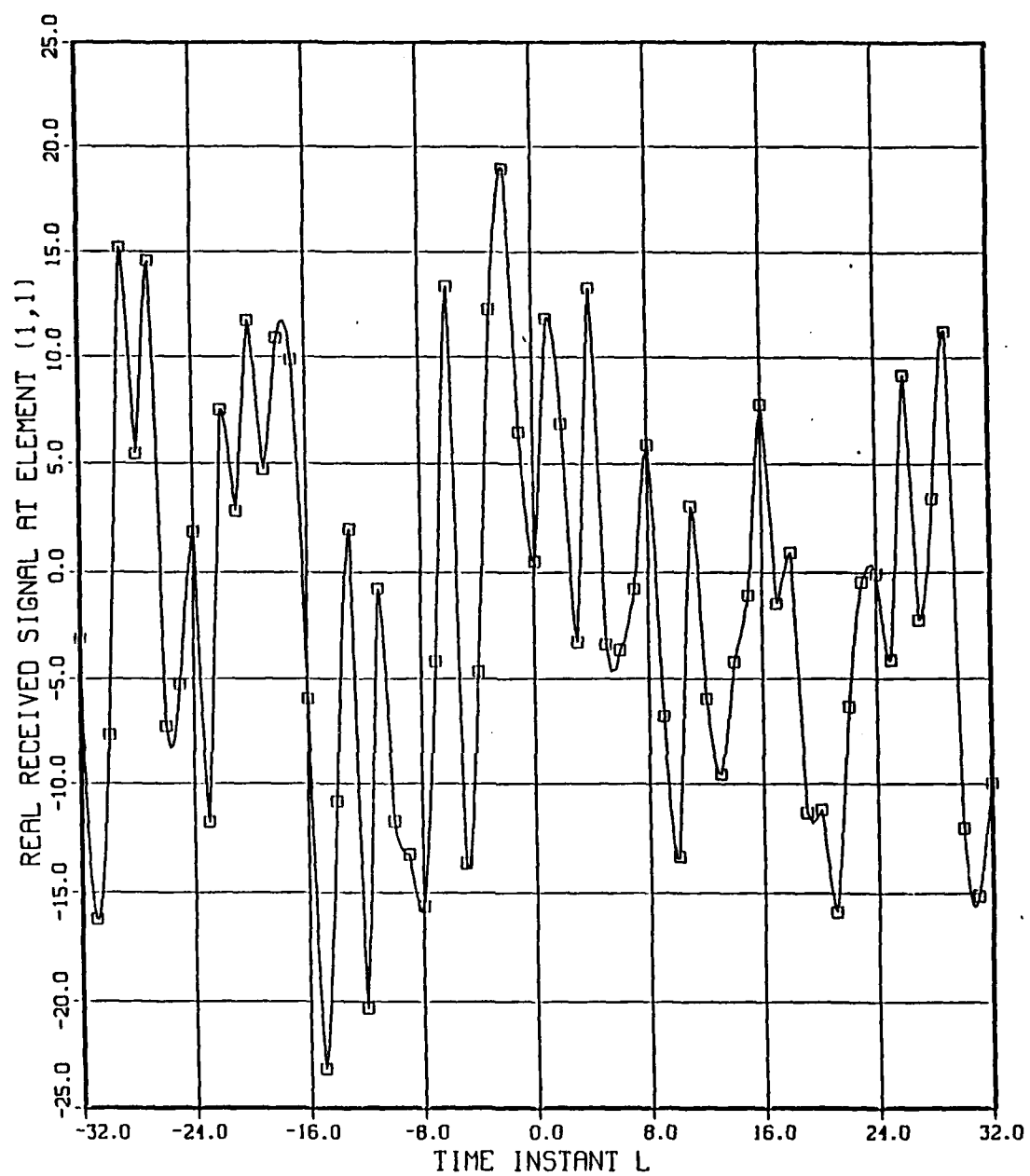
Figure 4.    Real Received Signal at Element (1,1), for Case LMS2 : SNR = -9dB

## A.  CASE 1

Case 1 placed a single broadband target at broadside relative to the planar array (i.e., $\theta_0 = 0^\circ$). This was considered the simplest case for both of the algorithms since it is at broadside that the far-field beam pattern has its narrowest beamwidth and, as a result, both algorithms should provide good angular resolution [Ref. 4]. The general plane-wave field radiated by the target consisted of six harmonics.

Figures 5, 6 and 7 present the average estimation errors of the depression angle ($e_{\theta_0}$) versus SNR for Case LMS1 at 1000 Hz, 3000 Hz and 6000 Hz, respectively. Results for bearing angle estimation errors in the broadside case are irrelevant since the target is directly above the array, and the bearing angle has no meaning. From these figures, we can see two trends. Increasing the SNR results in smaller magnitudes of the average estimation errors of the depression angle and as the harmonic number(q) increases, the magnitude of the estimation error decreases. These two trends were expected. As we increase the SNR, the noise components of the received signals are less dominant. An increase of the harmonic number (q) represents an increase in the frequency and, as a result, the beamwidth of the far-field beam pattern decreases. The decreased beamwidth increases the angular resolution of the algorithm and, as result, decreases the estimation error.

Figures 8, 9 and 10 present estimates of the direction cosines $U_0$ and $V_0$ for Case ALP1 at SNR = -3 dB and frequencies 1000 Hz, 3000 Hz, and 6000 Hz, respectively. Similarly, Figures 11, 12 and 13, and 14, 15, and 16 present estimates of the direction cosines $U_0$ and $V_0$ for Case ALP1 with the same order of frequency as above and for SNR = -6 dB and SNR = -9 dB, respectively. As we discussed in Chapter 2, the location of the peaks of the magnitude of the synthesis filter transfer function in dB give the $U_0$ and $V_0$ estimates. From these figures we can clearly observe that as the SNR decreases, the difference between the peak and the background noise in the transfer function plots decreases. Also, the harmonic number is important, because increasing the harmonic number produces sharper peaks in the transfer function plots resulting in more accurate estimation.

Figures 17, 18 and 19 present the average estimation error of the depression angle ($e_{\theta_0}$) versus SNR for Case ALP1 at 1000 Hz, 3000 Hz and 6000 Hz. The trends which were present in Case LMS1 are apparent here, that is, as SNR increases, the magnitude of the estimation error decreases and, as the harmonic number (q) increases, the magnitude of the estimation error decreases.

26

Finally Tables 1 and 2 in the Appendix A present the numerical data for Cases LMS1 and ALP1 respectively for all six harmonics. Comparing the two algorithms using these tables, we can conclude that for Case 1, both algorithms give small magnitude estimation errors in low SNR with a little better performance for the LMS1 particularly at 1000 Hz.
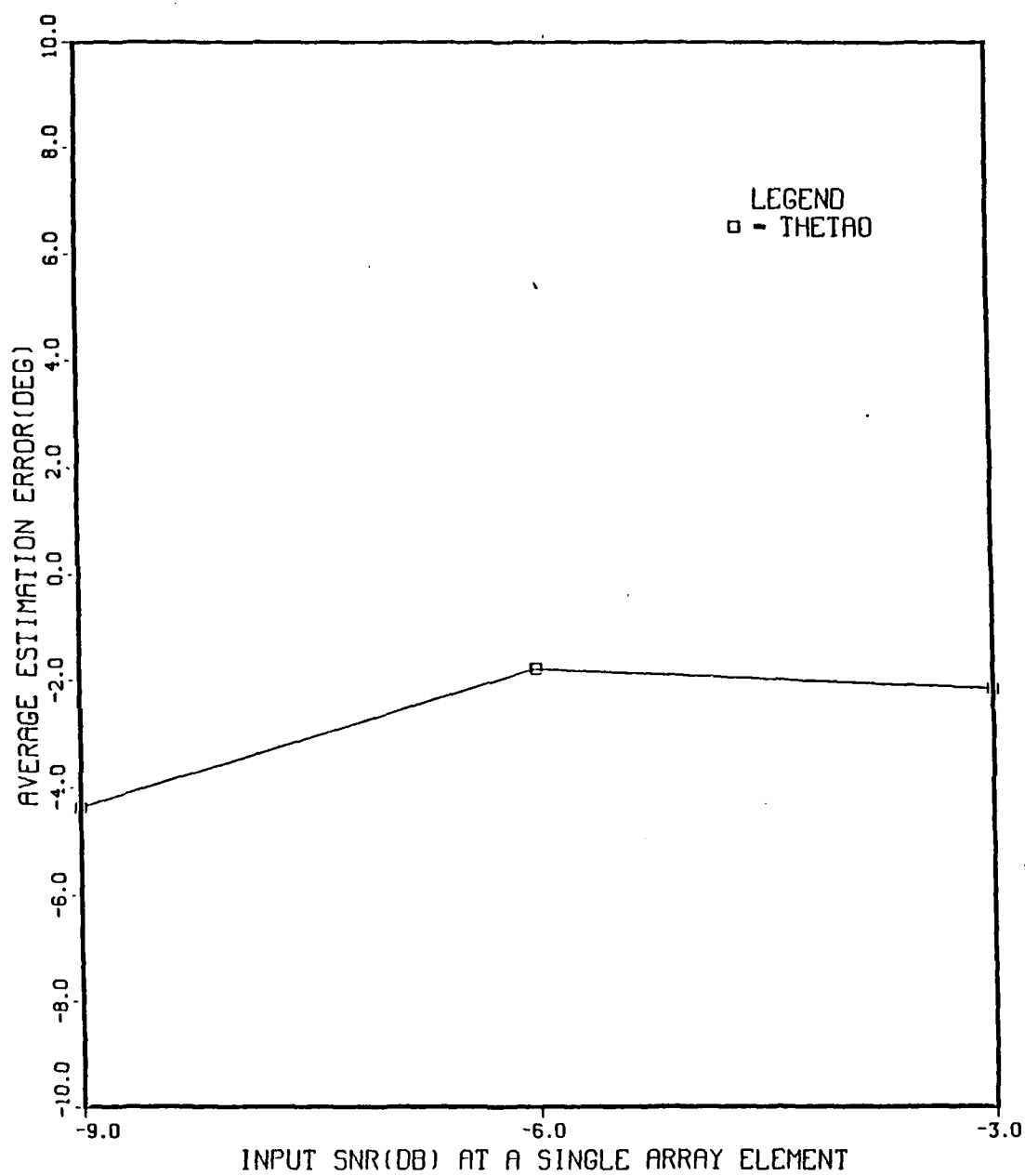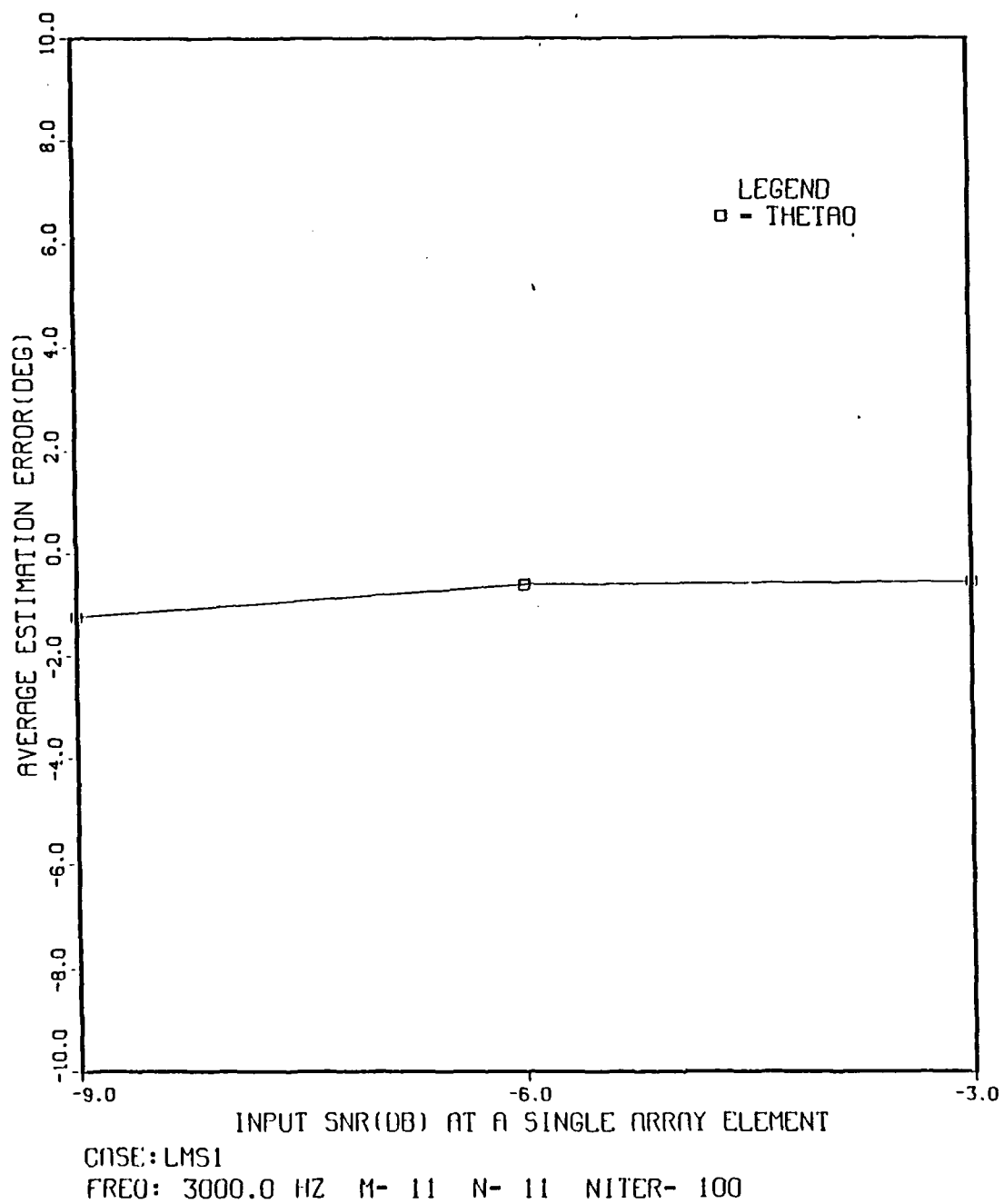
Figure 5.   Average Estimation Error of Depression Angle vs. SNR at 1000 Hz for Case LMS1.

Figure 6.    Average Estimation Error of Depression Angle vs. SNR at 3000 Hz for Case LMS1.
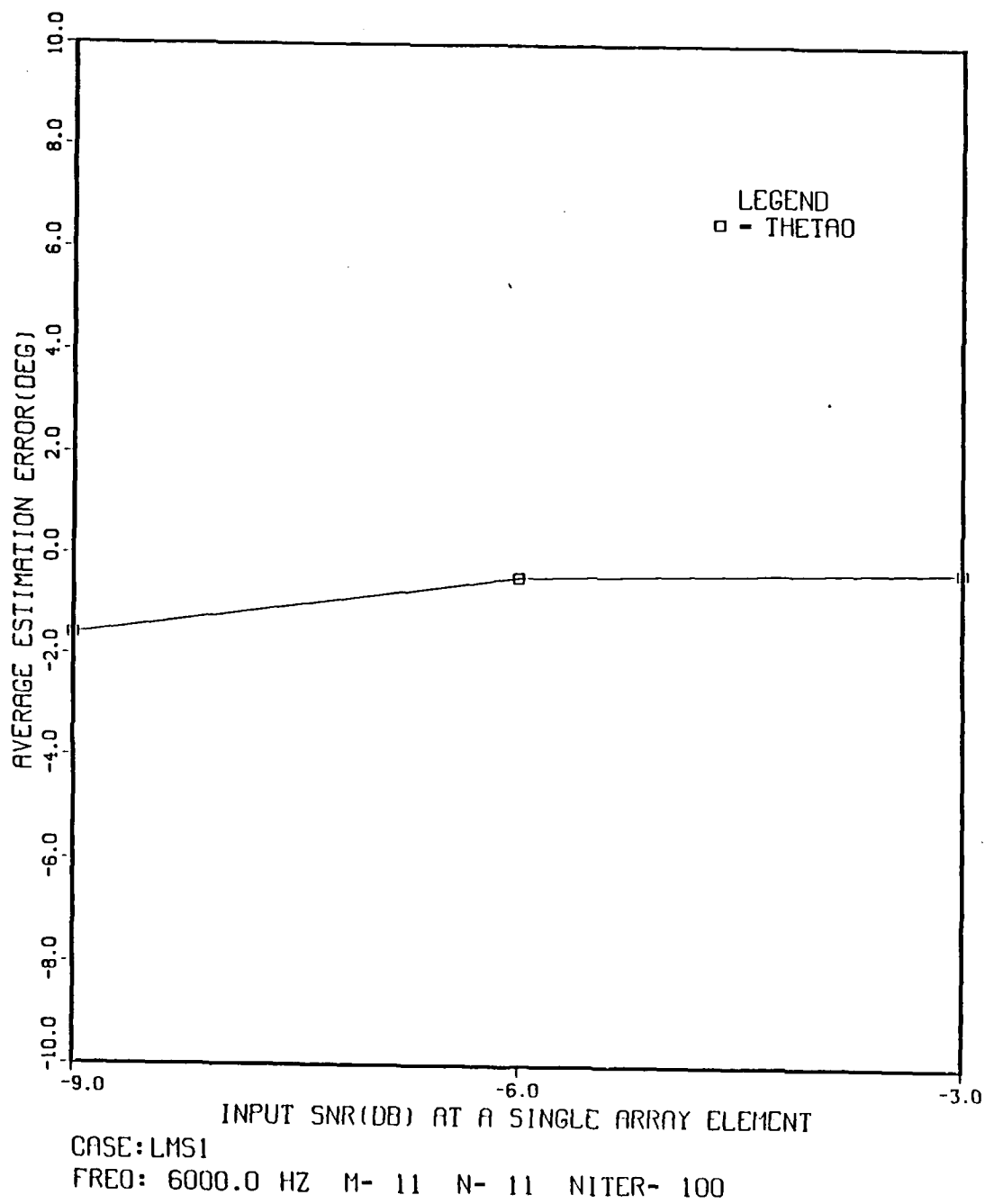
Figure 7.   Average Estimation Error of Depression Angle vs. SNR at 6000 Hz for Case LMS1.
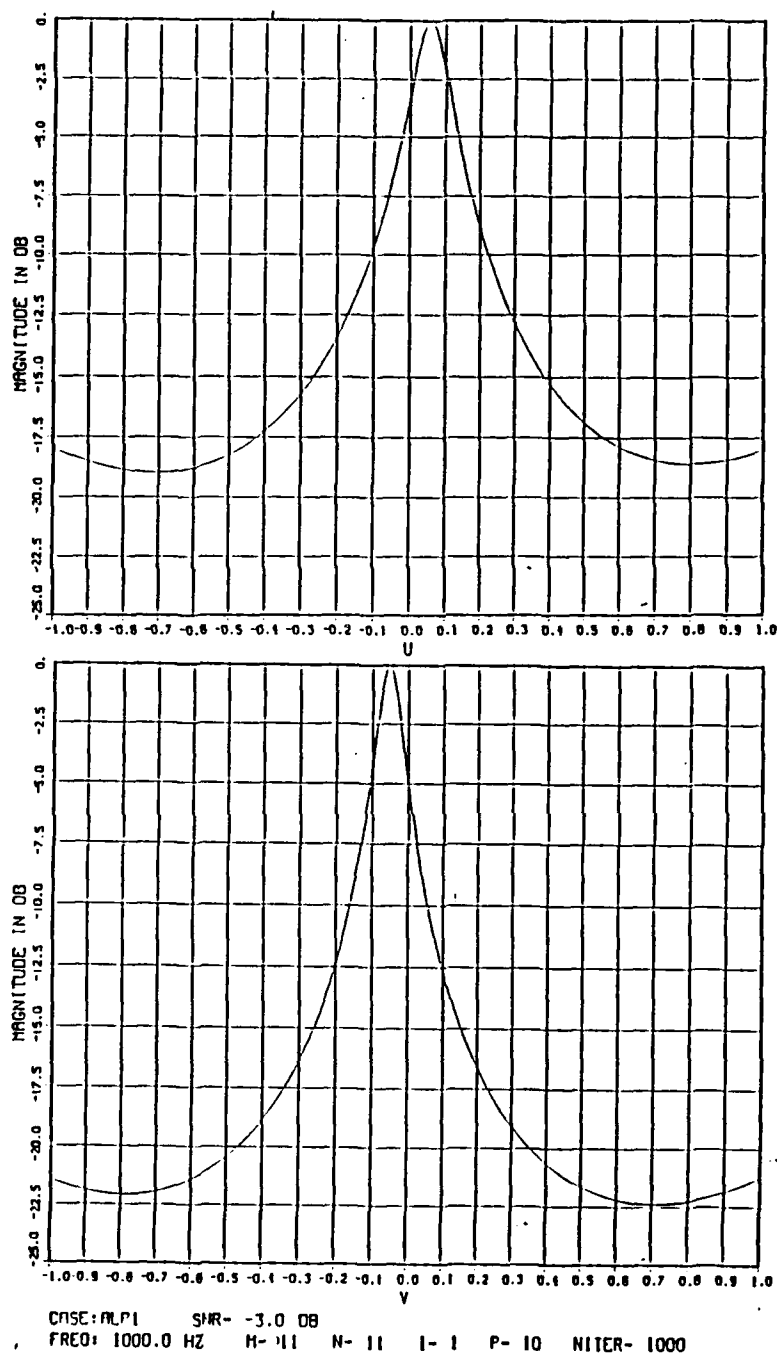
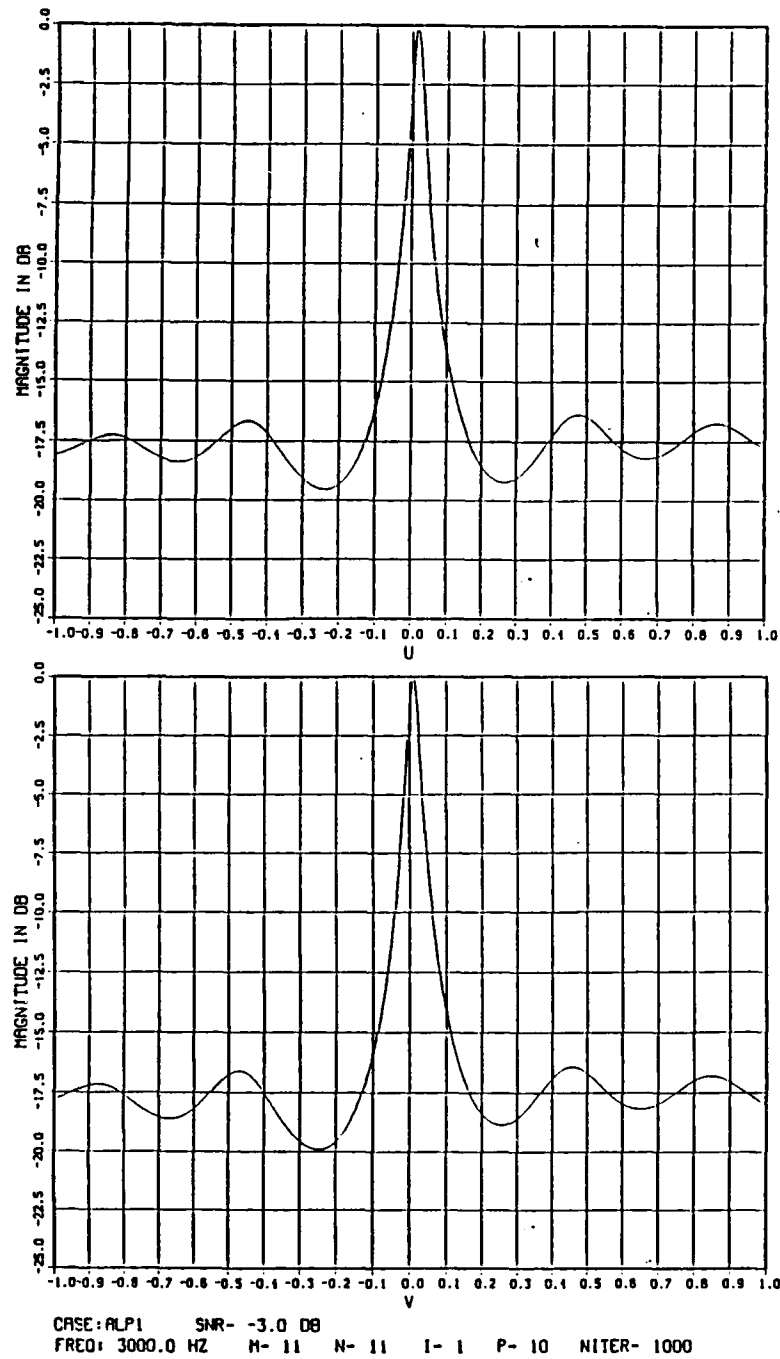Figure 8.    Estimates of Direction Cosines U0 and V0, Case ALP1: SNR = -3dB and
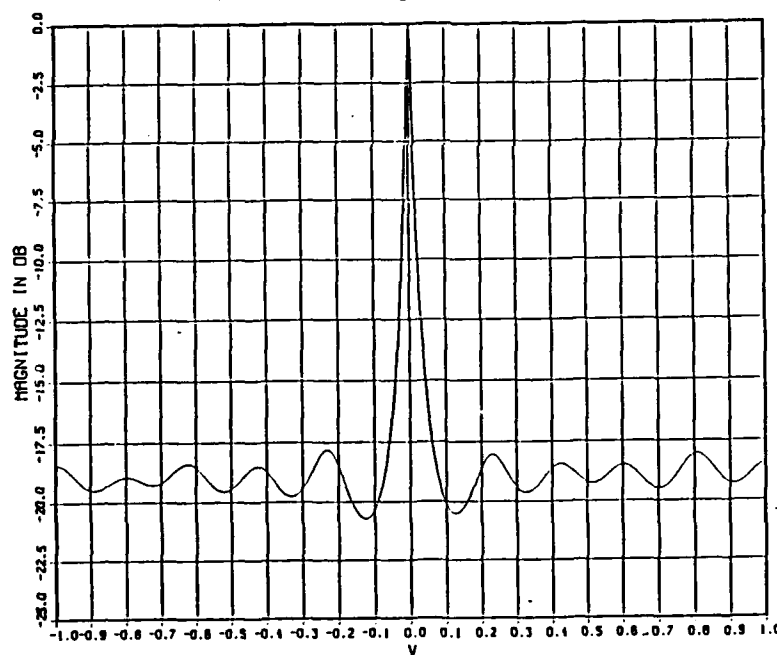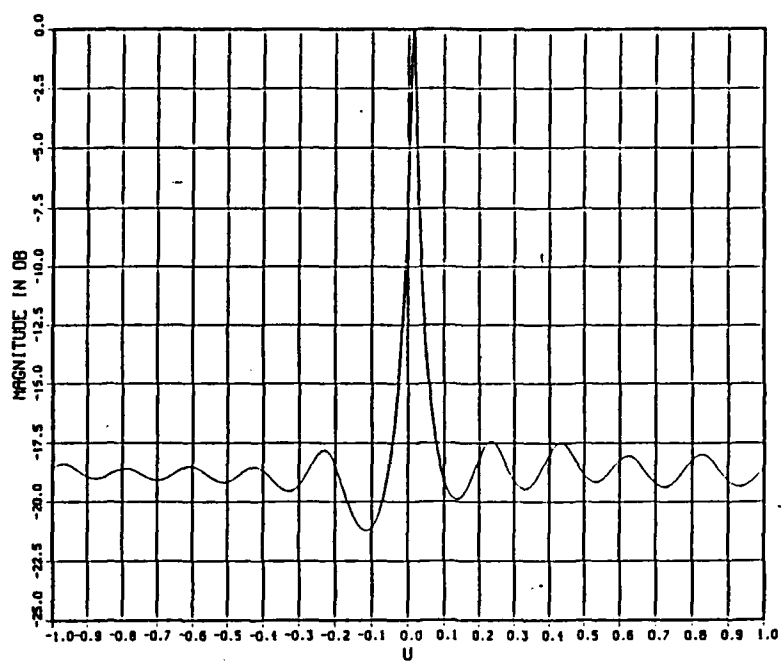             q = 1

**Figure 9.** Estimates of Direction Cosines U0 and V0, Case ALP1: SNR = -3dB and q = 3

CASE: ALP1    SNR= -3.0 DB
FREQ: 6000.0 HZ    M- 11    N- 11    I- 1    P- 10    NITER- 1000

**Figure 10.**    Estimates of Direction Cosines U0 and V0, Case ALP1: SNR = -3dB and
q = 6

33

CASE: ALP1    SNR- -6.0 DB
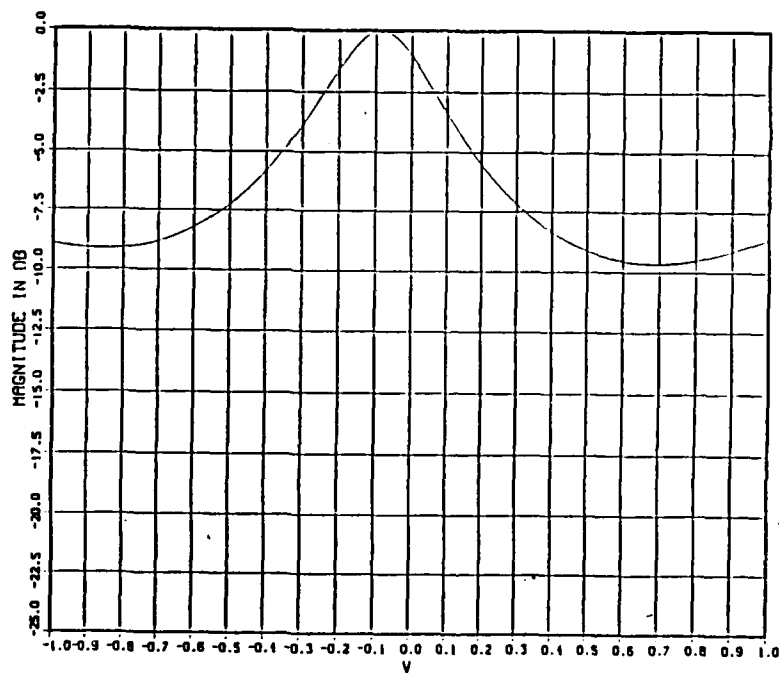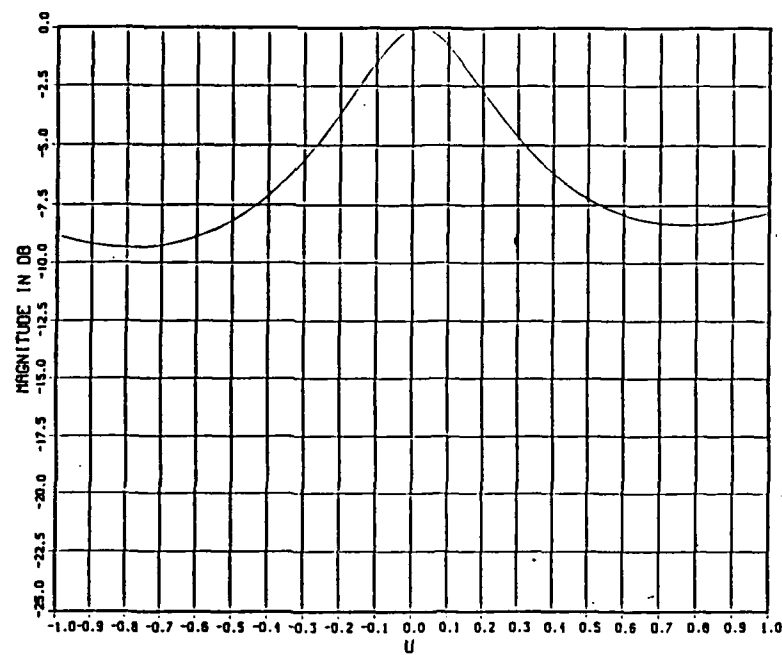FREQ: 1000.0 HZ    M- 11    N- 11    I- 1    P- 10    NITER- 1000

Figure 11.    Estimates of Direction Cosines U0 and V0, Case ALP1: SNR = -6dB and
q = 1

34

CASE:ALP1    SNR- -6.0 DB
FREQ: 3000.0 HZ    M- 11    N- 11    I- 1    P- 10    NITER- 1000

Figure 12.    Estimates of Direction Cosines U0 and V0, Case ALP1: SNR = -6dB and
q = 3

35
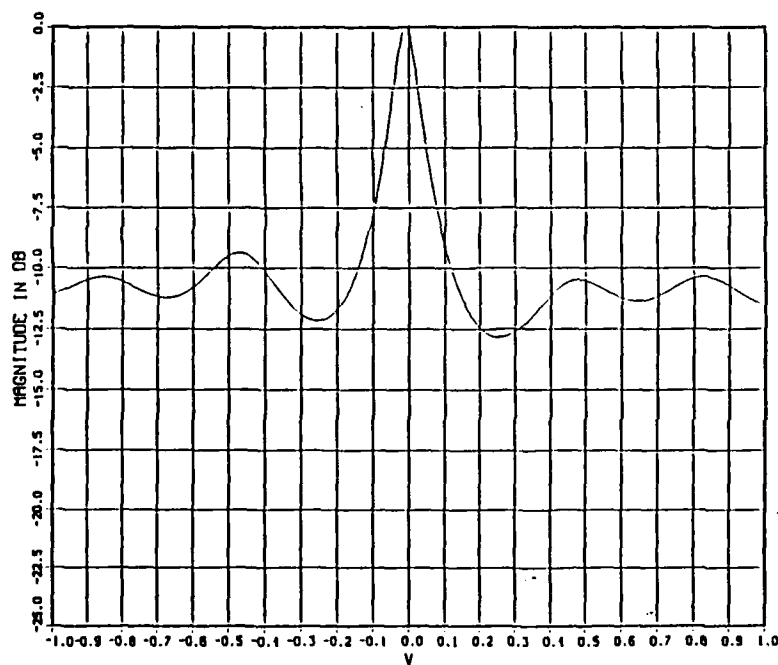
CASE: ALP1 SNR= -6.0 DB
FREQ: 6000.0 HZ M- 11 N- 11 I- 1 P- 10 NITER- 1000

Figure 13. Estimates of Direction Cosines U0 and V0, Case ALP1: SNR = -6dB and q = 6
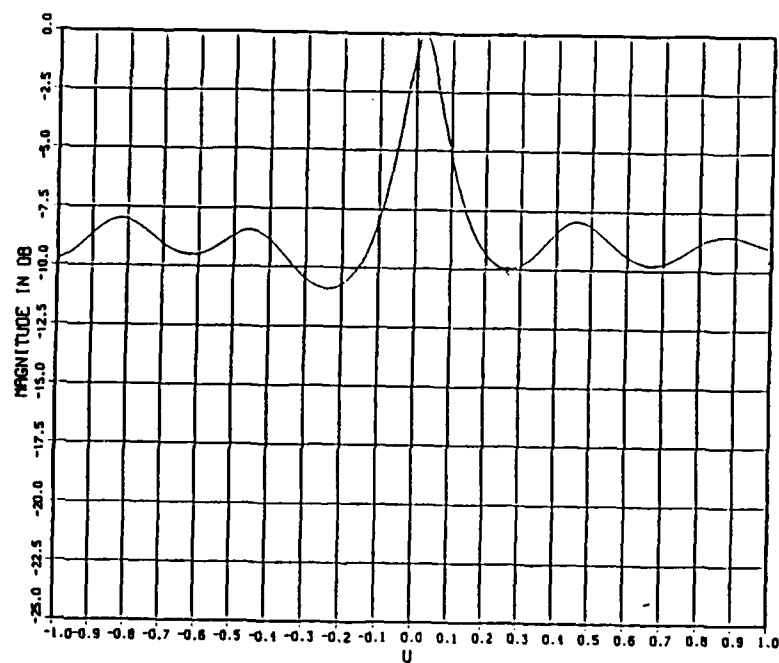
CASE:ALP1    SNR- -9.0 DB
FREQ: 1000.0 HZ    M- 11    N- 11    I- 1    P- 10    NITER- 1000

**Figure 14.**    **Estimates of Direction Cosines U0 and V0, Case ALP1: SNR = -9dB and**
q = 1

37
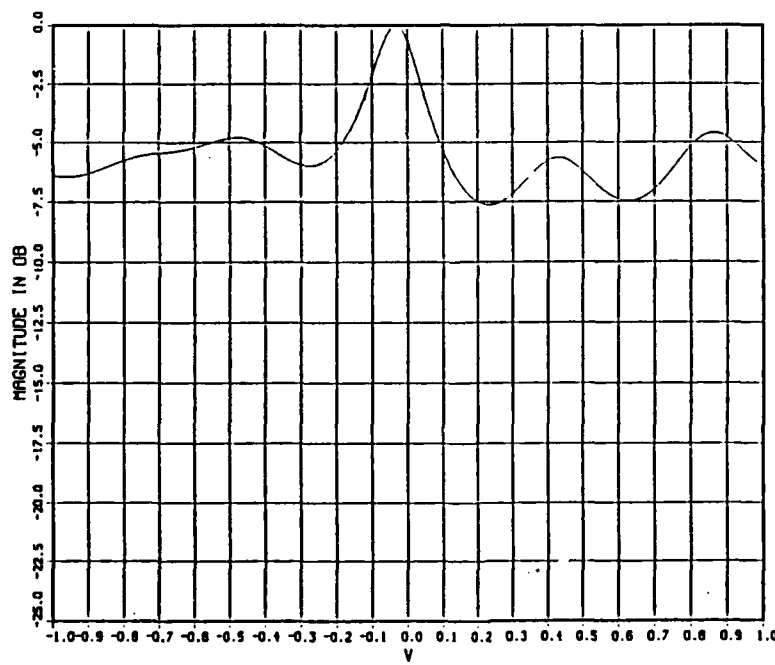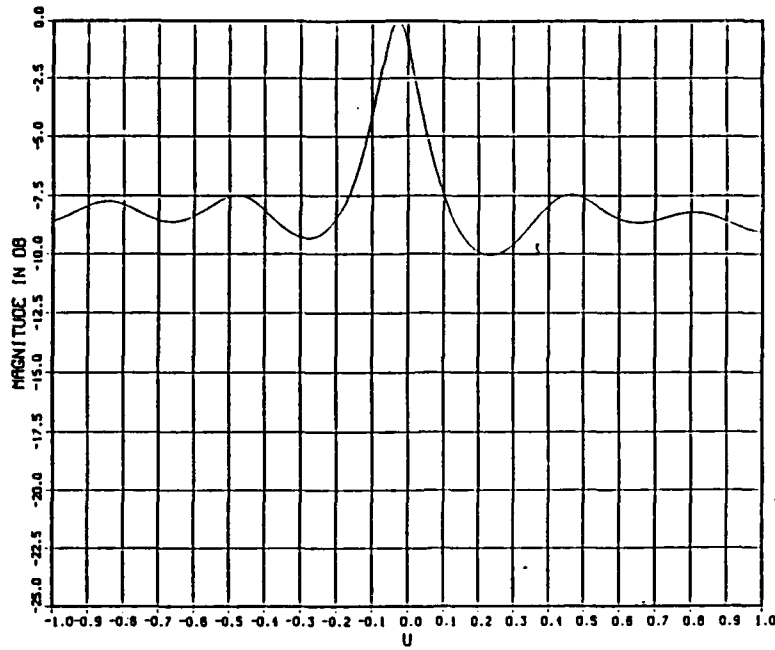
CASE:ALP1      SNR- -9.0 DB
FREQ: 3000.0 HZ      M- 11      N- 11      I- 1      P- 10      NITER- 1000

**Figure 15.** Estimates of Direction Cosines U0 and V0, Case ALP1: SNR = -9dB and
q = 3

38
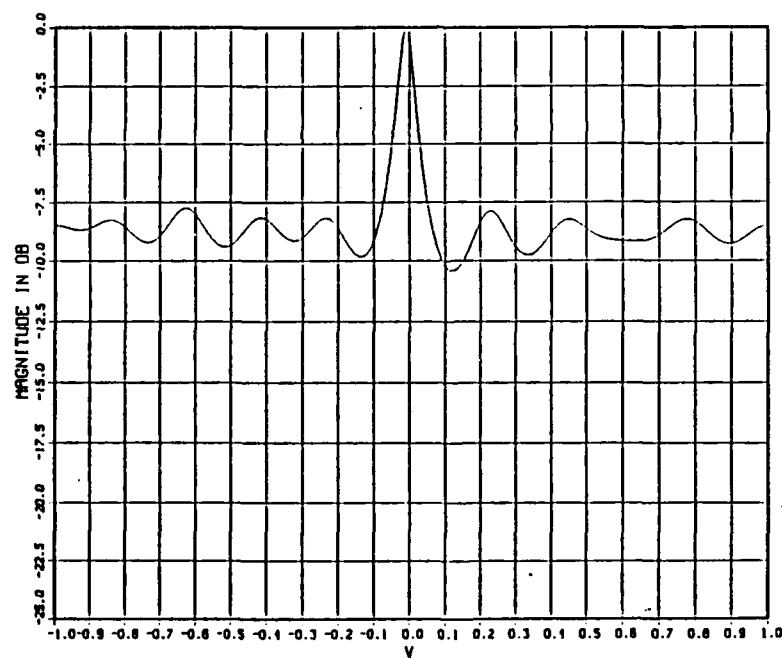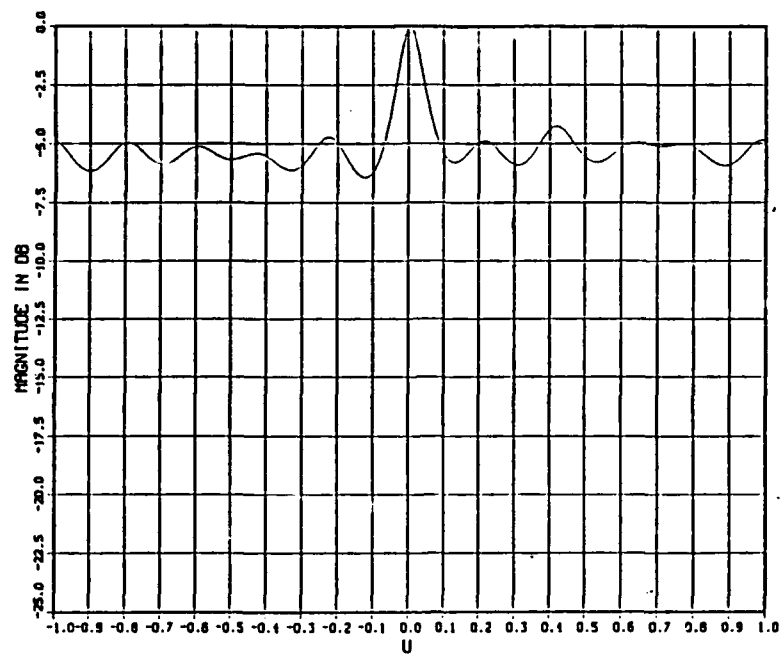
CASE: ALP1      SNR- -9.0 DB
FREQ: 6000.0 HZ      M- 11      N- 11      I- 1      P- 10      NITER- 1000

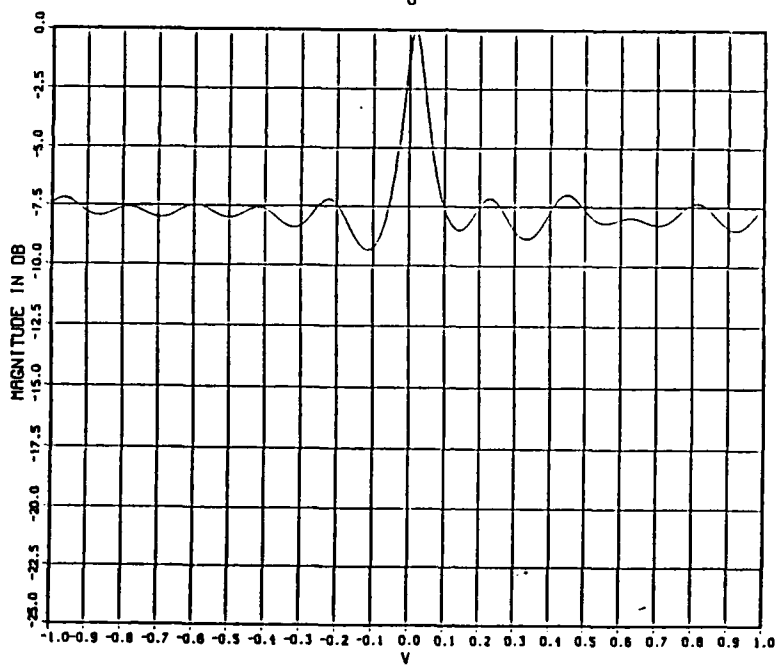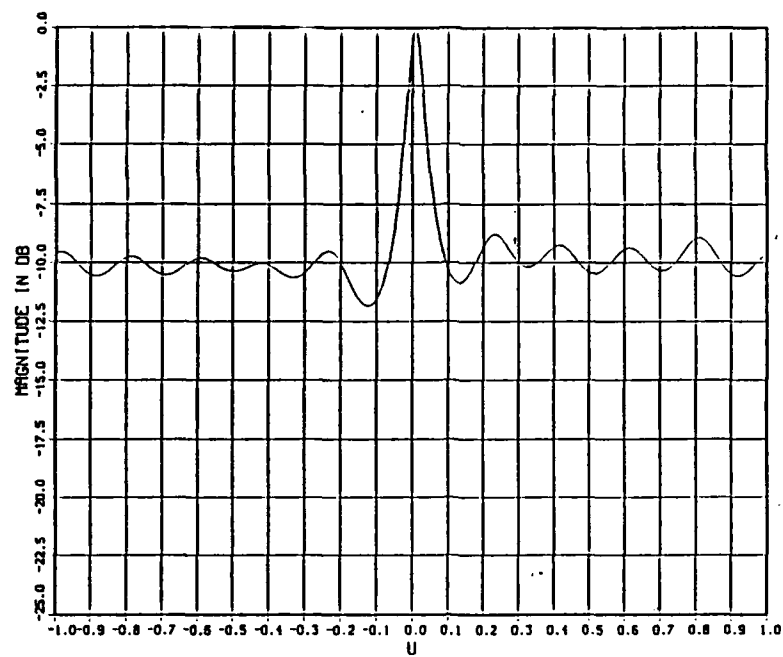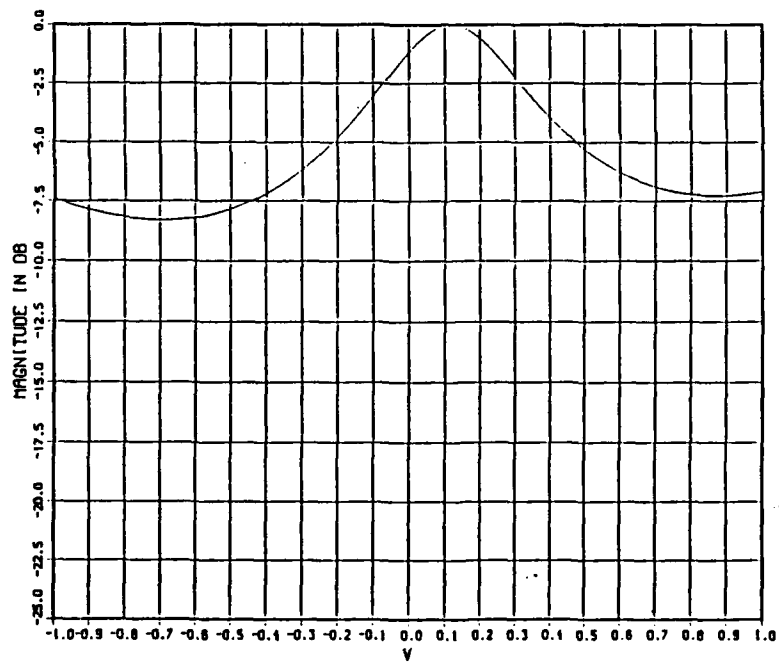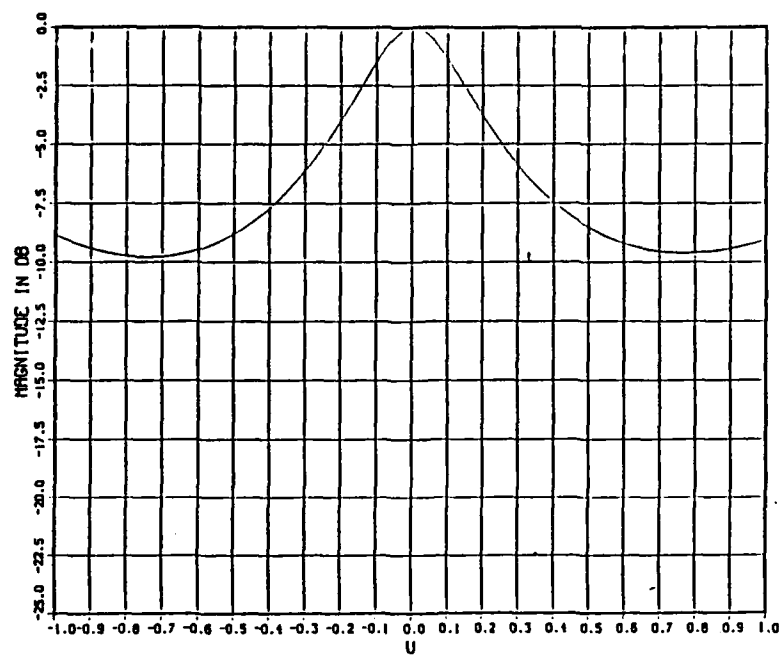Figure 16.  Estimates of Direction Cosines U0 and V0, Case ALP1: SNR = -9dB and
            q = 6

39

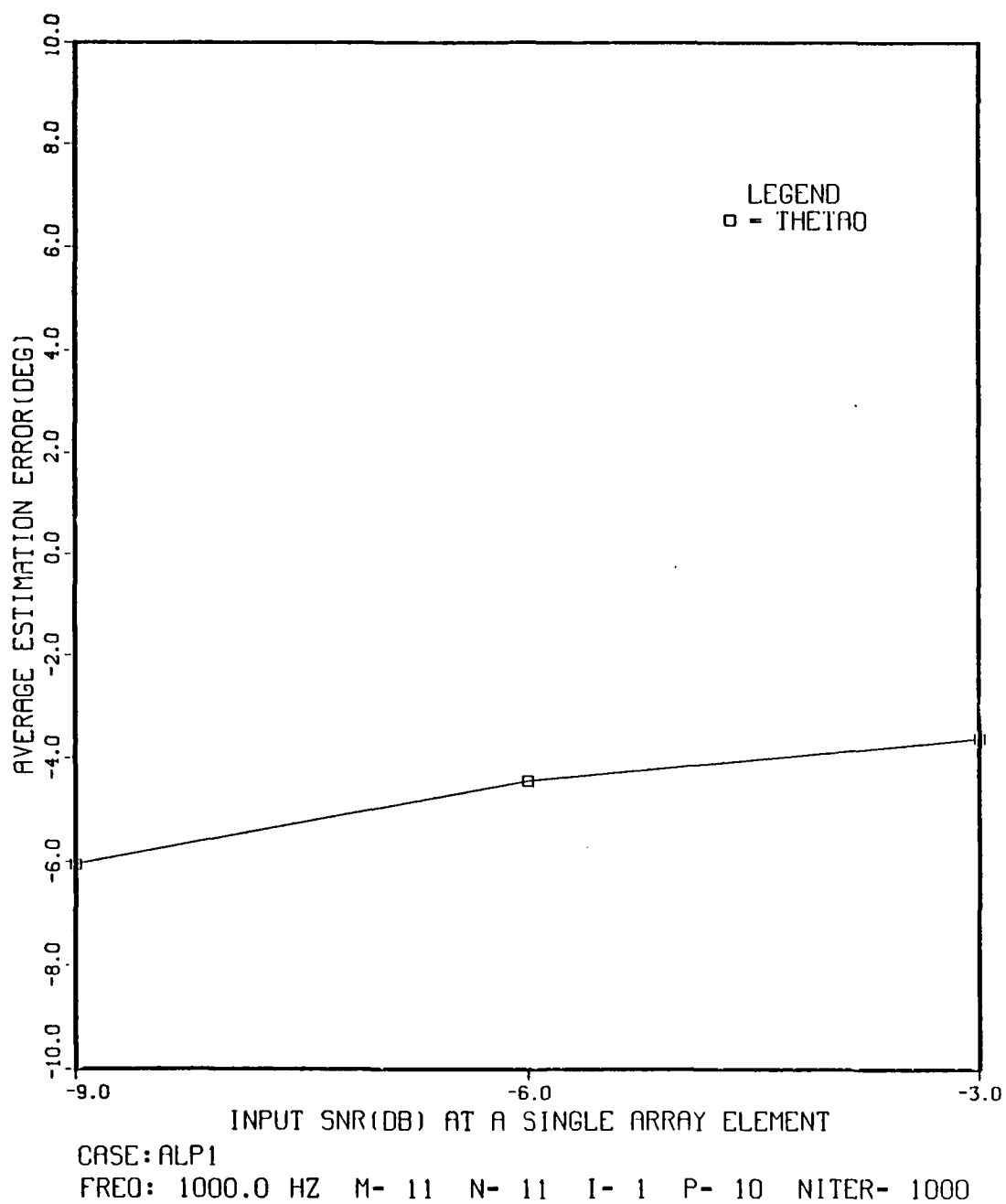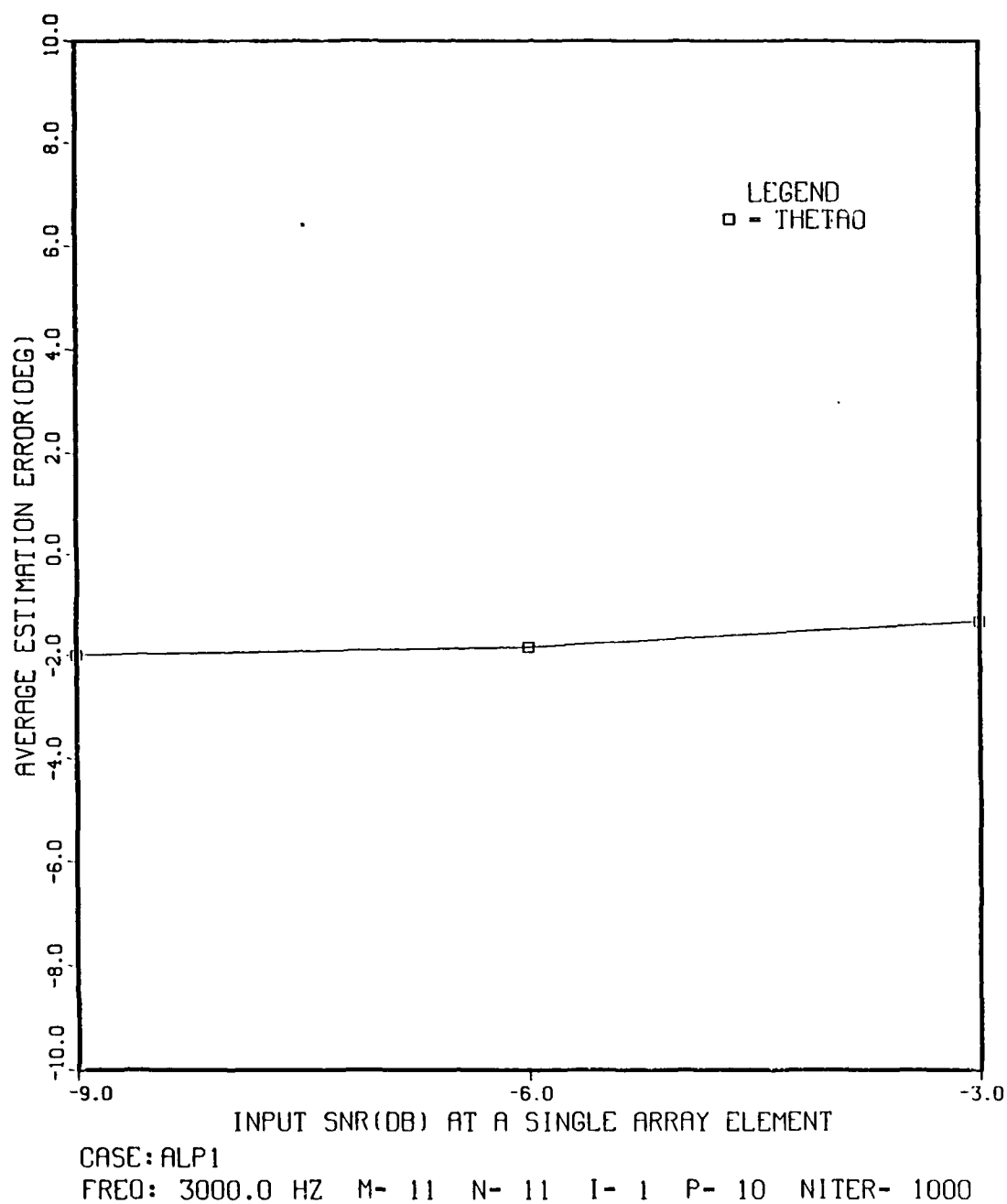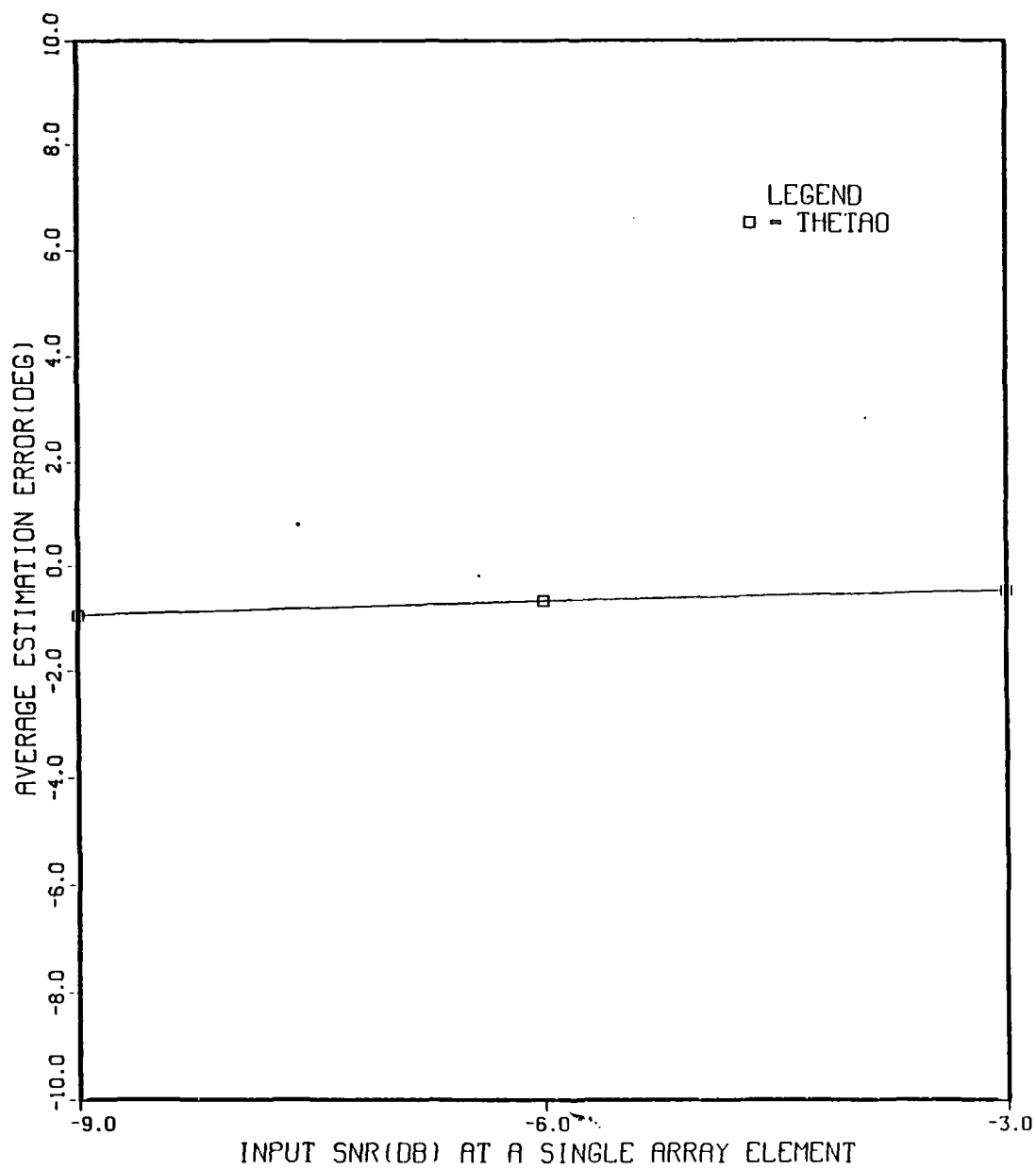Figure 17.  Average Estimation Error of Depression Angle vs. SNR at 1000 Hz for Case ALP1.

Figure 18.  Average Estimation Error of Depression Angle vs. SNR at 3000 Hz for Case ALP1.

**Figure 19.** Average Estimation Error of Depression Angle vs. SNR at 6000 Hz for Case ALP1.

## B. CASE 2

Case 2 placed three broadband targets at random locations. The general plane-wave field radiated by each of the targets contained two unique harmonics . Target 1 was located at ($\theta_0 = 49^o$, $\psi_0 = 38^o$) and radiated harmonics 1 and 6. Target 2 was located at ($\theta_0 = 5^o$, $\psi_0 = 137^o$) and radiated harmonics 2 and 5. Target 3 was located at ($\theta_0 = 77^o$, $\psi_0 = 307^o$) and radiated harmonics 3 and 4. Since there are three incident plane-wave fields, each containing two unique harmonics, the output electrical signal from each element in the array exhibits a total of six harmonics.

Figures 20 through 25 present the average estimation errors of the depression ($e_{\theta_0}$) and bearing ($e_{\psi_0}$) angles versus SNR for Case LMS2 for all the harmonics in increasing order of the harmonic number (q), respectively. The same trend about the SNR as in Case 1 holds here, that is increasing the SNR results in smaller magnitude of the average estimation error. These general results can be explained using the same arguments presented for Case 1.

Figures 26 through 43 present estimates of the direction cosines $U_0$ and $V_0$ for all the harmonics placed in increasing order of the harmonic number (q) at SNR's -3 dB, -6 dB and -9 dB, respectively. Again, the two trends observed in Case ALP1 are apparent here, that is, decreasing the SNR decreases the difference between the peak and the background noise and increasing the harmonic number (q) produces sharper peaks in the transfer function plots.

Figures 44 through 49 present the average estimation errors of the depression ($e_{\theta_0}$) and bearing ($e_{\psi_0}$) angles versus SNR for Case ALP2 for all the harmonics in increasing order of the harmonic number (q), respectively. The same trends as in LMS2 hold, with the exception that now the magnitude of the average estimation error for both angles is smaller than in LMS2 . Note the difference in scaling between the error plots for Case LMS2 and Case ALP2.

Finally, Tables 3 and 4 in the Appendix A present the numerical data for Cases LMS2 and ALP2, respectively, for all six harmonics. Comparing the two algorithms using these tables, we can conclude that for Case 2, the ALP algorithm gives smaller magnitude estimation errors in most instances than the LMS algorithm especially for low SNR.
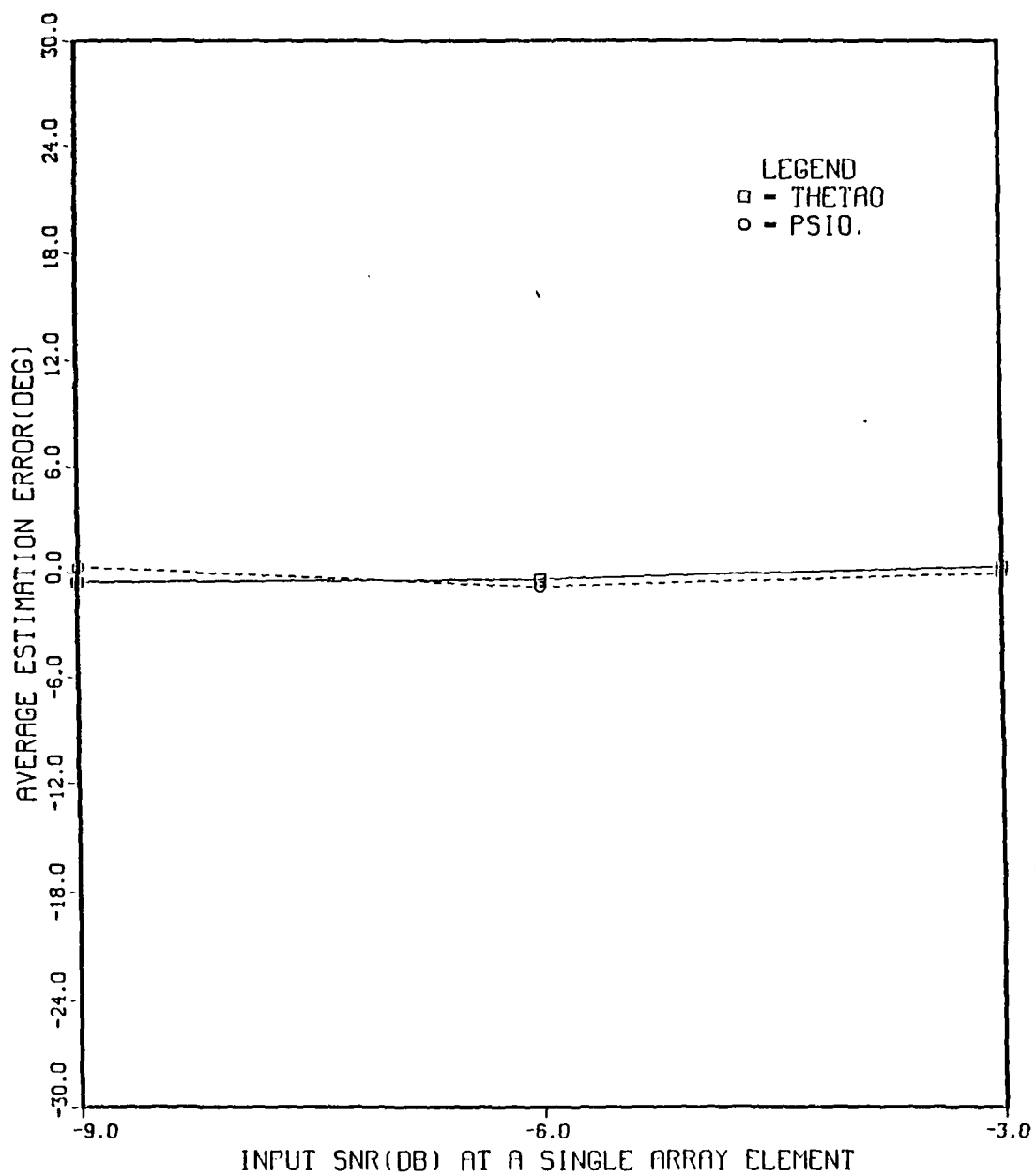
Figure 20.    Average Estimation Errors of Depression and Bearing Angles vs. SNR
             at 1000 Hz for Case LMS2.

44
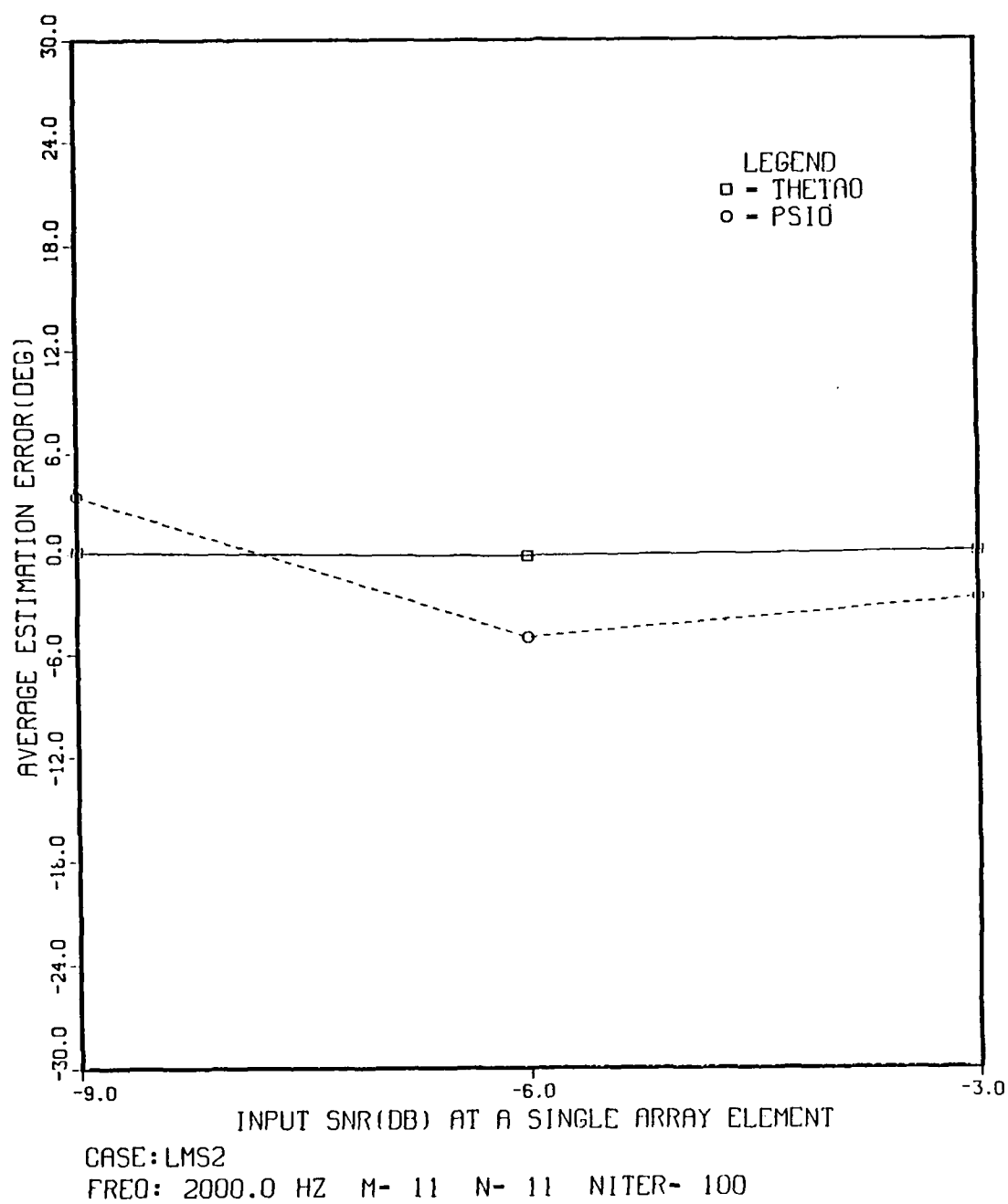
Figure 21.  Average Estimation Errors of Depression and Bearing Angles vs. SNR at 2000 Hz for Case LMS2.

45
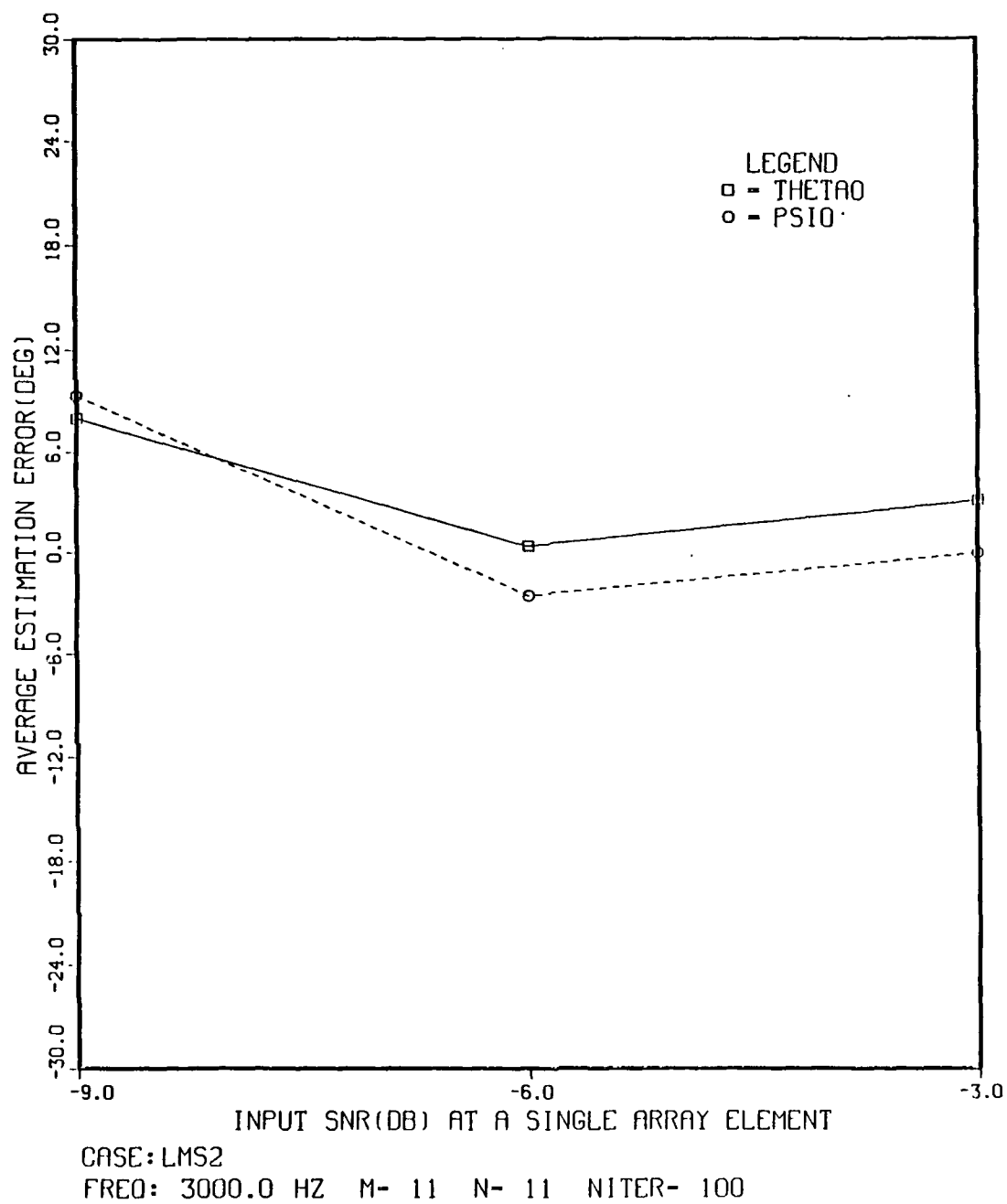
Figure 22.   Average Estimation Errors of Depression and Bearing Angles vs. SNR
at 3000 Hz for Case LMS2.
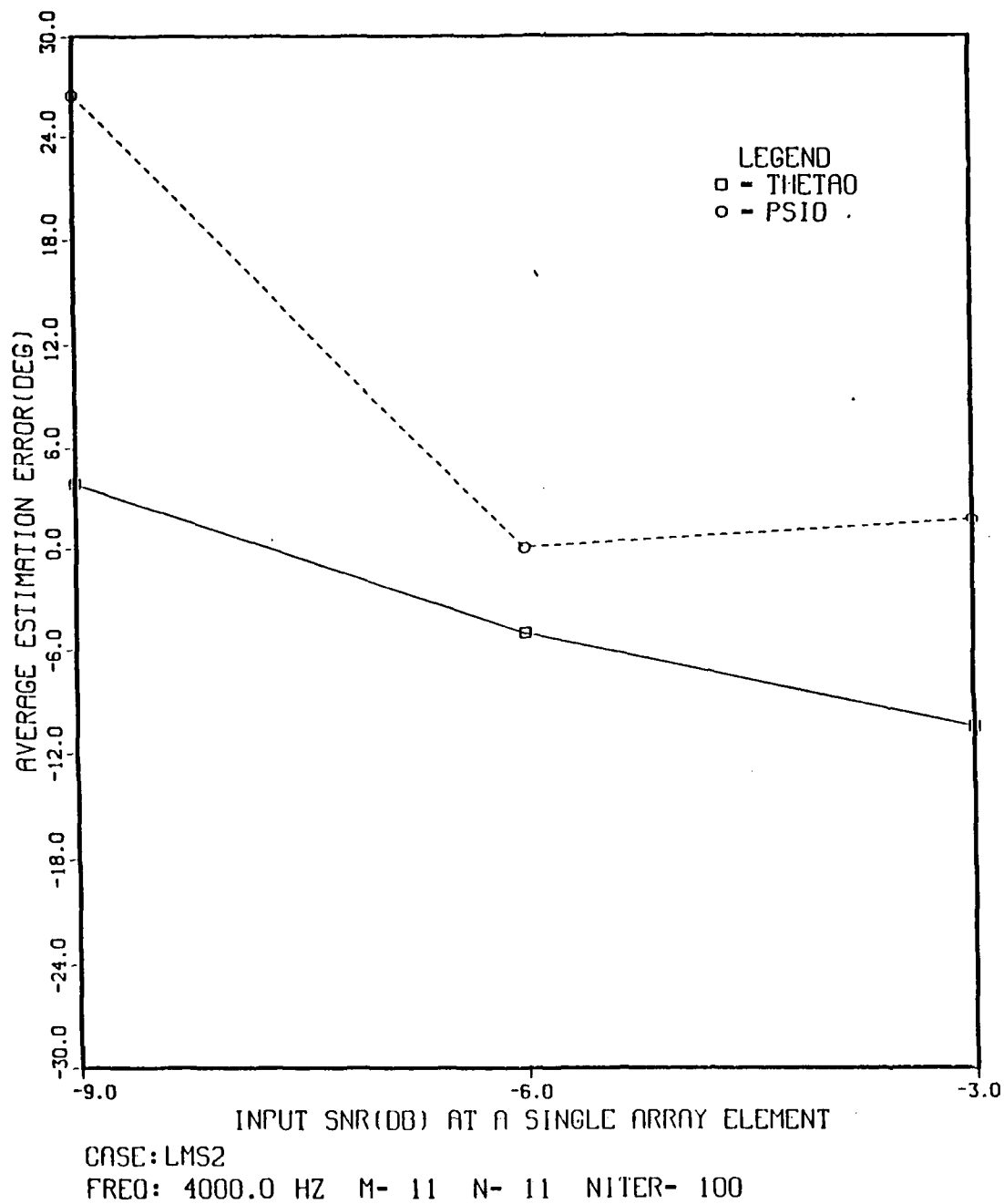
Figure 23.    Average Estimation Errors of Depression and Bearing Angles vs. SNR
at 4000 Hz for Case LMS2.

47
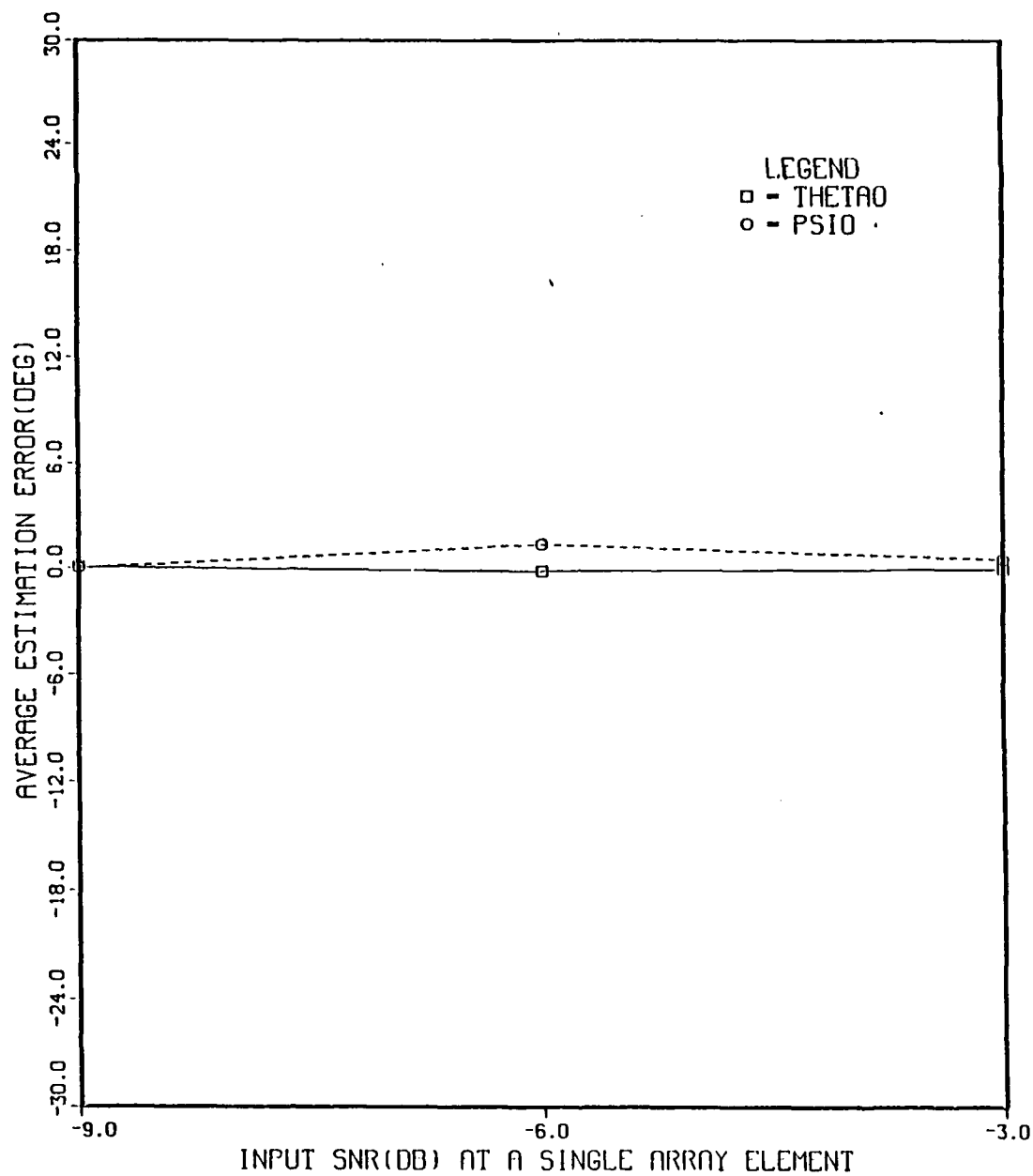
**Figure 24.** Average Estimation Errors of Depression and Bearing Angles vs. SNR at 5000 Hz for Case LMS2.
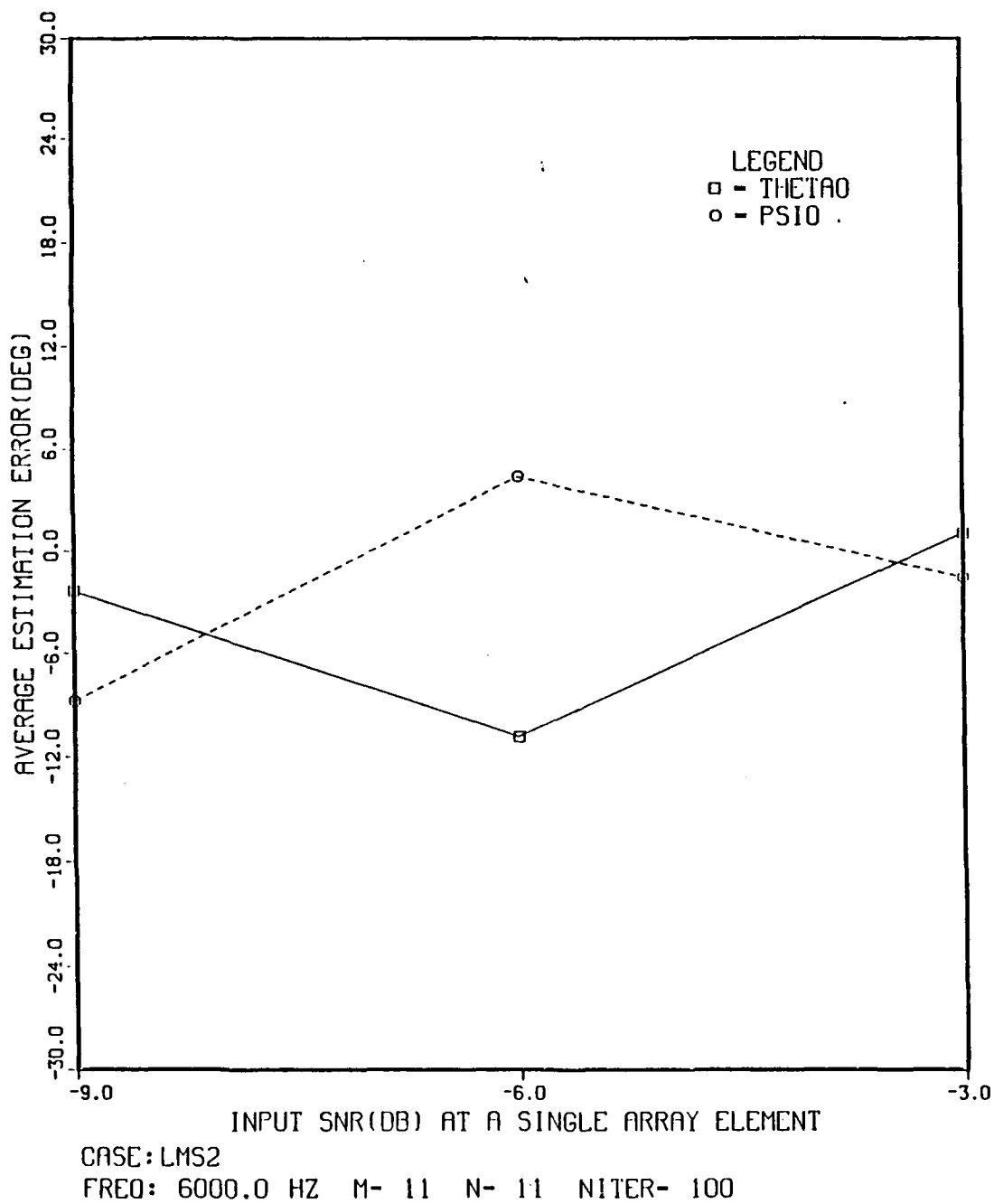
Figure 25.  Average Estimation Errors of Depression and Bearing Angles vs. SNR
at 6000 Hz for Case LMS2.

49
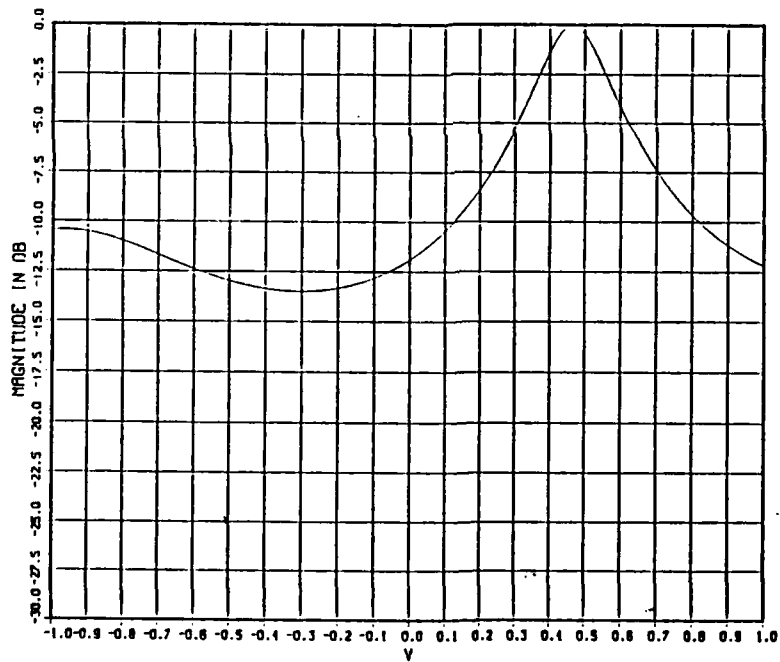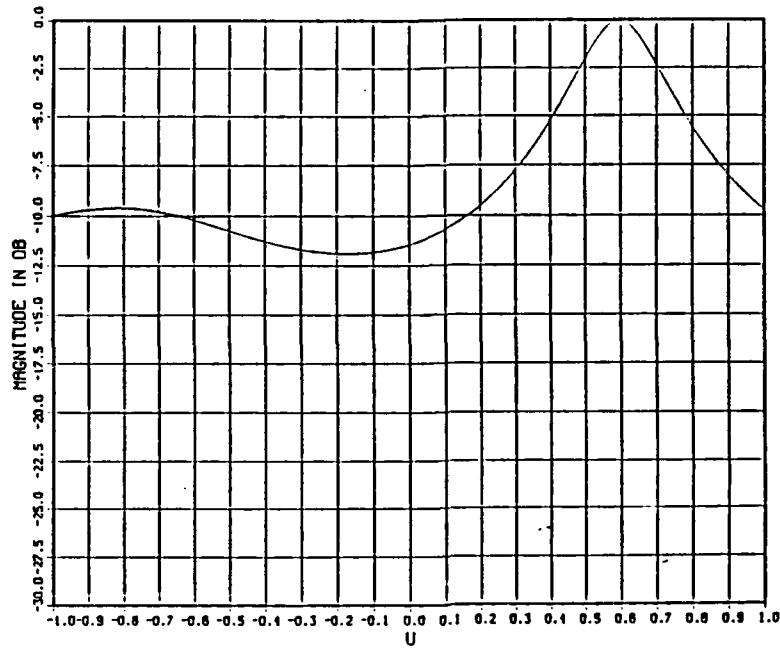
Figure 26. Estimates of Direction Cosines U0 and V0, Case ALP2: SNR = -3dB and q = 1
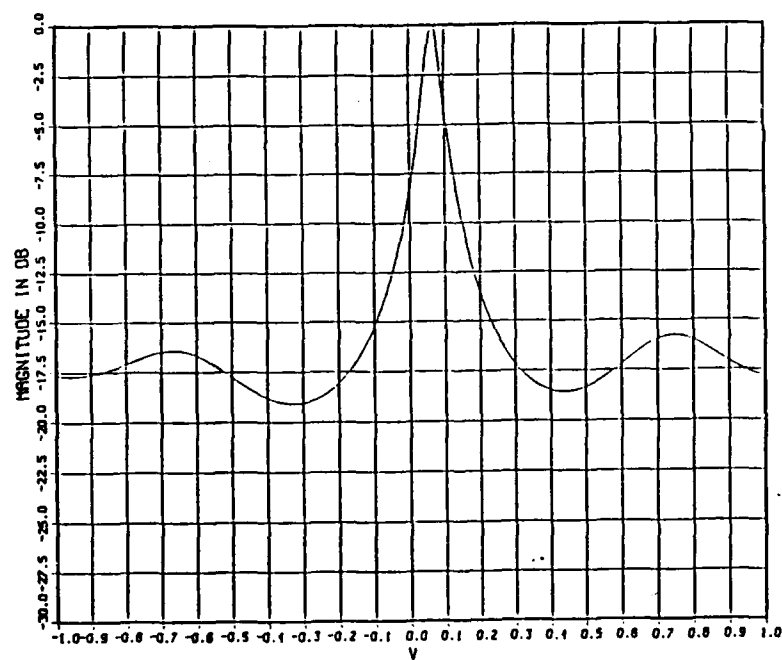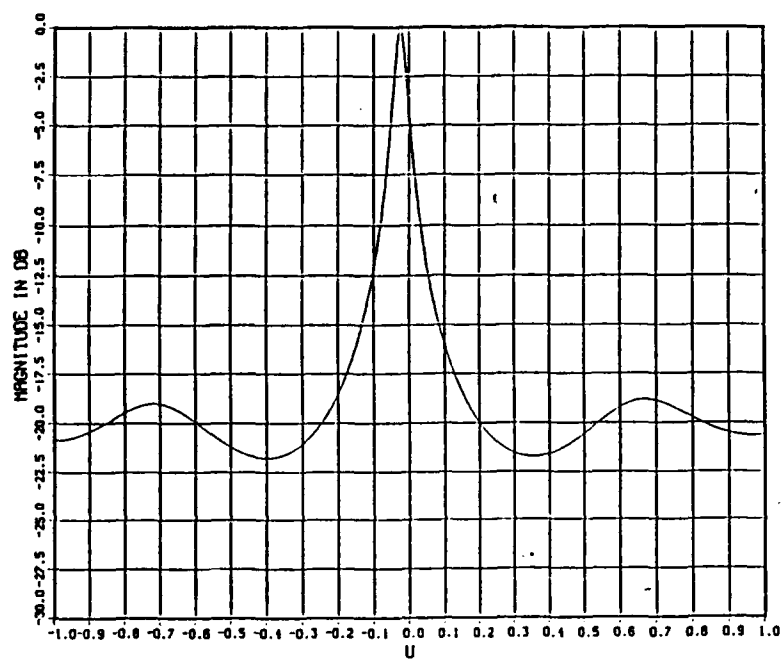
CASE: ALP2    SNR= -3.0 DB
FREO: 2000.0 HZ    M- 11    N- 11    I- 1    P- 10    NITER- 1000

Figure 27.    Estimates of Direction Cosines U0 and V0, Case ALP2: SNR = -3dB and
q = 2

51

CASE: ALP2    SNR- -3.0 DB
FREQ: 3000.0 HZ    M- 11    N- 11    I- 1    P- 10    NITER- 1000

Figure 28.    Estimates of Direction Cosines U0 and V0, Case ALP2: SNR = -3dB and
q = 3

CASE:ALP2    SNR- -3.0 DB
FREO: 4000.0 HZ    M- 11    N- 11    I- 1    P- 10    NITER- 1000

Figure 29.    Estimates of Direction Cosines U0 and V0, Case ALP2: SNR = -3dB and
q = 4

53

Figure 30.  Estimates of Direction Cosines U0 and V0, Case ALP2: SNR = -3dB and q = 5

CASE:ALP2    SNR- -3.0 DB
FREO: 6000.0 HZ    M- 11    N- 11    I- 1    P- 10    NITER- 1000

Figure 31.    Estimates of Direction Cosines U0 and V0, Case ALP2: SNR = -3dB and
q = 6

55

CASE:ALP2    SNR- -6.0 DB
FREQ: 1000.0 HZ    M- 11    N- 11    I- 1    P- 10    NITER- IC00

**Figure 32.    Estimates of Direction Cosines U0 and V0, Case ALP2: SNR = -6dB and q = 1**

56

Figure 33. Estimates of Direction Cosines U0 and V0, Case ALP2: SNR = -6dB and q = 2

57

CASE: ALP2    SNR= -6.0 DB
FREQ: 3000.0 HZ    M- 11    N- 11    I- 1    P- 10    NITER- 1000

Figure 34.    Estimates of Direction Cosines U0 and V0, Case ALP2: SNR = -6dB and
q = 3

58

CASE:ALP2    SNR- -6.0 DB
FREO: 4000.0 HZ    M- 11    N- 11    I- 1    P- 10    NITER- 1000

**Figure 35.    Estimates of Direction Cosines U0 and V0, Case ALP2: SNR = -6dB and**
**q = 4**

Figure 36. Estimates of Direction Cosines U0 and V0, Case ALP2: SNR = -6dB and q = 5

Figure 37. Estimates of Direction Cosines U0 and V0, Case ALP2: SNR = -6dB and q = 6

CASE:ALP2    SNR- -9.0 DB
FREQ: 1000.0 HZ    M- 11    N- 11    I- 1    P- 10    NITER- 1000

**Figure 38.    Estimates of Direction Cosines U0 and V0, Case ALP2: SNR = -9dB and**
$q = 1$

62

CASE:ALP2    SNR= -9.0 DB
FREO: 2000.0 HZ    M- 11    N- 11    I- 1    P- 10    NITER- 1000

Figure 39.    Estimates of Direction Cosines U0 and V0, Case ALP2: SNR = -9dB and

q = 2

63

CASE:ALP2     SNR- -9.0 DB
FREO: 3000.0 HZ     M- 11    N- 11    I- 1    P- 10    NITER- 1000

Figure 40.    Estimates of Direction Cosines U0 and V0, Case ALP2: SNR = -9dB and
q = 3

64

CASE: ALP2    SNR- -9.0 DB
FREQ: 1000.0 HZ    M- 11    N- 11    I- 1    P- 10    NITER- 1000

Figure 41.   Estimates of Direction Cosines U0 and V0, Case ALP2: SNR = -9dB and
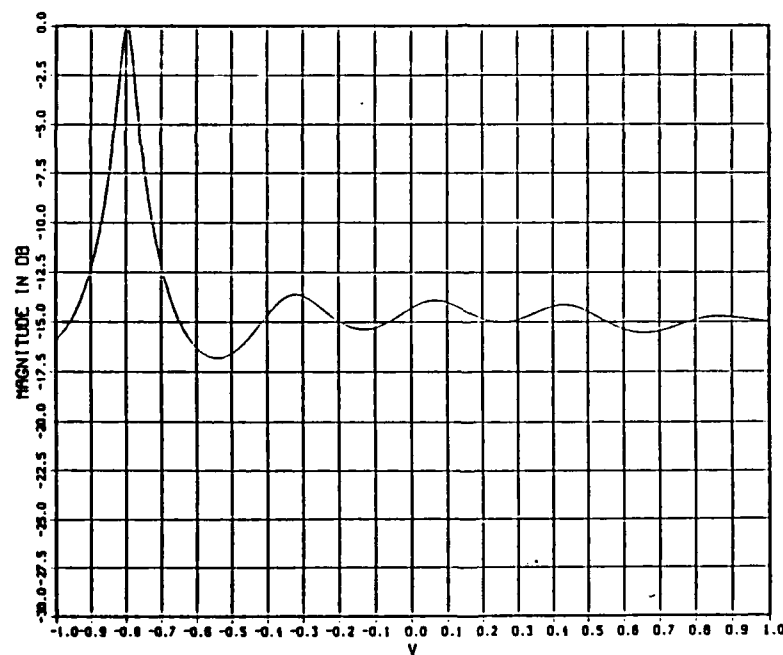q = 4

CASE:ALP2     SNR- -9.0 DB
FREQ: 5000.0 HZ     H- 11     N- 11     I- 1     P- 10     NITER- 1000

Figure 42.     Estimates of Direction Cosines U0 and V0, Case ALP2: SNR = -9dB and q = 5

66
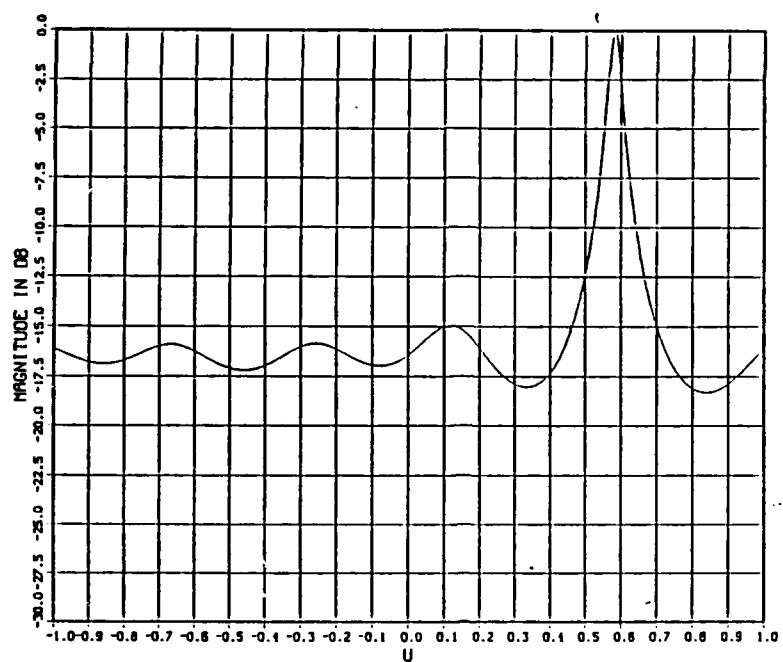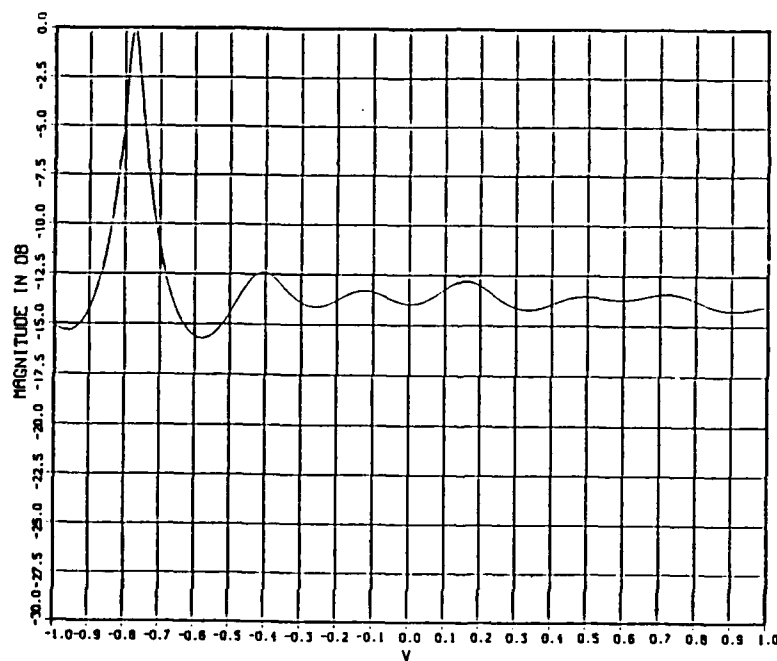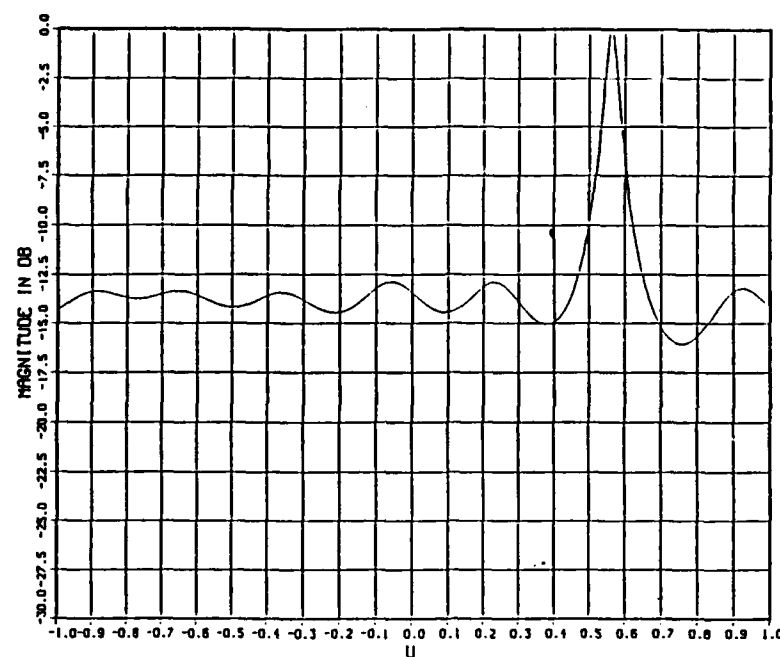
CASE:ALP2     SNR- -9.0 DB
FREO: 6000.0 HZ     M- 11     N- 11     I- 1     P- 10     NITER- 1000

Figure 43.     Estimates of Direction Cosines U0 and V0, Case ALP2: SNR = -9dB and q = 6

67
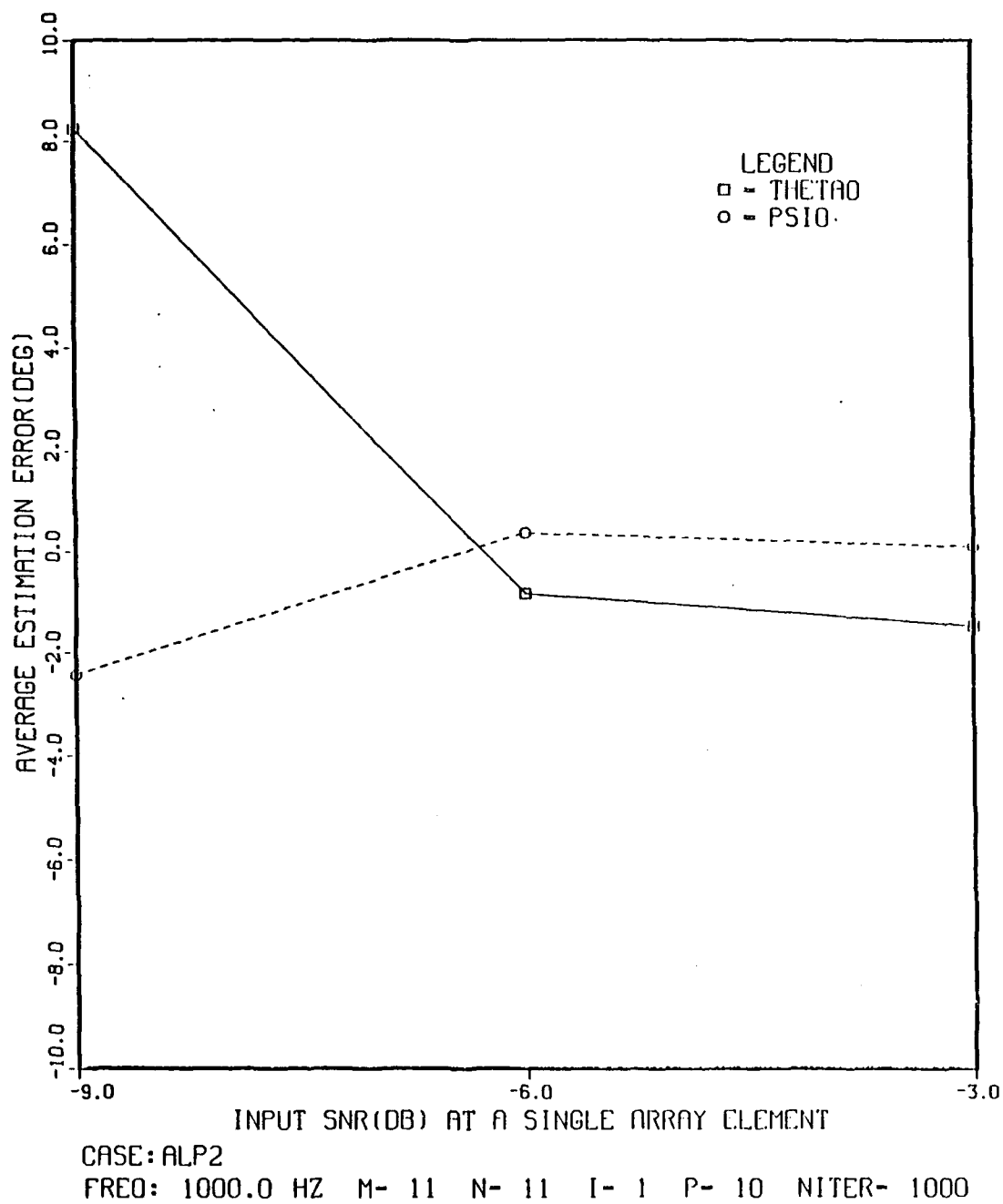
Figure 44.   Average Estimation Errors of Depression and Bearing Angles vs. SNR
at 1000 Hz for Case ALP2.
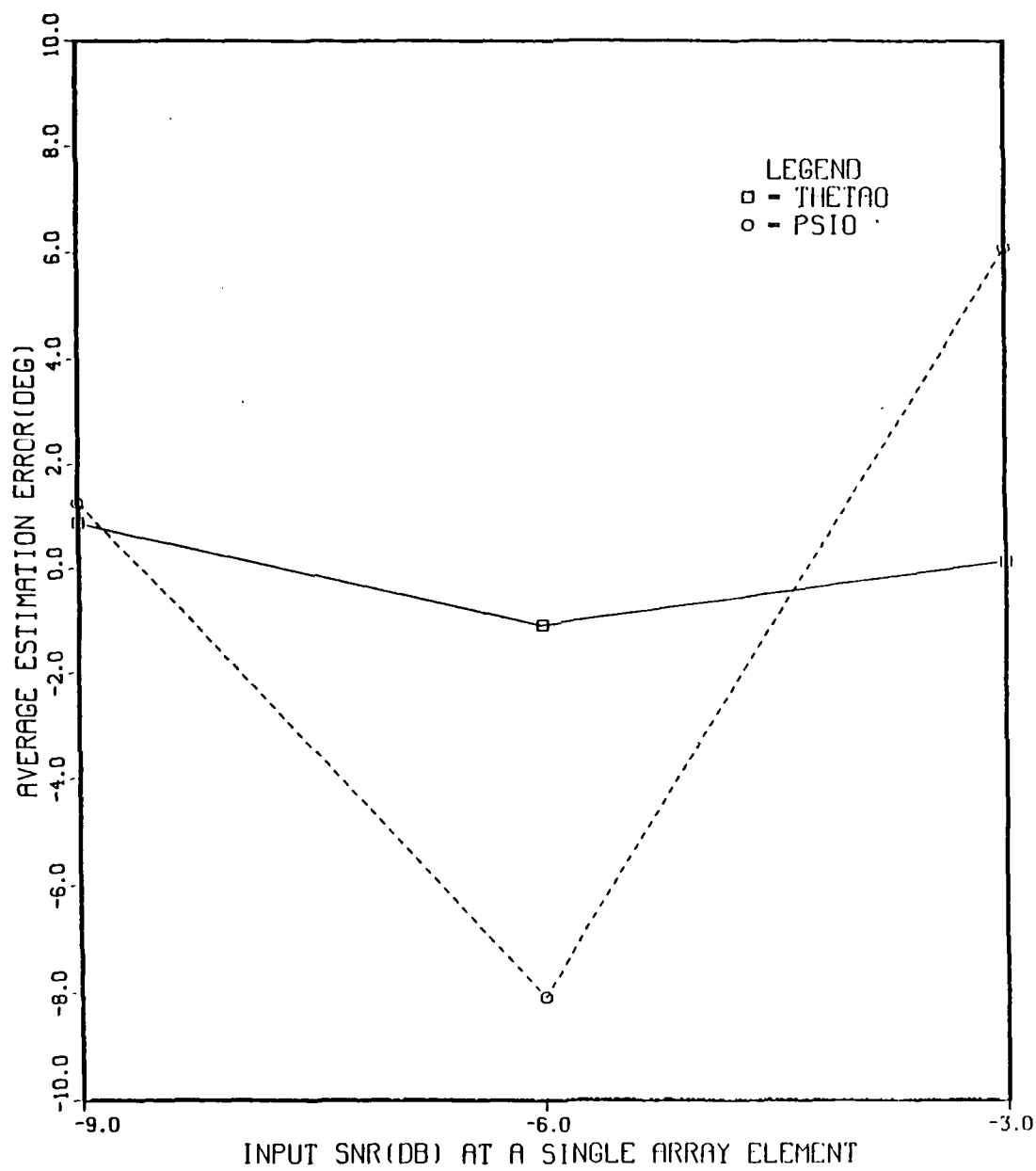
Figure 45.    Average Estimation Errors of Depression and Bearing Angles vs. SNR
at 2000 Hz for Case ALP2.
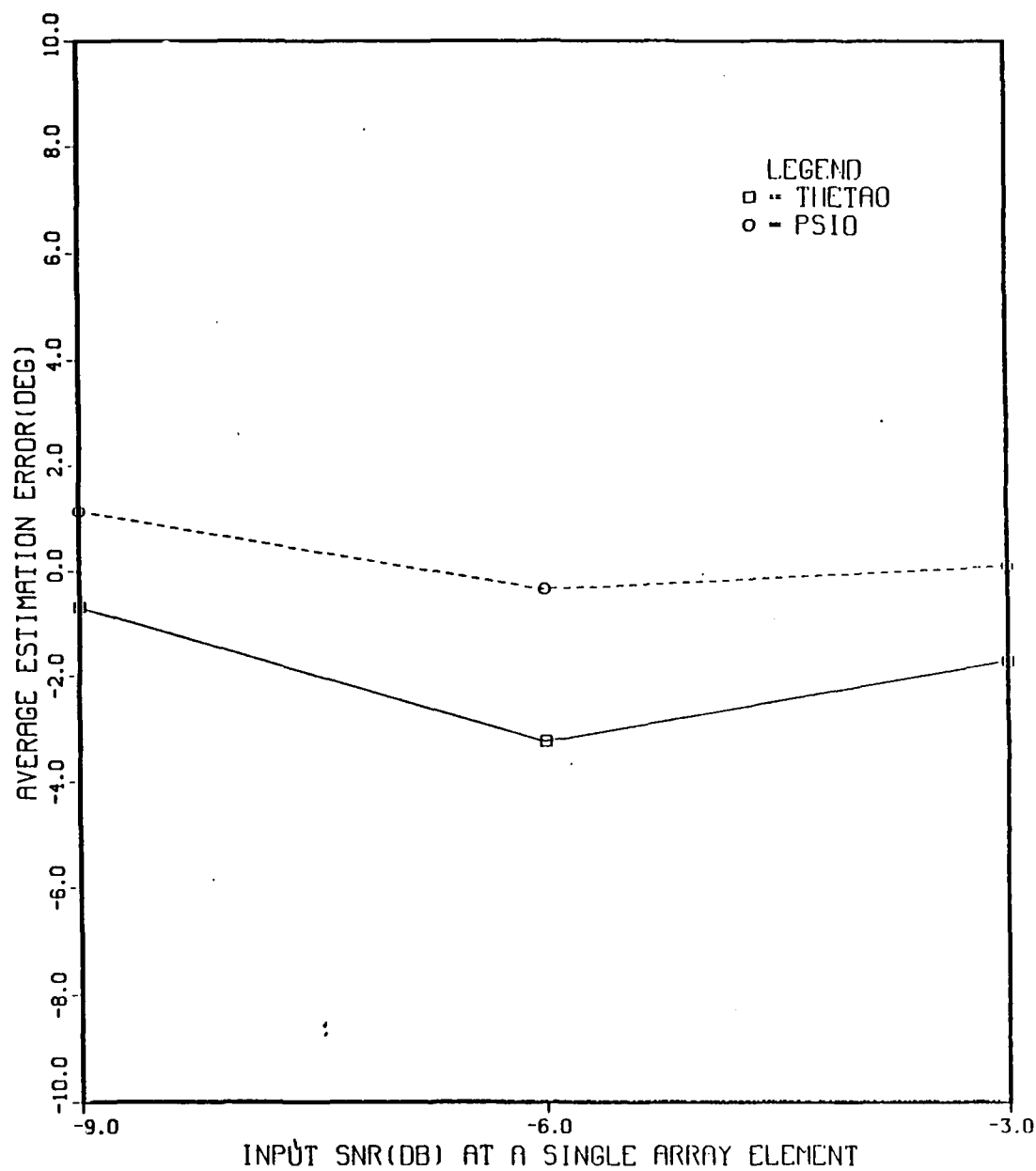
**Figure 46.** Average Estimation Errors of Depression and Bearing Angles vs. SNR at 3000 Hz for Case ALP2.
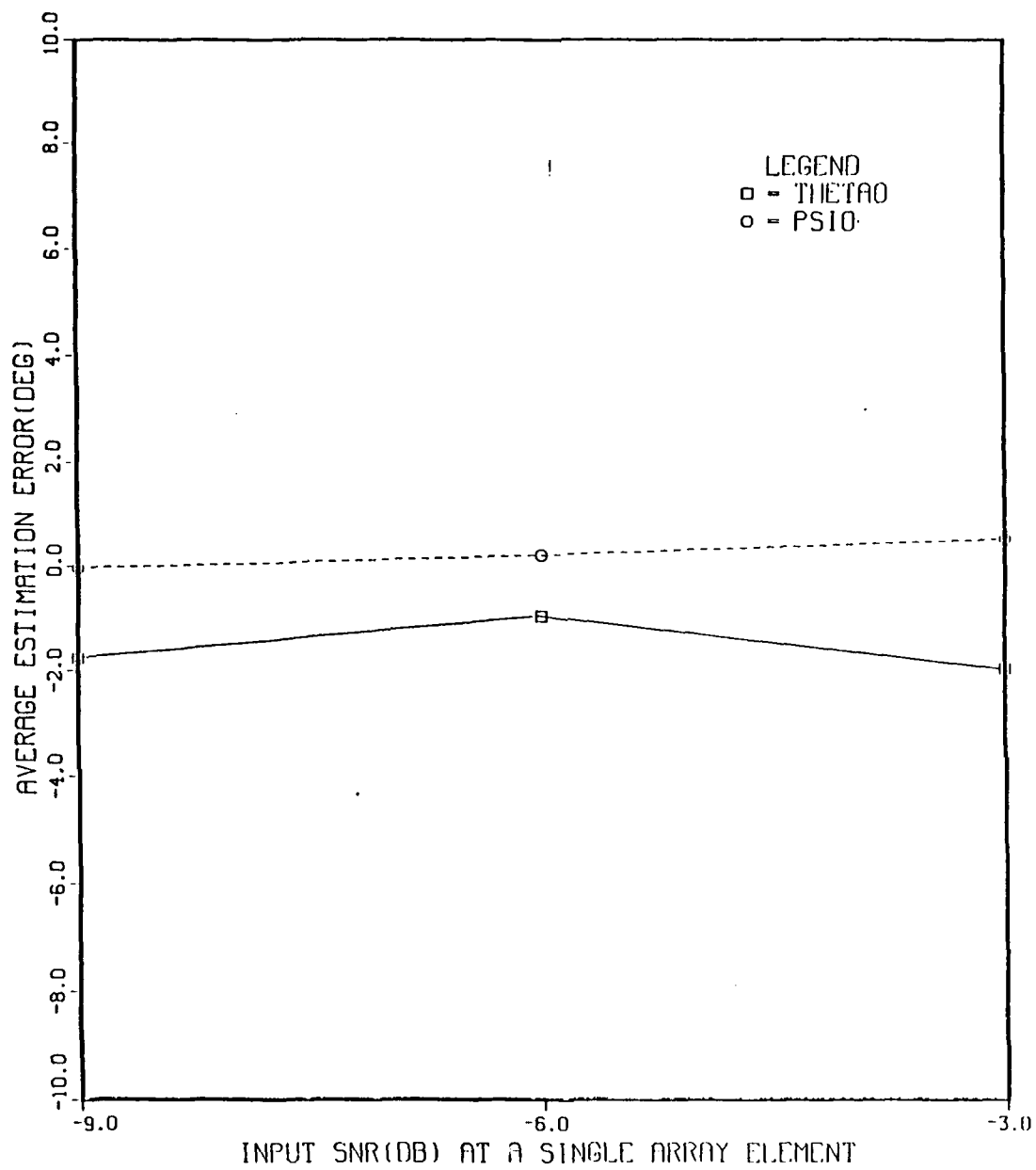
70

Figure 47.    Average Estimation Errors of Depression and Bearing Angles vs. SNR
at 4000 Hz for Case ALP2.
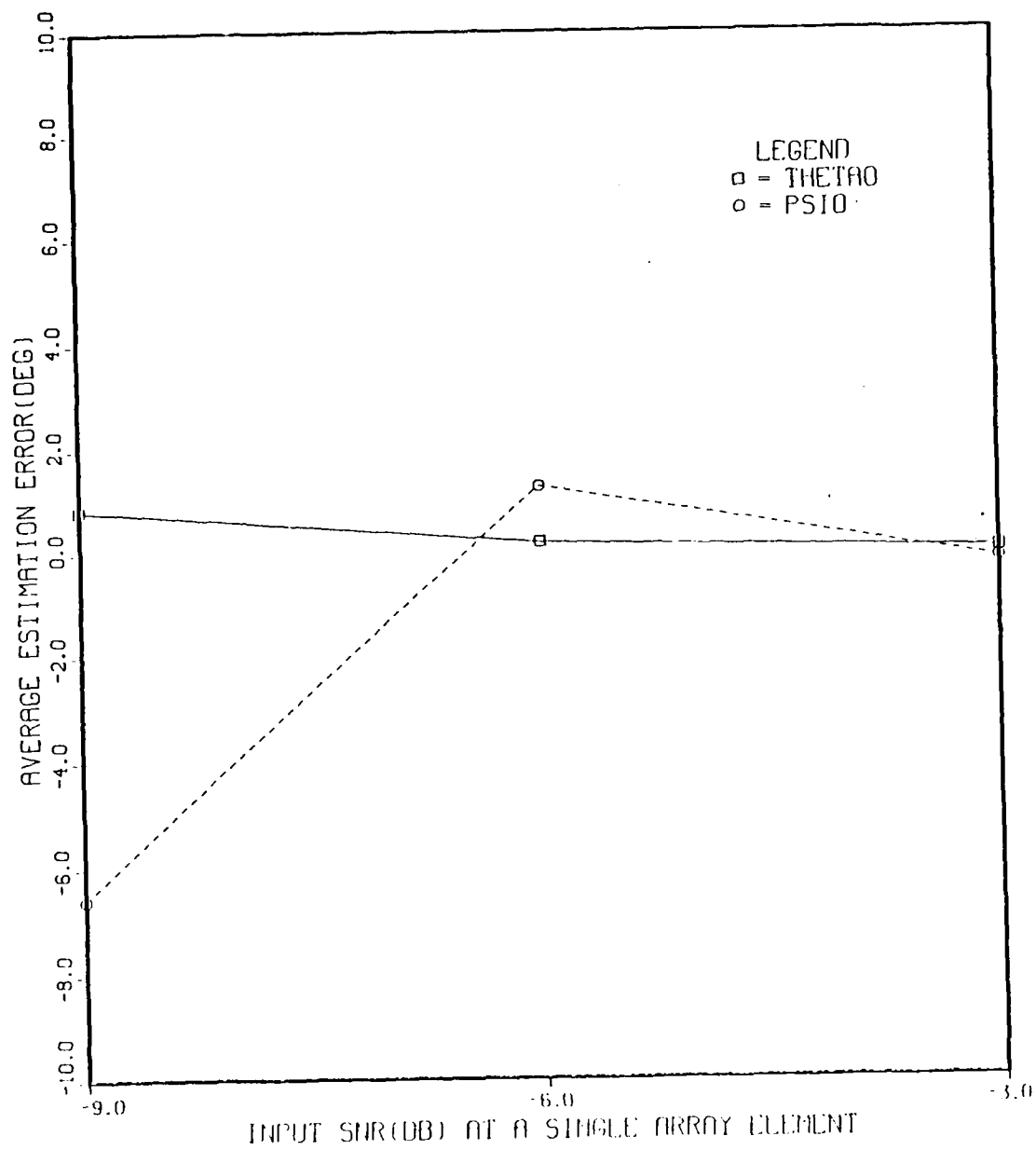
Figure 48.  Average Estimation Errors of Depression and Bearing Angles vs. SNR
at 5000 Hz for Case ALP2.
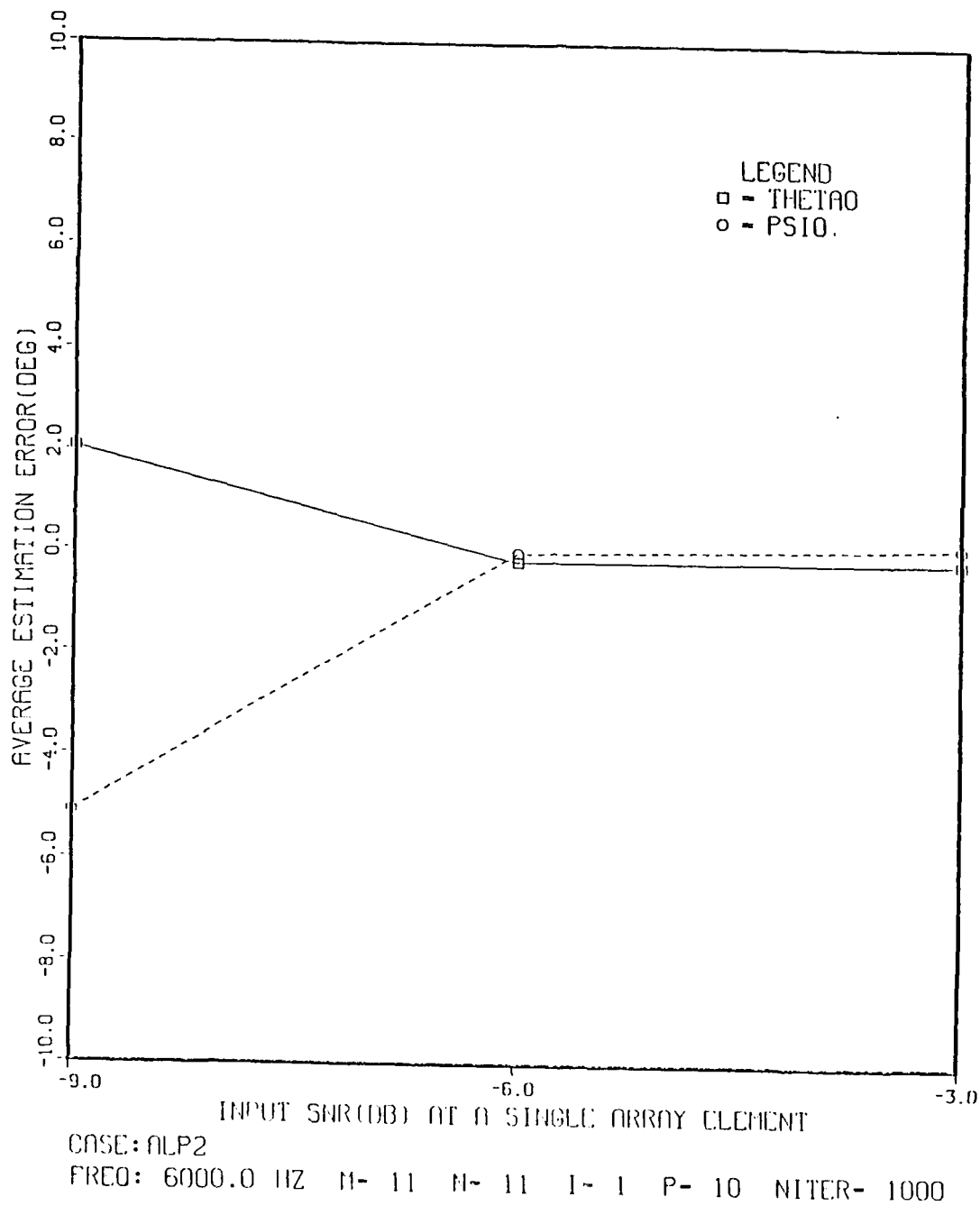
Figure 49.    Average Estimation Errors of Depression and Bearing Angles vs. SNR at 6000 Hz for Case ALP2.

## C. CASE 3

Case 3 placed a single broadband target at endfire relative to the planar array (i.e., $\theta_0 = 90^\circ$, $\psi_0 = 90^\circ$). This case was considered the most difficult for both algorithms since it is at endfire that the far-field beam pattern beamwidth is broadest [Ref. 4]. The general plane-wave field radiated by the target consisted of six harmonics.

Figures 50 and 51 present the average estimation errors of the depression ($e_{\theta_0}$) and bearing ($e_{\psi_0}$) angles versus SNR for Case LMS3 at 1000 Hz and 3000 Hz, respectively. The estimation errors for the highest harmonic (6000 Hz) are not shown for Case LMS3 since the magnitude of these errors were between 45 and 90 degrees. This poor performance for the highest harmonic at endfire can be explained theoretically [Ref. 6].

Figures 52, 53, and 54 present estimates of the direction cosines $U_0$ and $V_0$ for Case ALP3 at SNR = -3 dB and frequencies 1000 Hz, 3000 Hz, and 6000 Hz, respectively. Similarly, Figures 55, 56, and 57, and 58, 59, and 60 present estimates of the direction cosines $U_0$ and $V_0$ for Case ALP3 with the same order of frequency as above and SNR = -6 dB and SNR = -9 dB, respectively. Here we can observe an ambiguity for the $V_0$ estimates at 6000 Hz which can be explained by examining the exponential term of Eq.(2-79). This term for the highest frequency component creates integer multiplies of $2\pi$ producing two peaks at $\pm 1$ for the $V_0$ estimates at 6000 Hz.

Figures 61, 62 and 63 present the average estimation errors of the depression ($e_{\theta_0}$) and bearing ($e_{\psi_0}$) angles versus SNR for Case ALP3 at 1000 Hz, 3000 Hz, and 6000 Hz, respectively. We can observe that in Case ALP3 at 6000 Hz we have acceptable estimates for depression angle ($\theta_c$). In Figure 63 the $\psi_0$ error plot is not shown since the magnitude of this error was between 45 and 90 degrees.

Finally, Tables 5 and 6 in Appendix A present the numerical data for Cases LMS3 and ALP3 respectively for all six harmonics. Comparing the two algorithms using these tables, we can conclude that for Case 3 the ALP algorithm gives smaller magnitude estimation errors in most instances than the LMS algorithm for both angles.
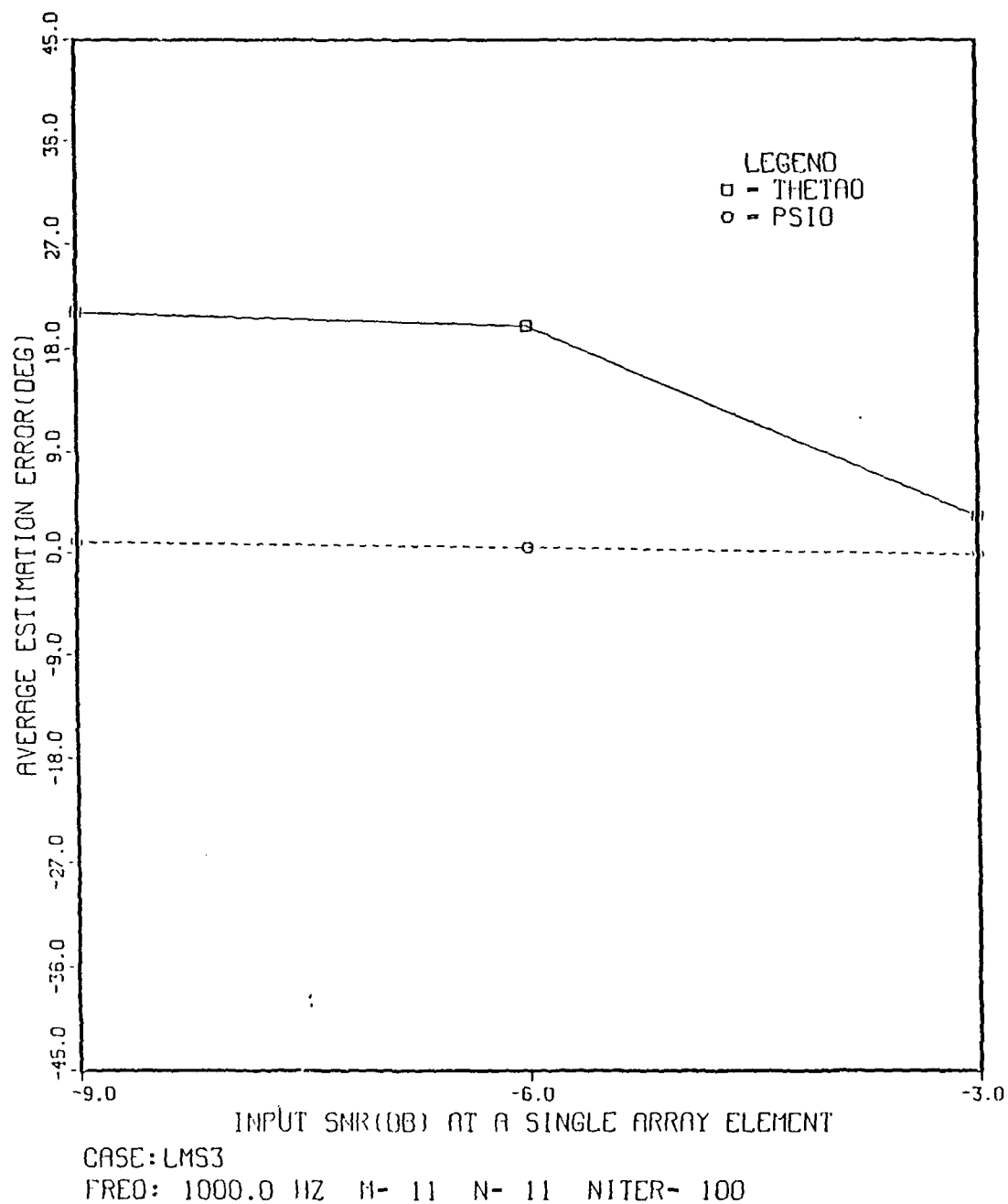
Figure 50. Average Estimation Errors of Depression and Bearing Angles vs. SNR at 1000 Hz for Case LMS3.

75
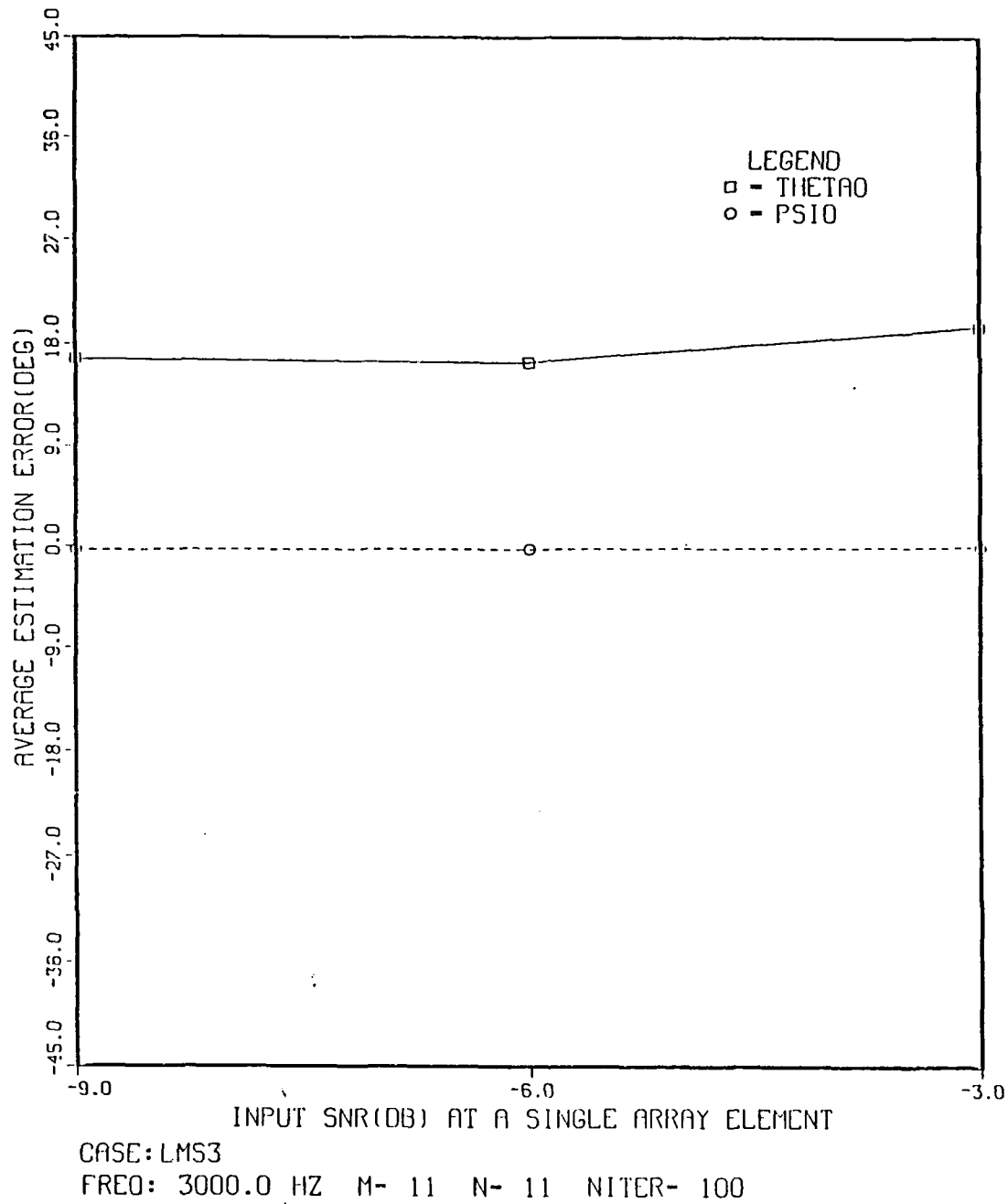
Figure 51. Average Estimation Errors of Depression and Bearing Angles vs. SNR at 3000 Hz for Case LMS3.
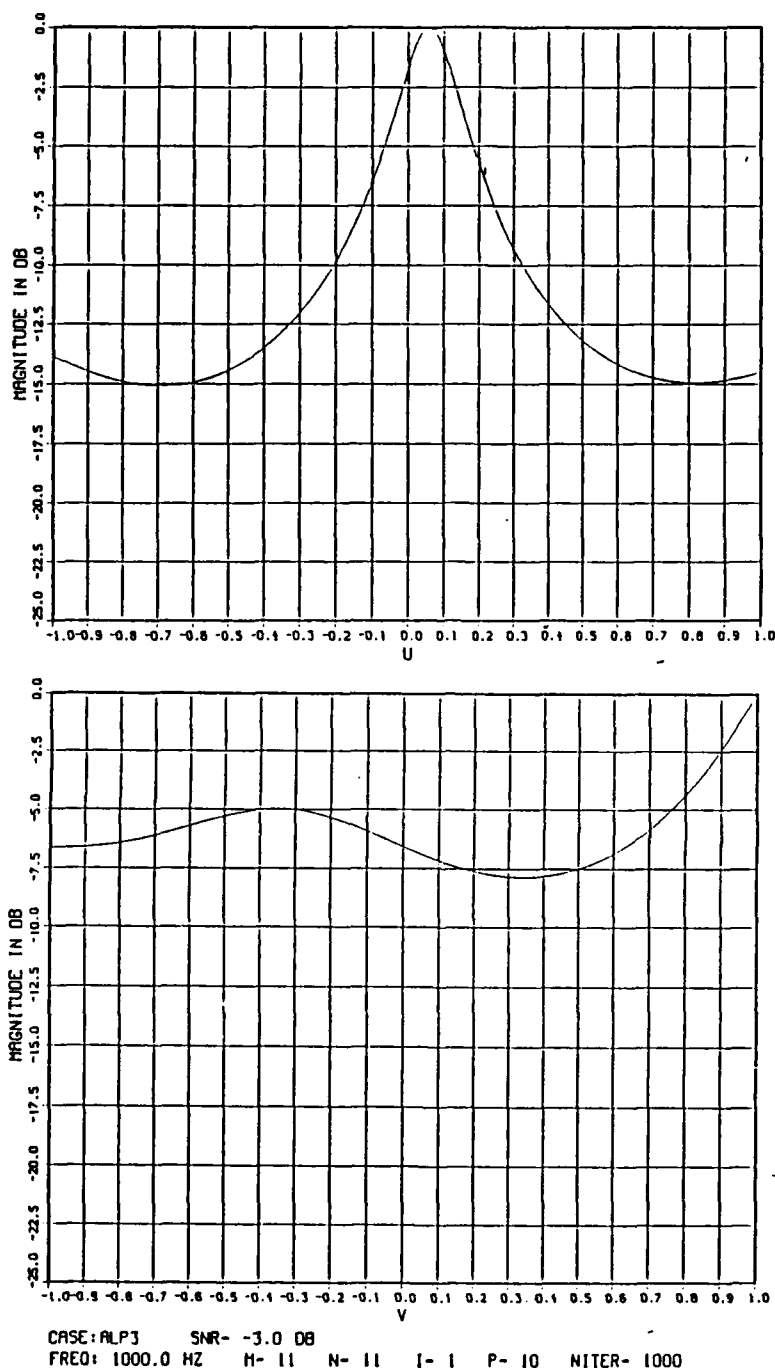
Figure 52. Estimates of Direction Cosines U0 and V0, Case ALP3: SNR = -3dB and q = 1

77

CASE:ALP3    SNR- -3.0 DB
FREQ: 3000.0 HZ    M- 11    N- 11    I- 1    P- 10    NITER- 1000
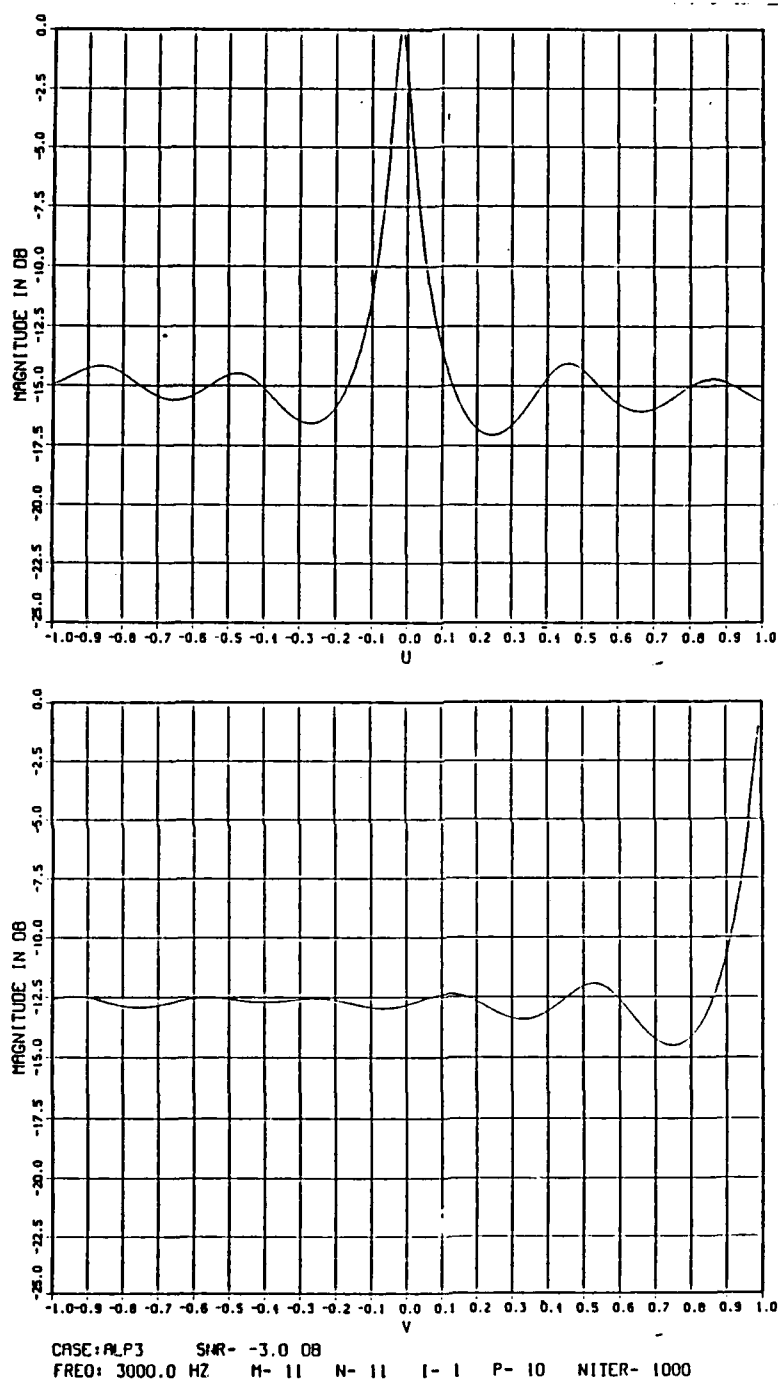
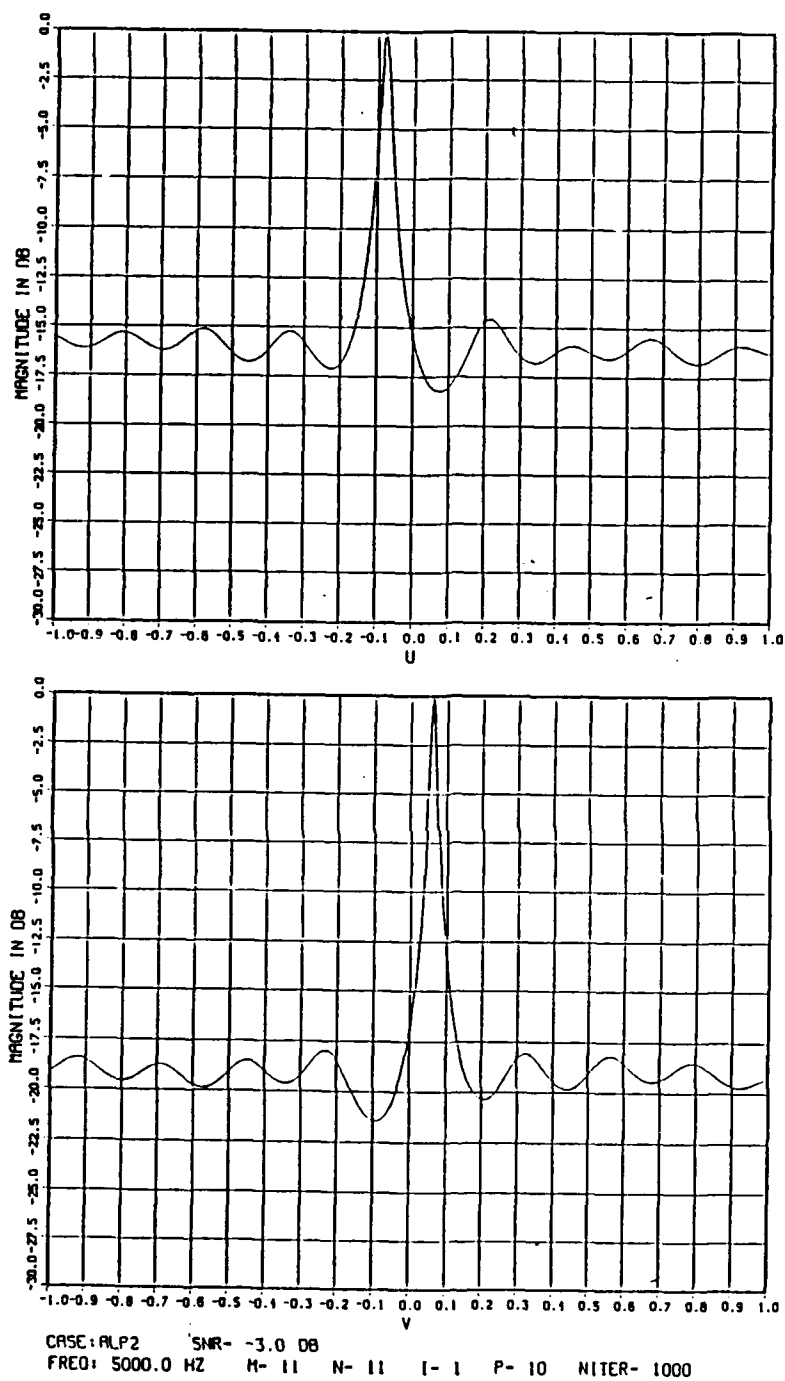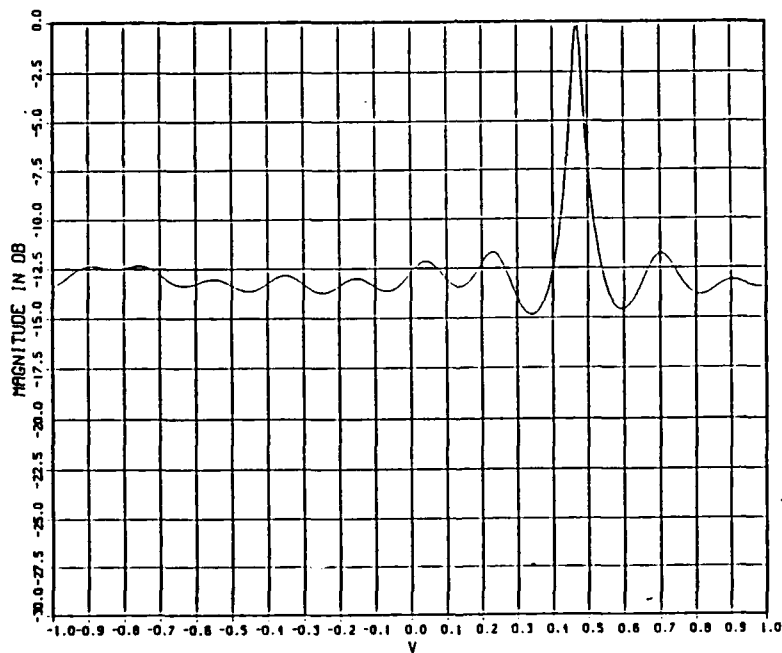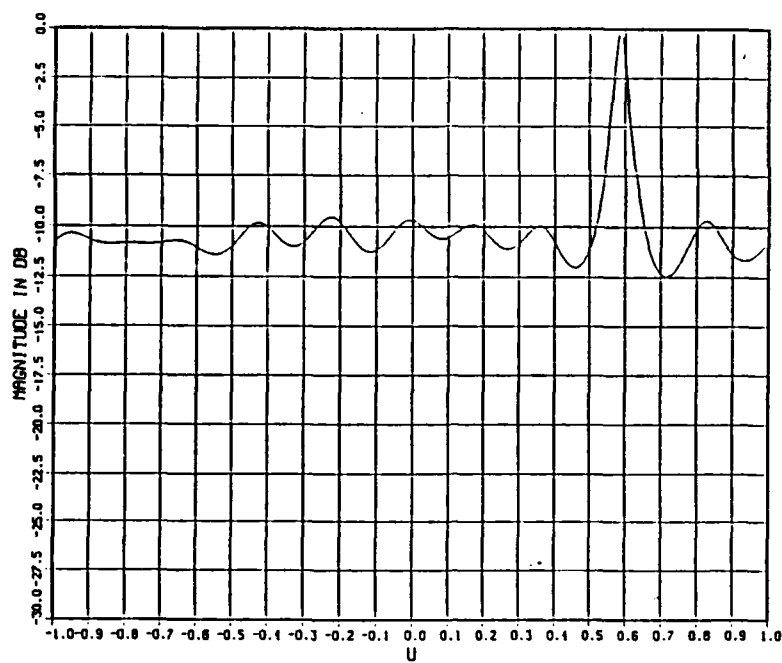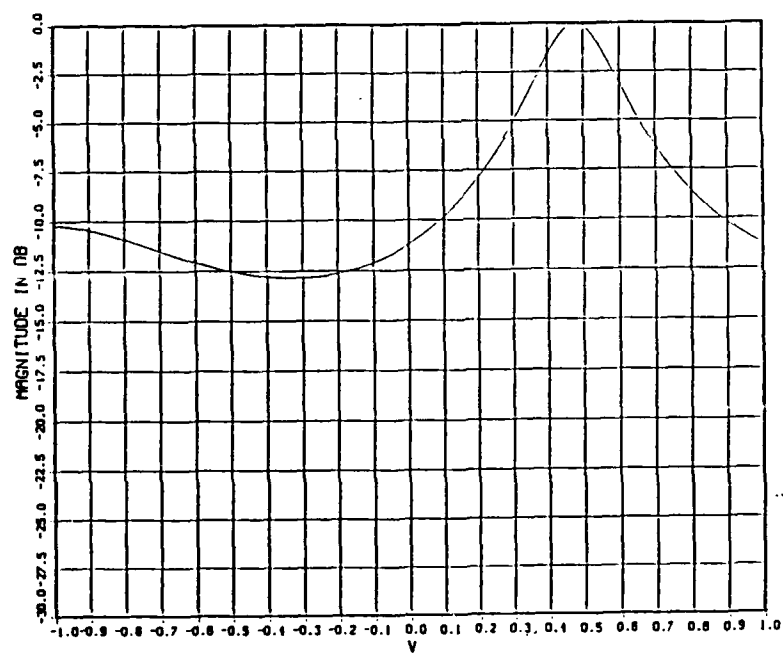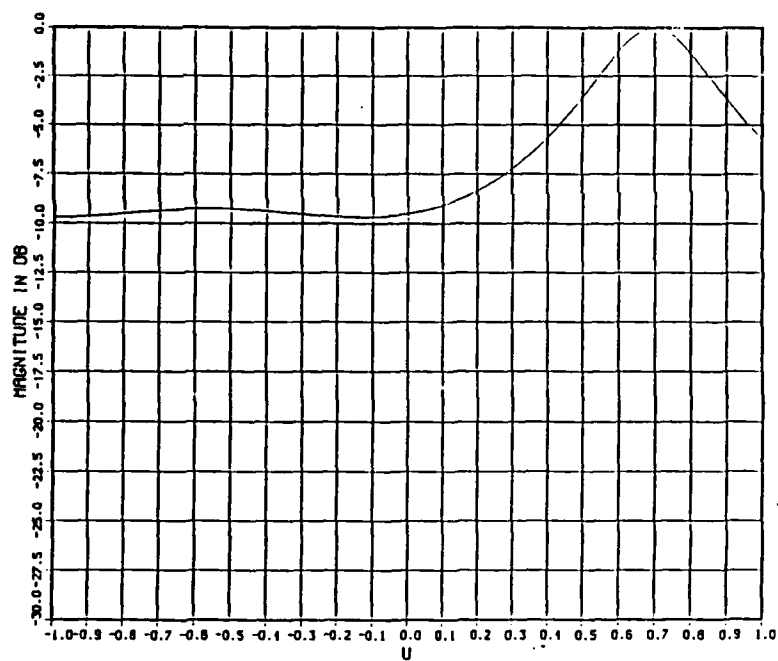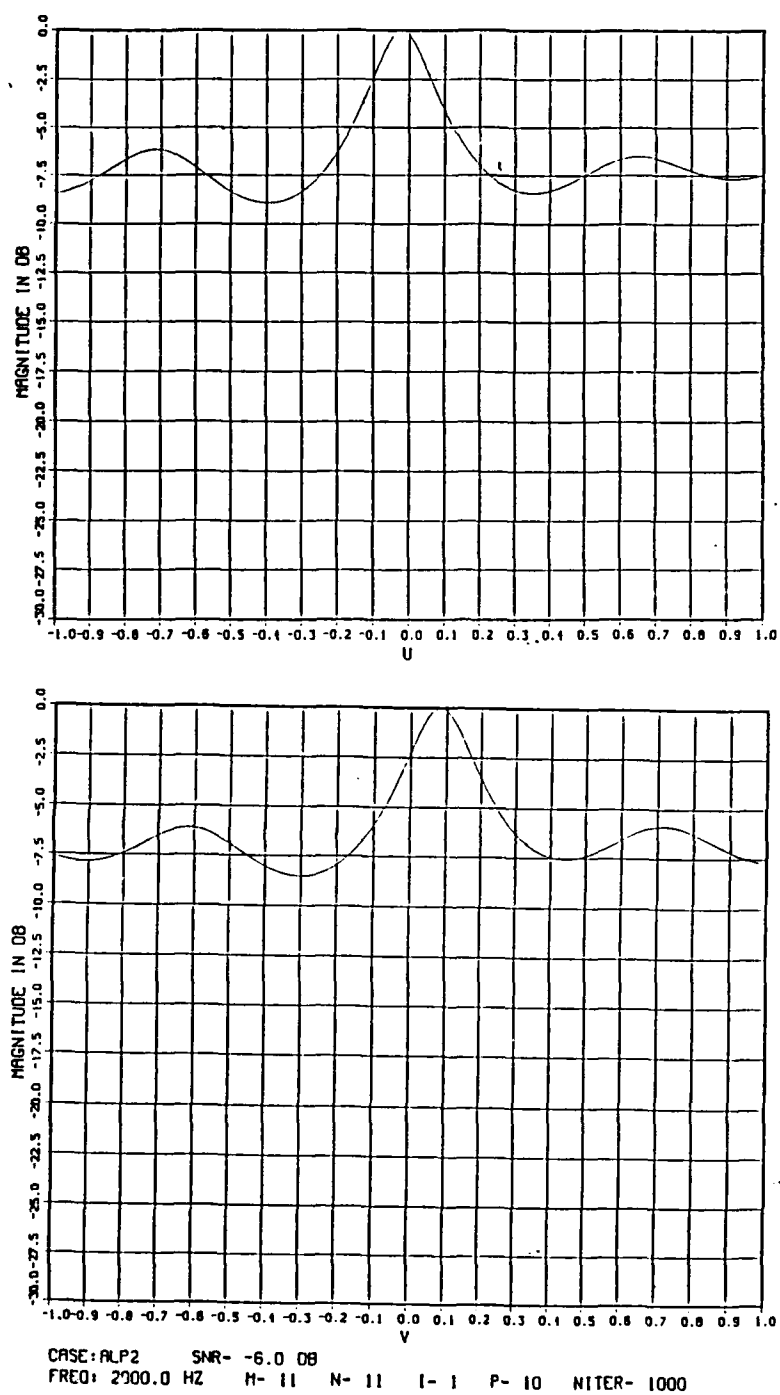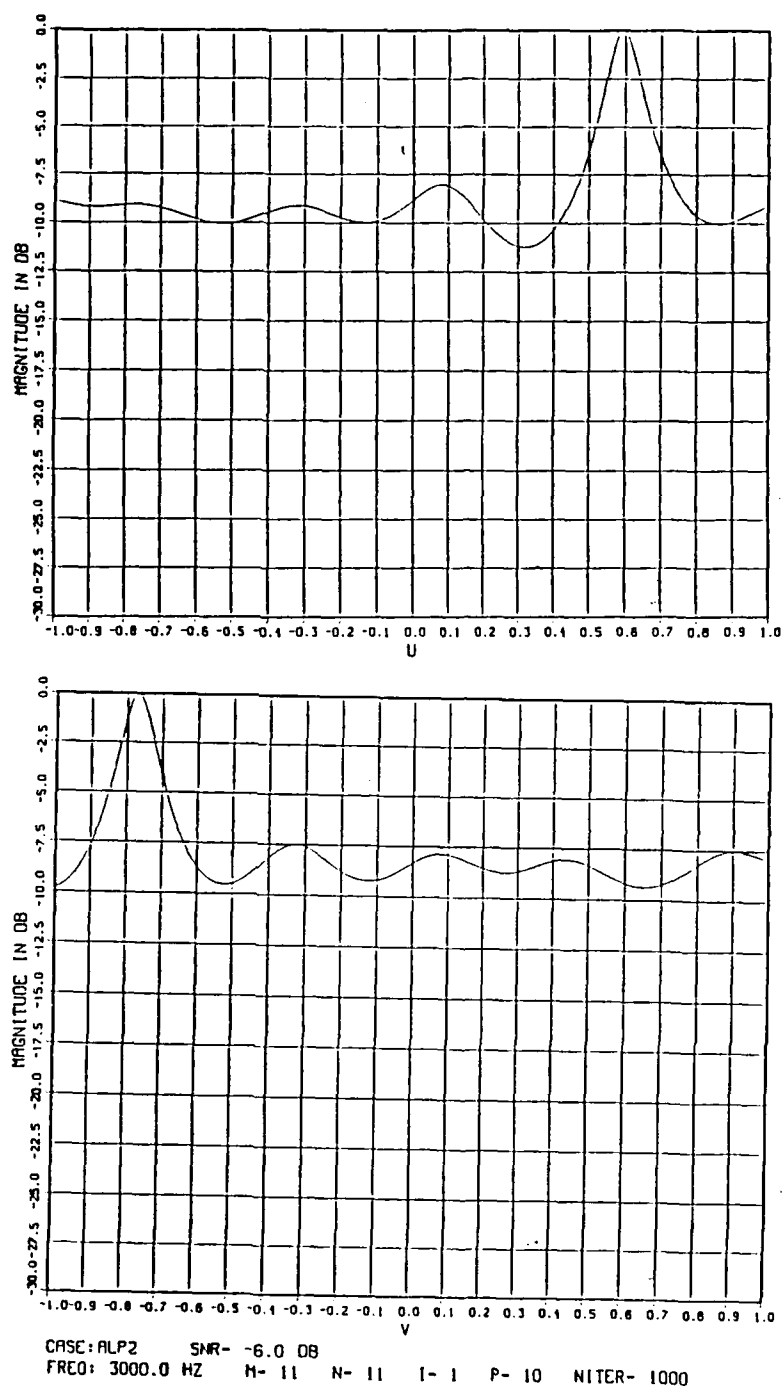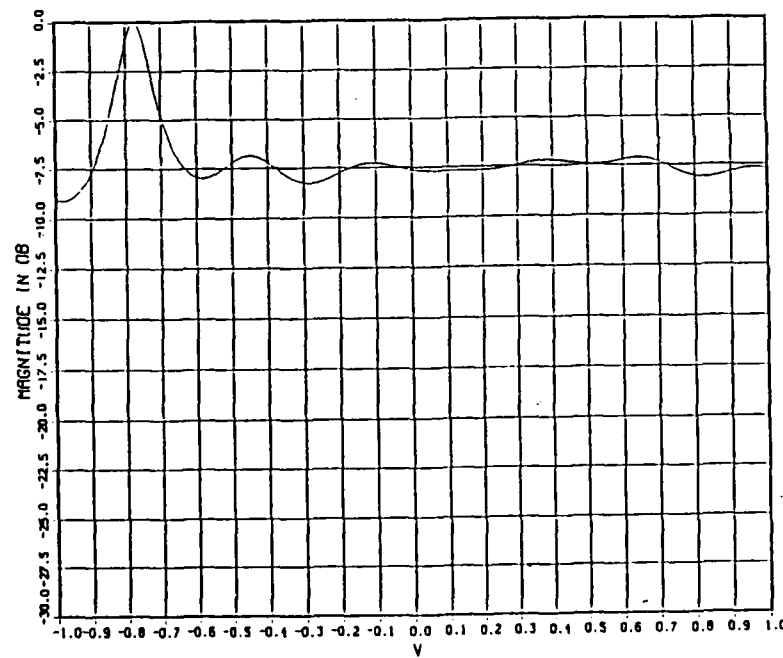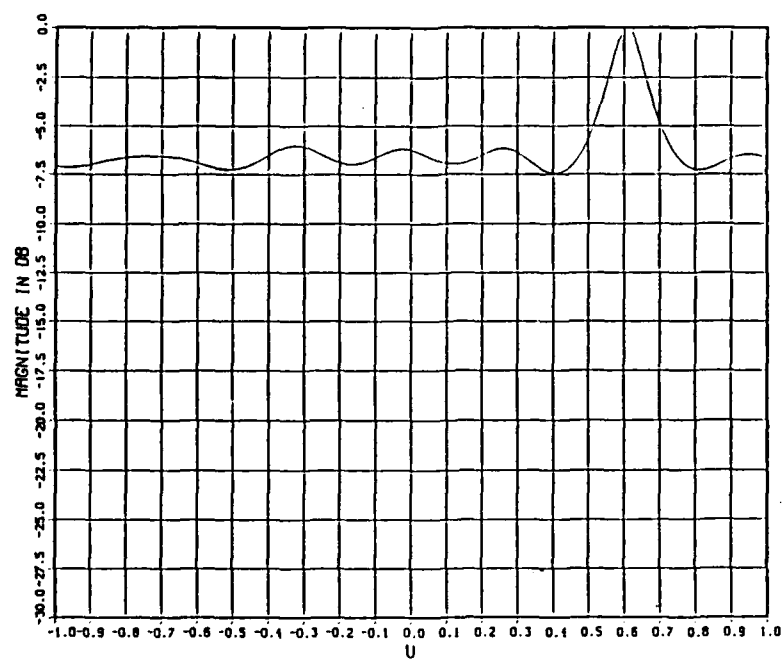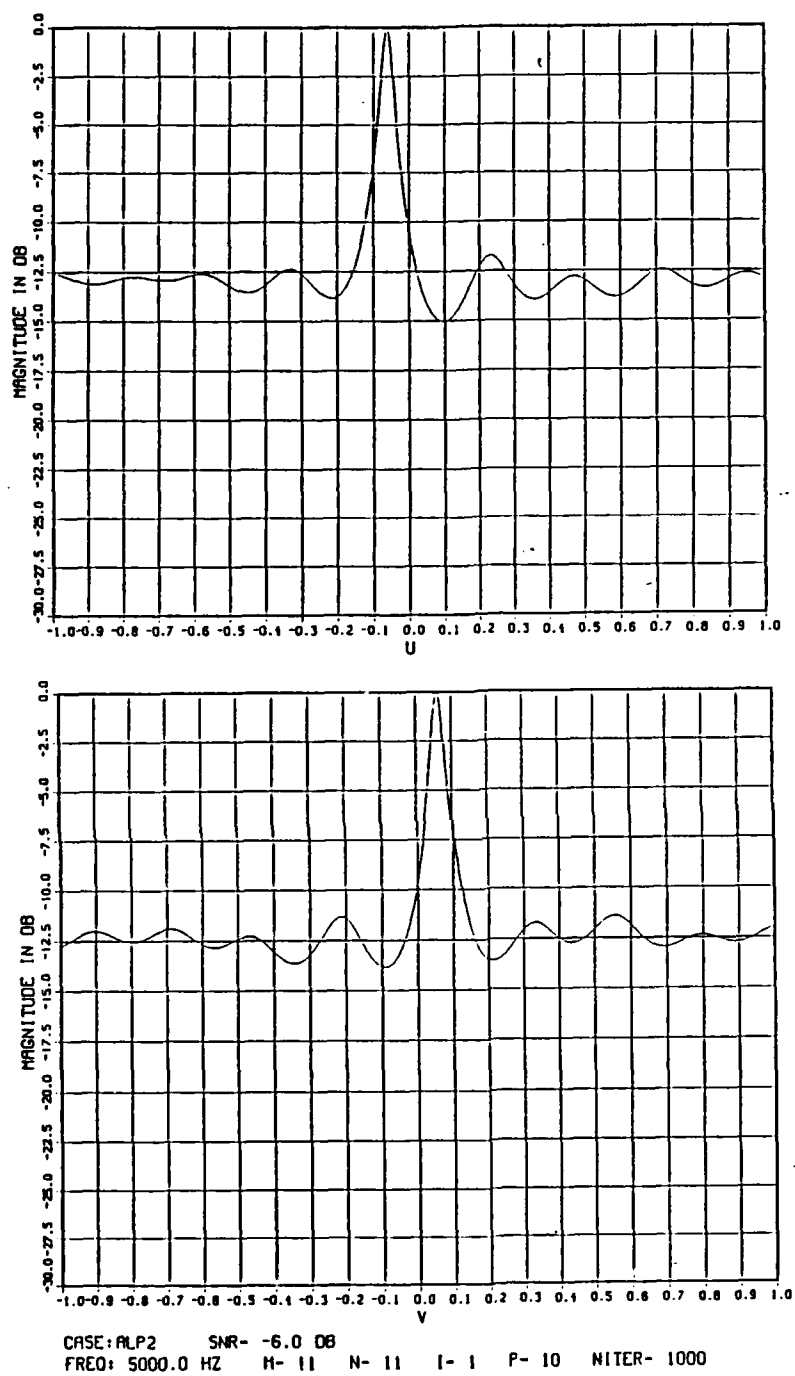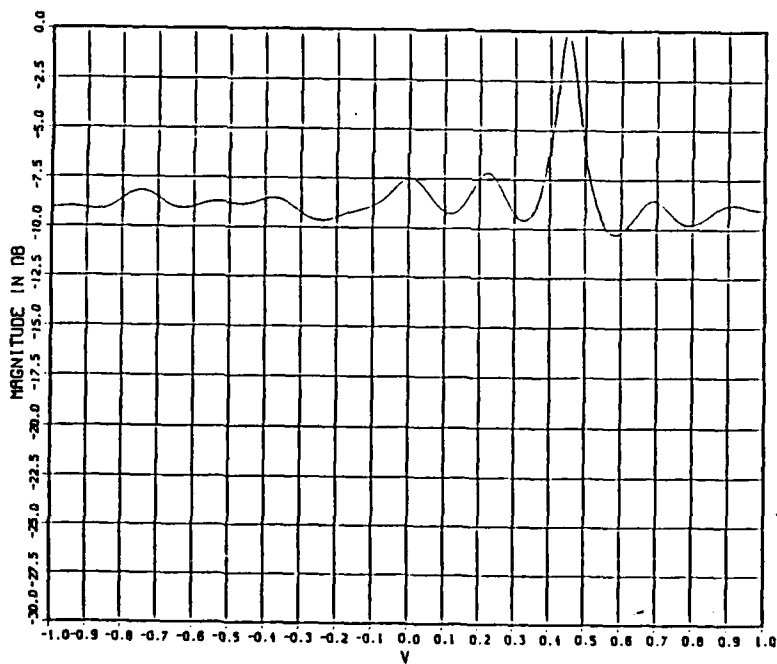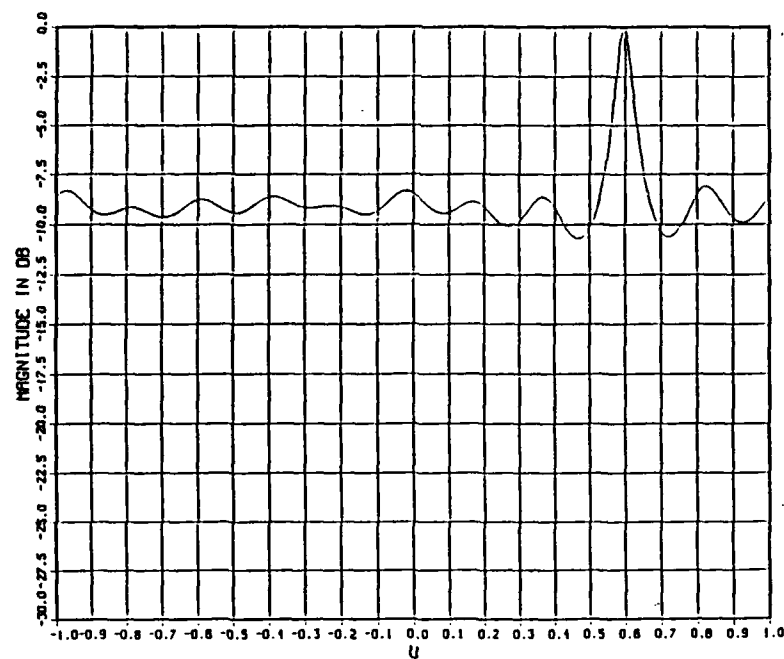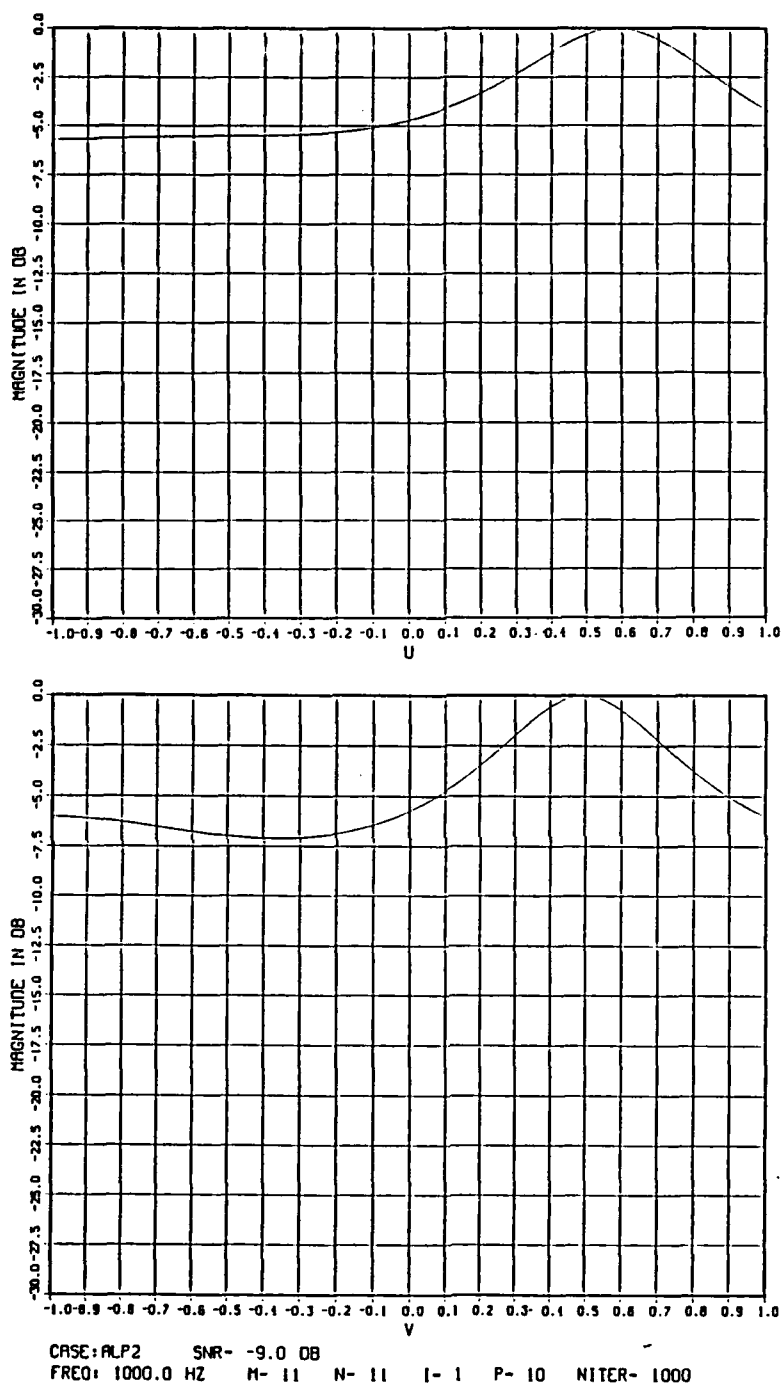Figure 53.    Estimates of Direction Cosines U0 and V0, Case ALP3: SNR = -3dB and
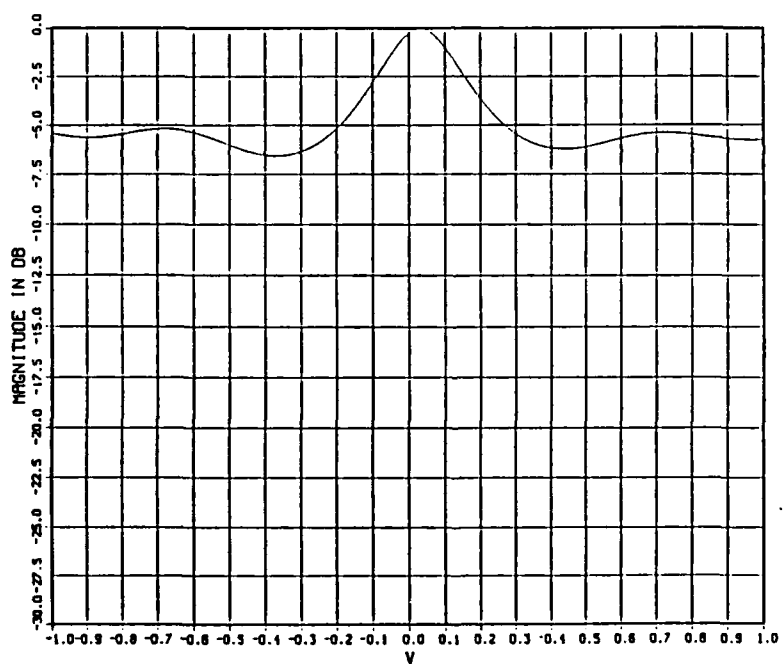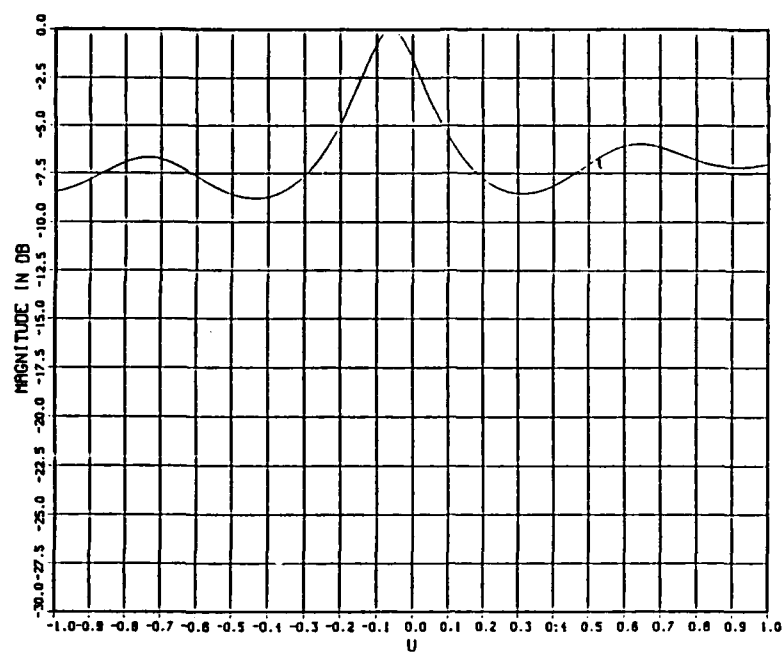q = 3

78
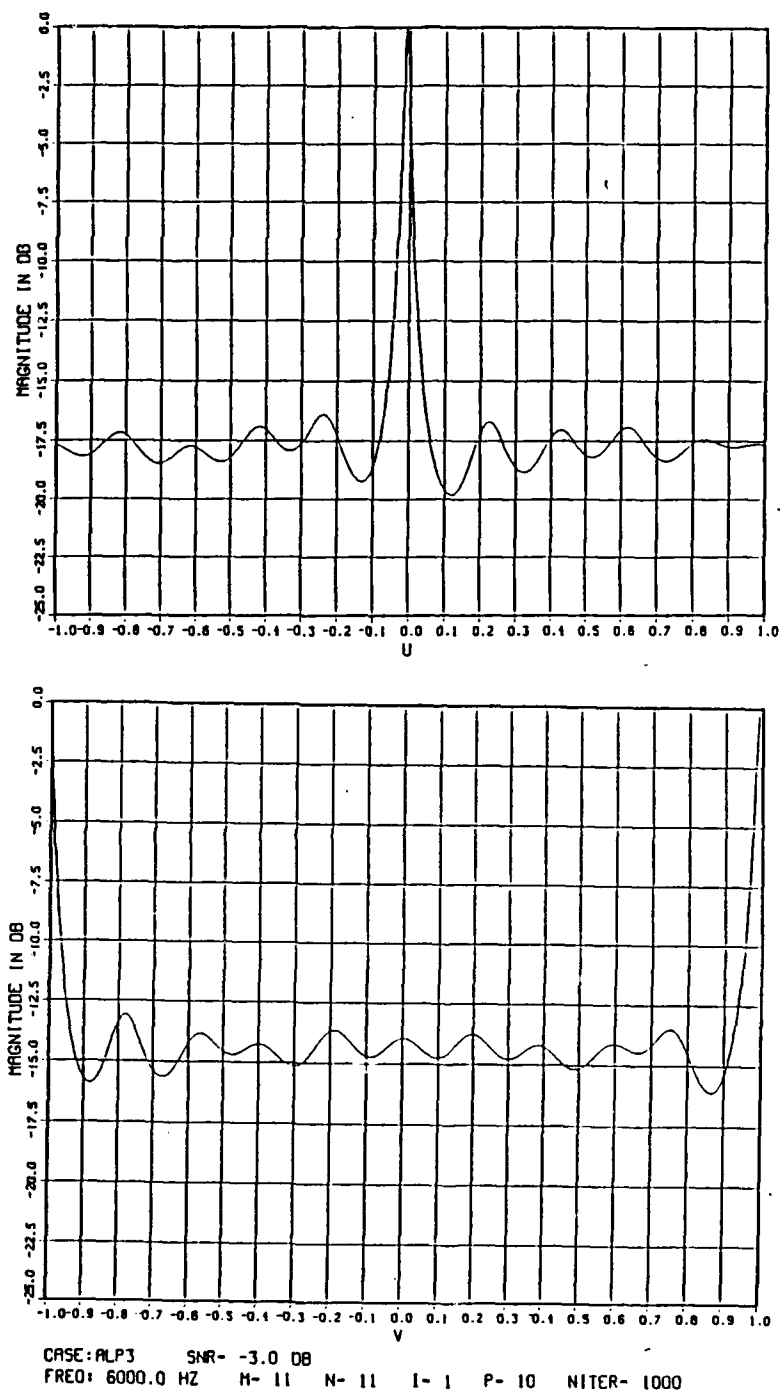
Figure 54. Estimates of Direction Cosines U0 and V0, Case ALP3: SNR = -3dB and q = 6

79
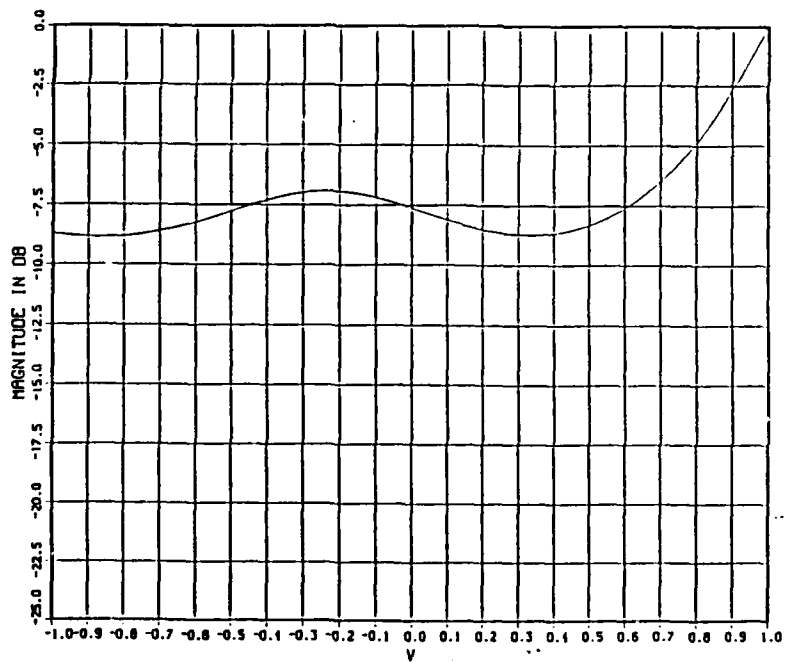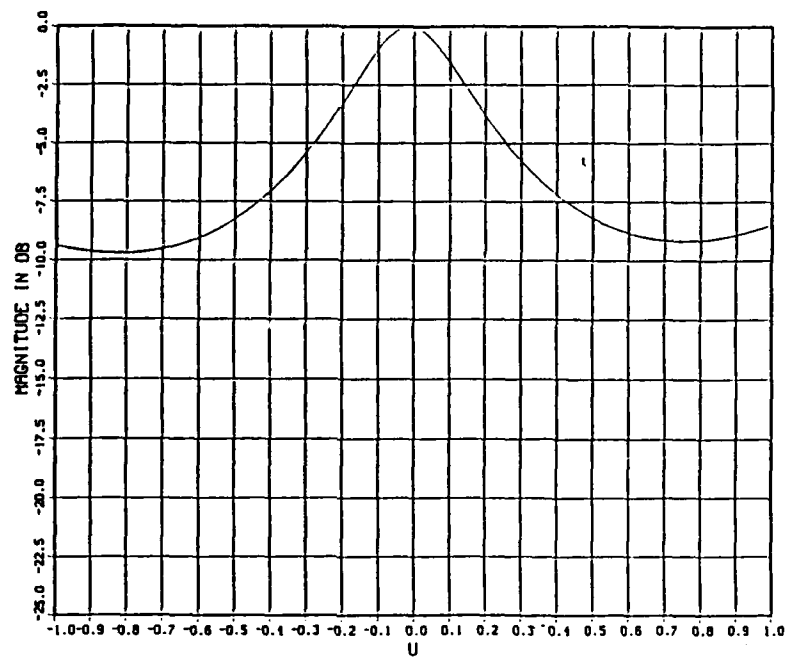
**Figure 55.** Estimates of Direction Cosines U0 and V0, Case ALP3: SNR = -6dB and q = 1
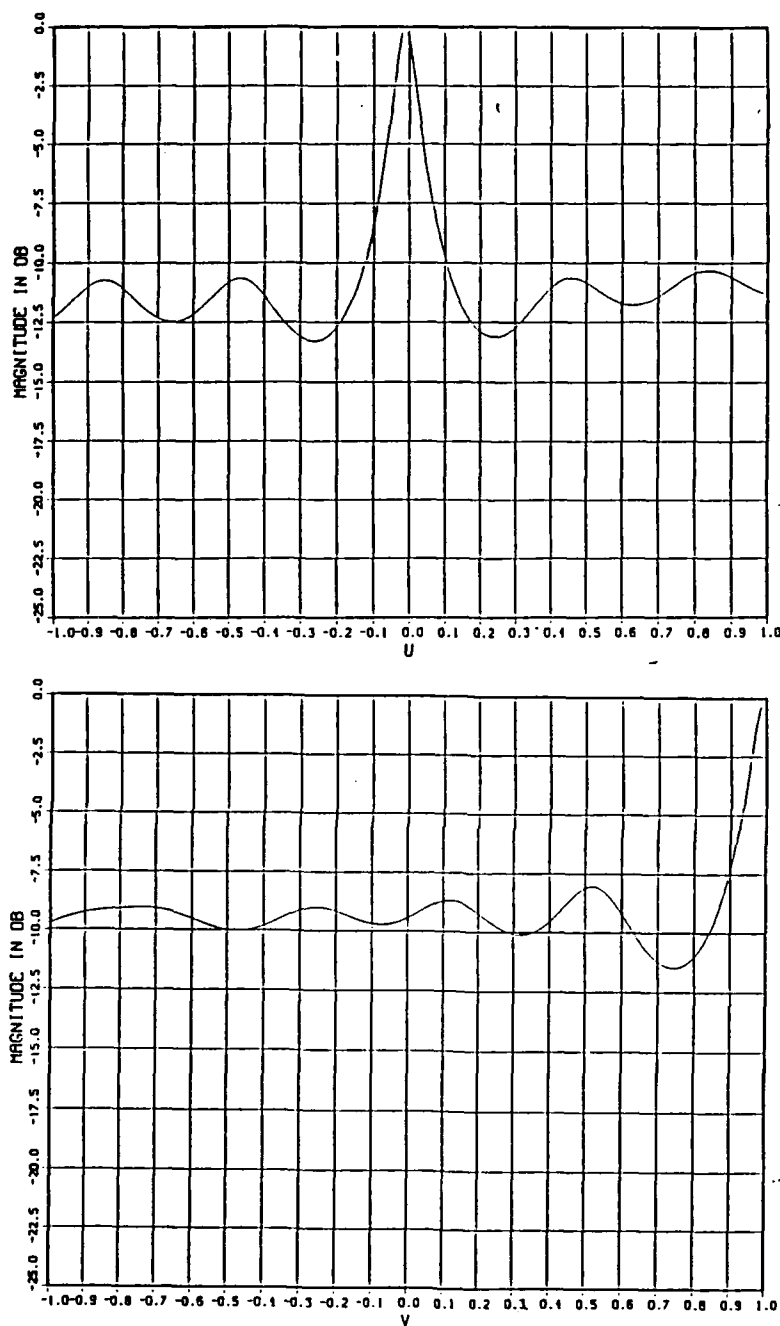
Figure 56. Estimates of Direction Cosines U0 and V0, Case ALP3: SNR = -6dB and q = 3

Figure 57.   Estimates of Direction Cosines U0 and V0, Case ALP3: SNR = -6dB and q = 6
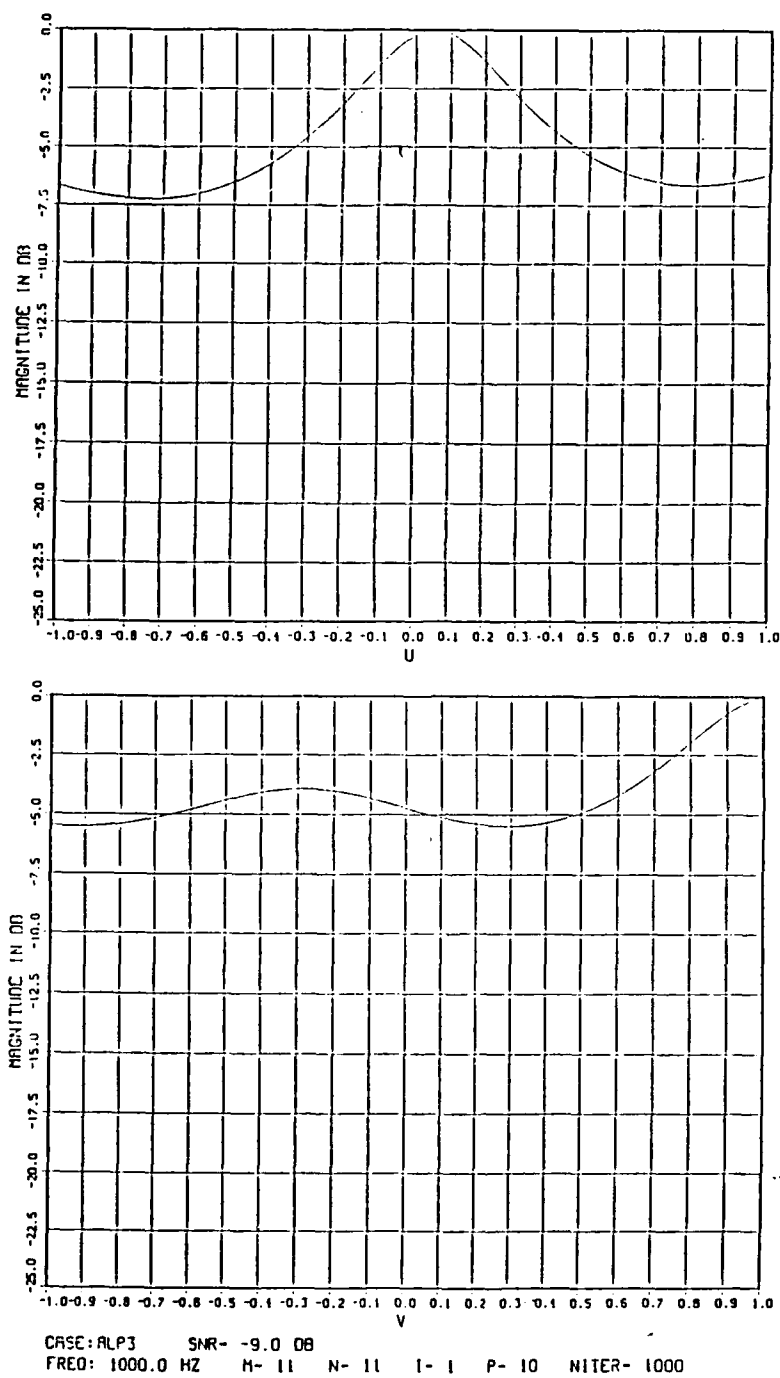
Figure 58.   Estimates of Direction Cosines U0 and V0, Case ALP3: SNR = -9dB and q = 1

CASE: ALP3     SNR- -9.0 DB
FREQ: 3000.0 HZ     M- 11     N- 11     I- 1     P- 10     NITER- 1000

Figure 59.     Estimates of Direction Cosines U0 and V0, Case ALP3: SNR = -9dB and q = 3
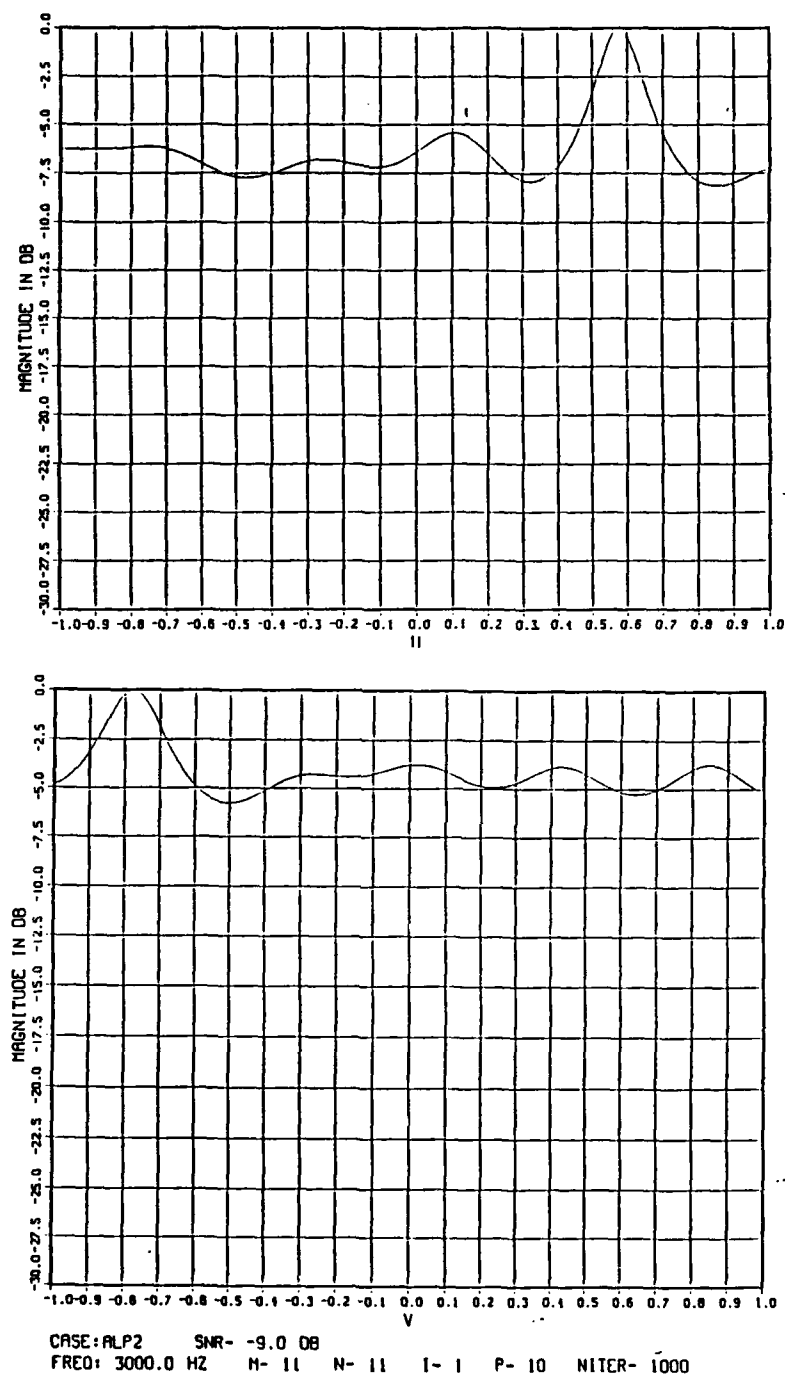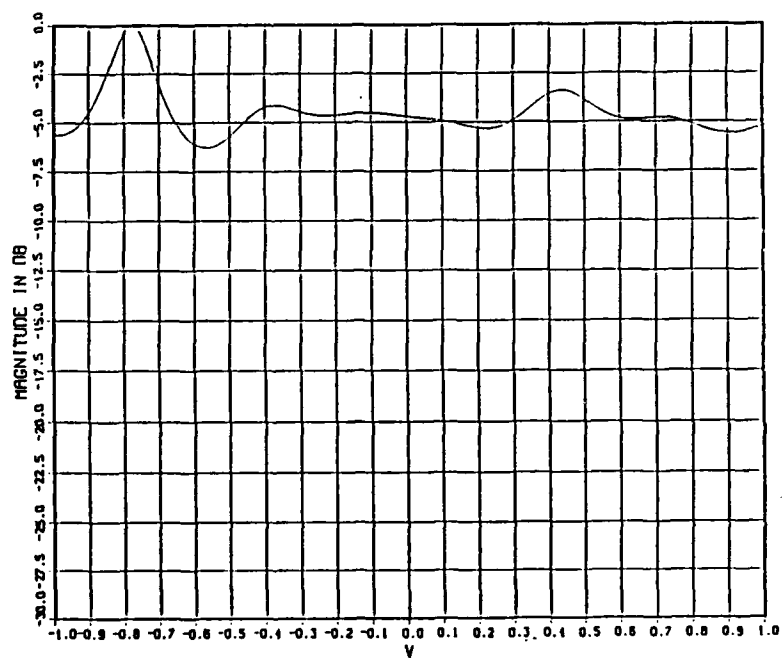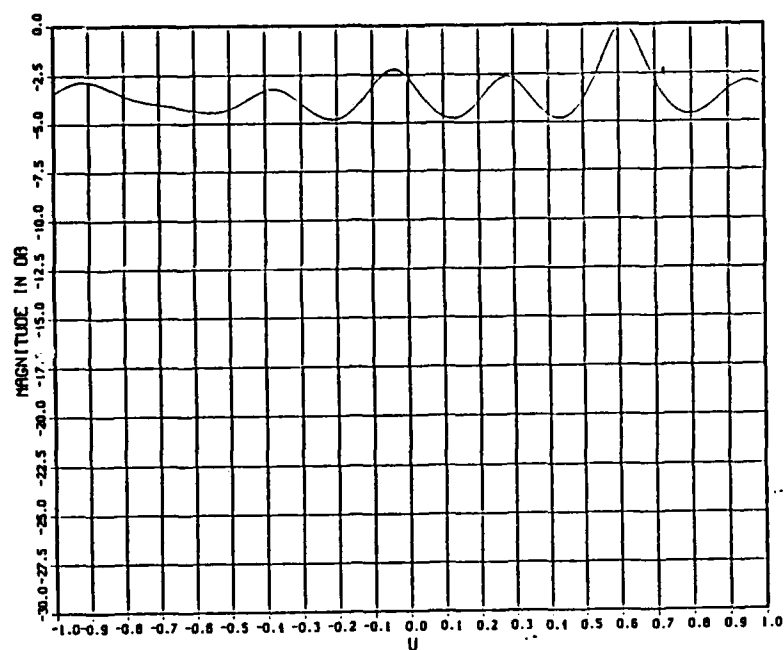
84
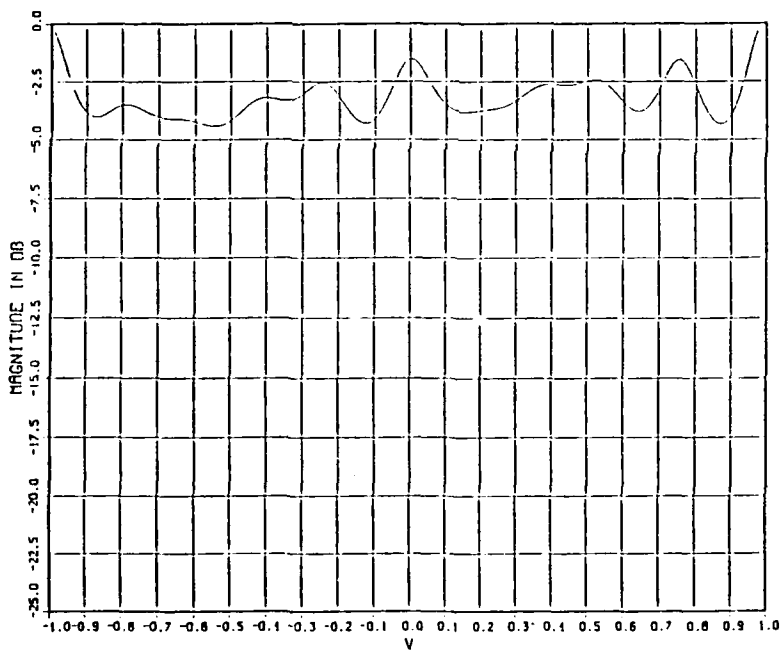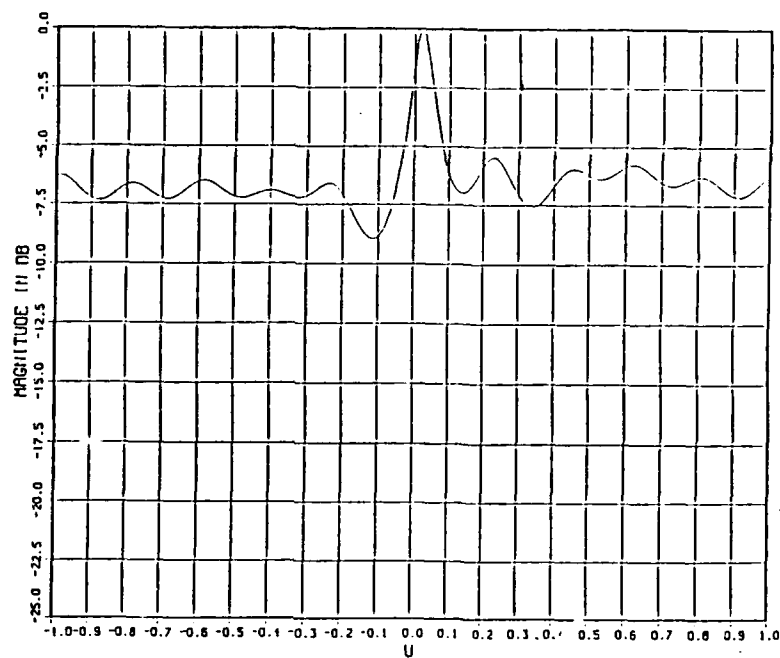
CASE: ALP3    SNR- -9.0 DB
FREQ: 6000.0 HZ    M- 11    N- 11    I- 1    P- 10    NITER- 1000

**Figure 60.** Estimates of Direction Cosines U0 and V0, Case ALP3: SNR = -9dB and q = 6
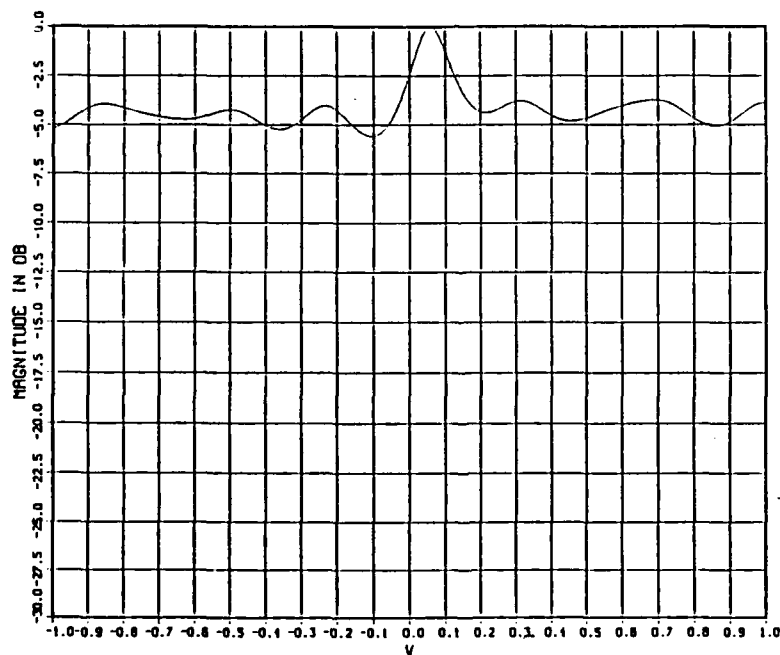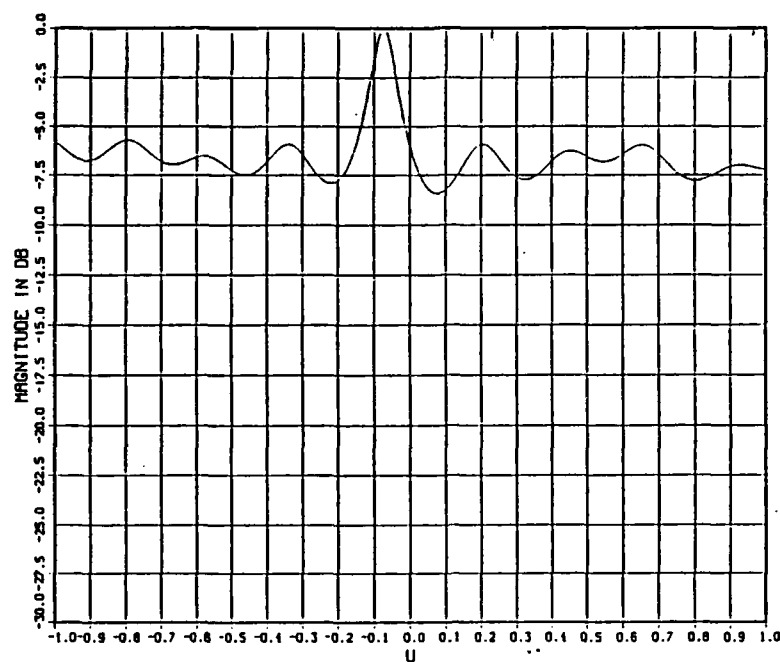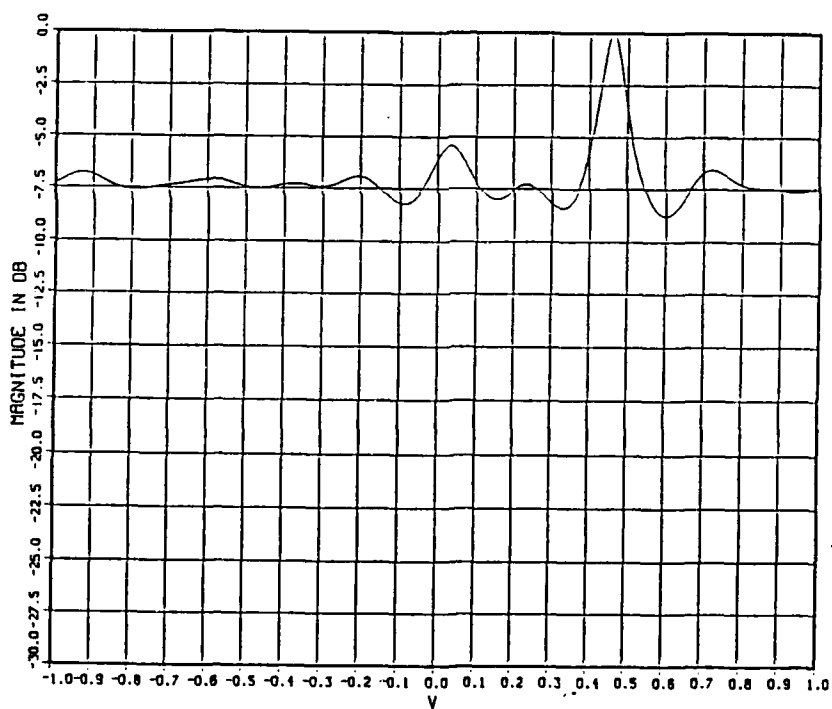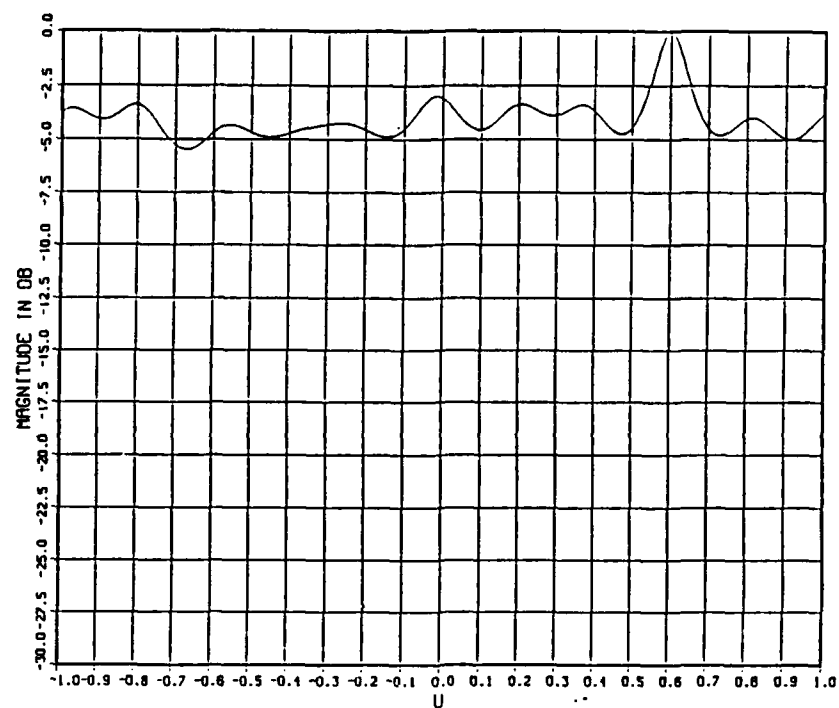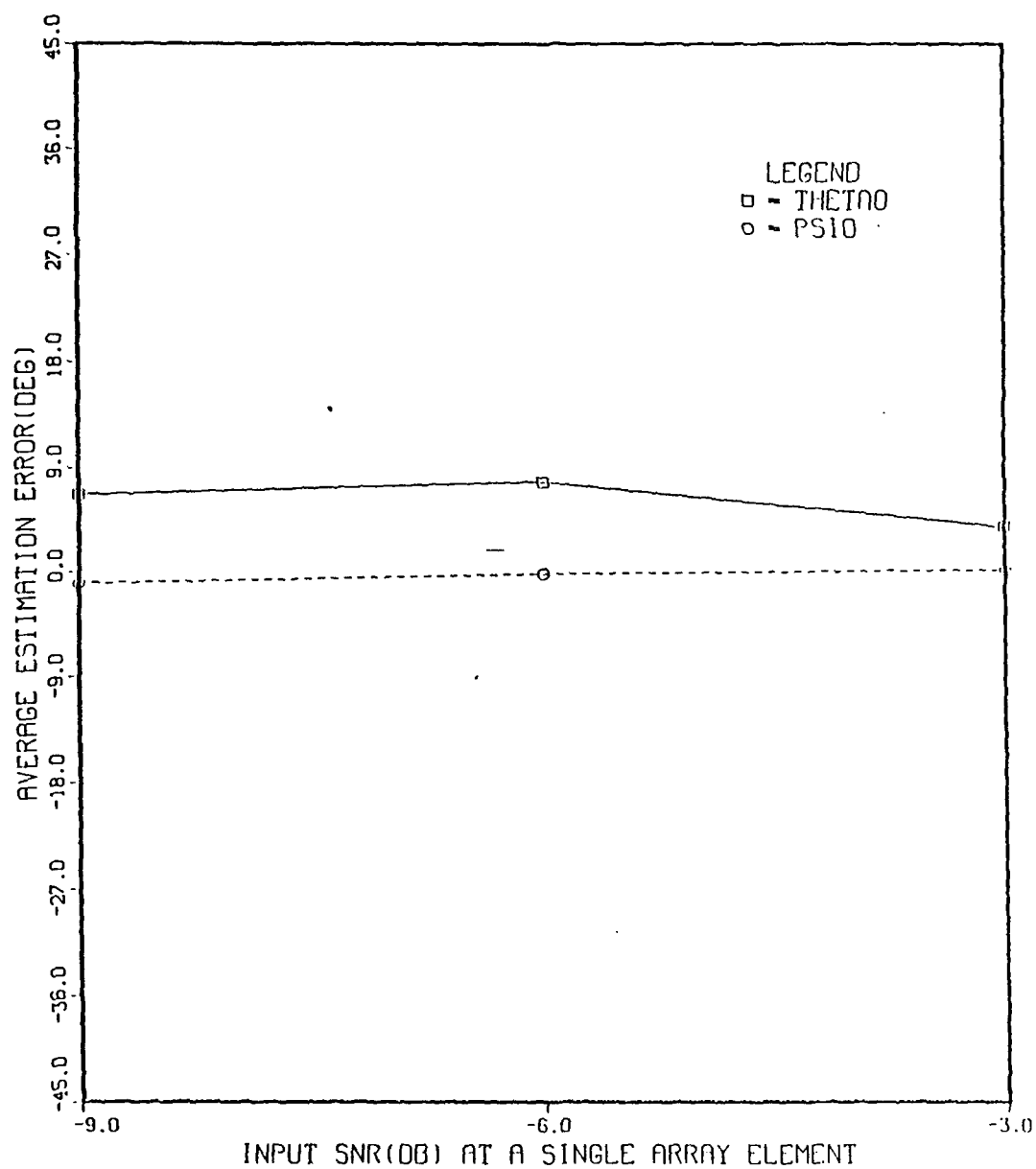
Figure 61. Average Estimation Errors of Depression and Bearing Angles vs. SNR at 1000 Hz for Case ALP3.
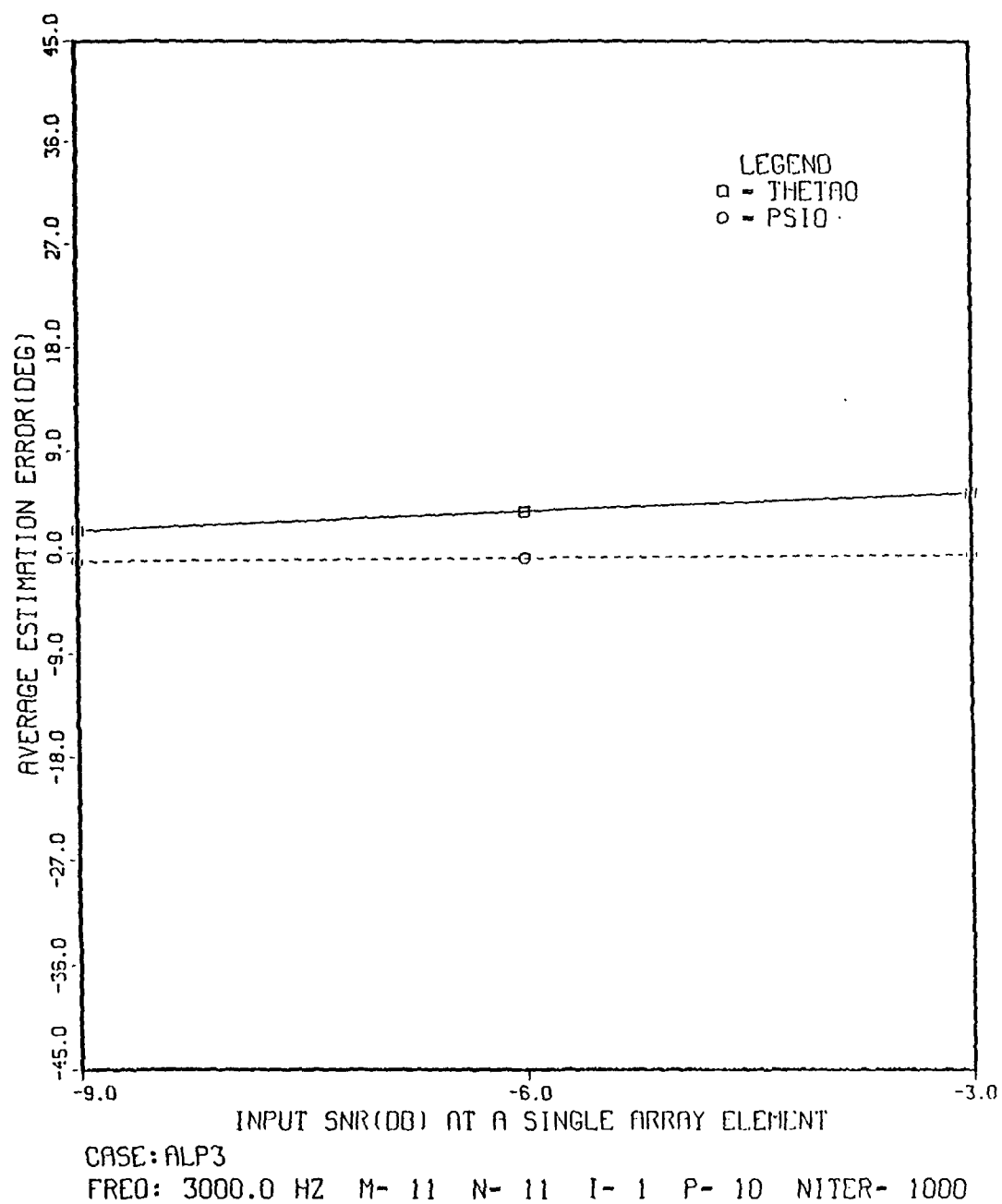
Figure 62.    Average Estimation Errors of Depression and Bearing Angles vs. SNR
at 3000 Hz for Case ALP3.

87
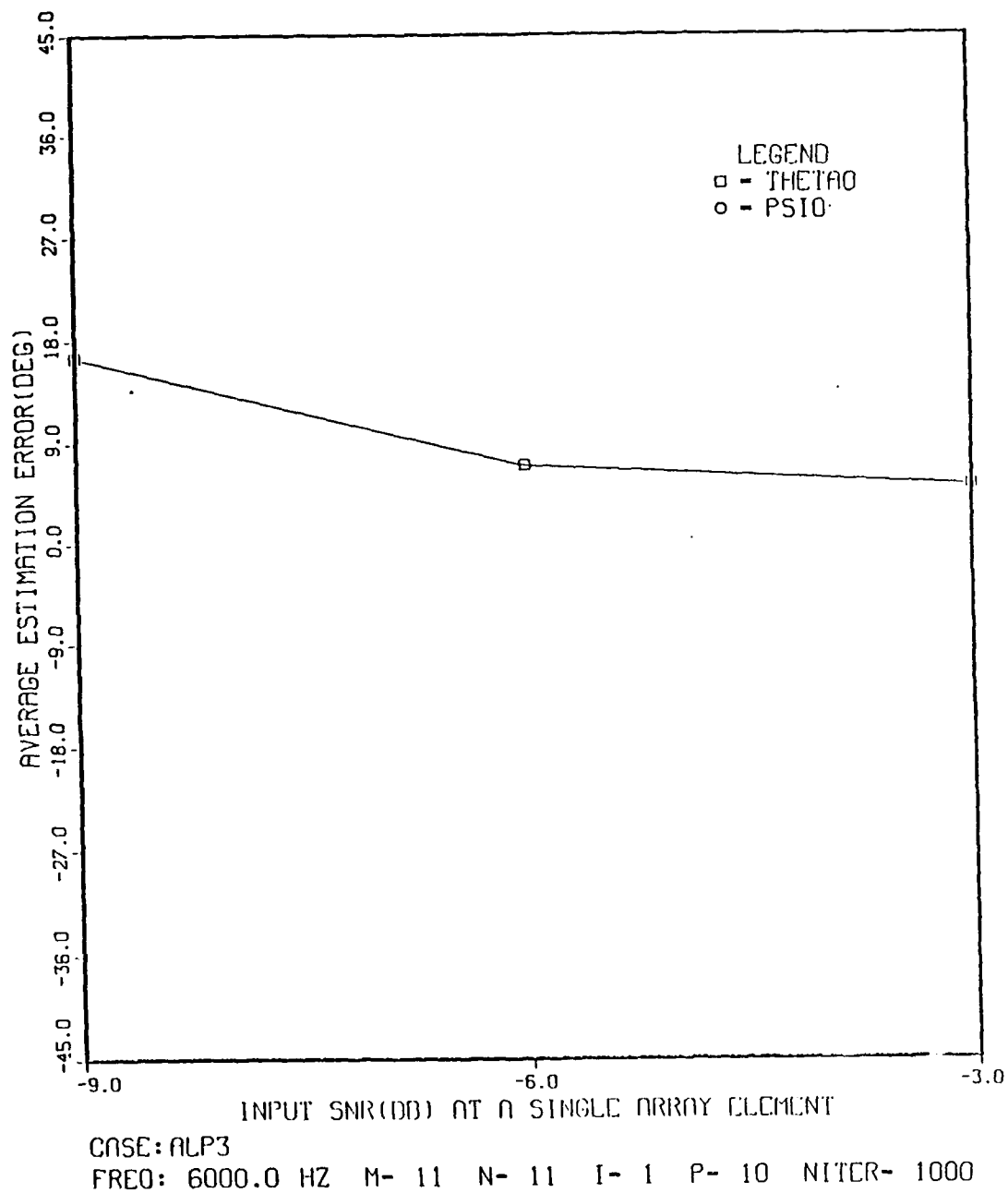
**Figure 63.** Average Estimation Errors of Depression and Bearing Angles vs. SNR at 6000 Hz for Case ALP3.

## D. CASE 4

Case 4 corresponds to three broadband targets being present two of which have a common harmonic. Target 1 was located at ($\theta_0 = 45^\circ$, $\psi_0 = 0^\circ$). Target 2 was located at ($\theta_0 = 45^\circ$, $\psi_0 = 180^\circ$). Target 3 was located at ( $\theta_0 = 33^\circ$ , $\psi_0 = 47^\circ$). A total of six harmonics were present in the output electrical signal. The following three subcases were examined:

- Case 4-A: Three targets, two of which are located in the same plane. Targets 1 and 2 have a common spectral line at 1000 Hz.

- Case 4-B: Three targets, two of which are located in the same plane. Targets 1 and 2 have a common spectral line at 3000 Hz.

- Case 4-C: Three targets two of which are located in the same plane. Targets 1 and 2 have a common spectral line at 6000 Hz.

For these cases, only no noise results were compiled for both algorithms in order to examine the ability of target discrimination when two targets are in the same plane and have a common harmonic.

Figures 64, 65 and 66 present estimates of the direction cosines $U_0$ and $V_0$ for each common harmonic, that is at 1000 Hz for Case ALP4-A, 3000 Hz for Case ALP4-B and at 6000 Hz for Case ALP4-C. Clearly, we can observe that except for case ALP4-A, the algorithm can discriminate the location of two targets.

Tables 7 through 12 in the Appendix A present numerical data for all the subcases of Case 4 for both algorithms. From these tables we can observe that for all the harmonics, except the common one, both algorithms correctly identified the location of the targets with zero degrees estimation errror. However, for the common harmonic, the LMS algorithm located a false fourth target, which was located exactly between the actual locations of targets 1 and 2. On the other hand the ALP algorithm, except for the subcase ALP4-A, for the common harmonic, identifies two different estimates of the direction cosine $U_0$ from the transfer function plots, which results in two different target locations.
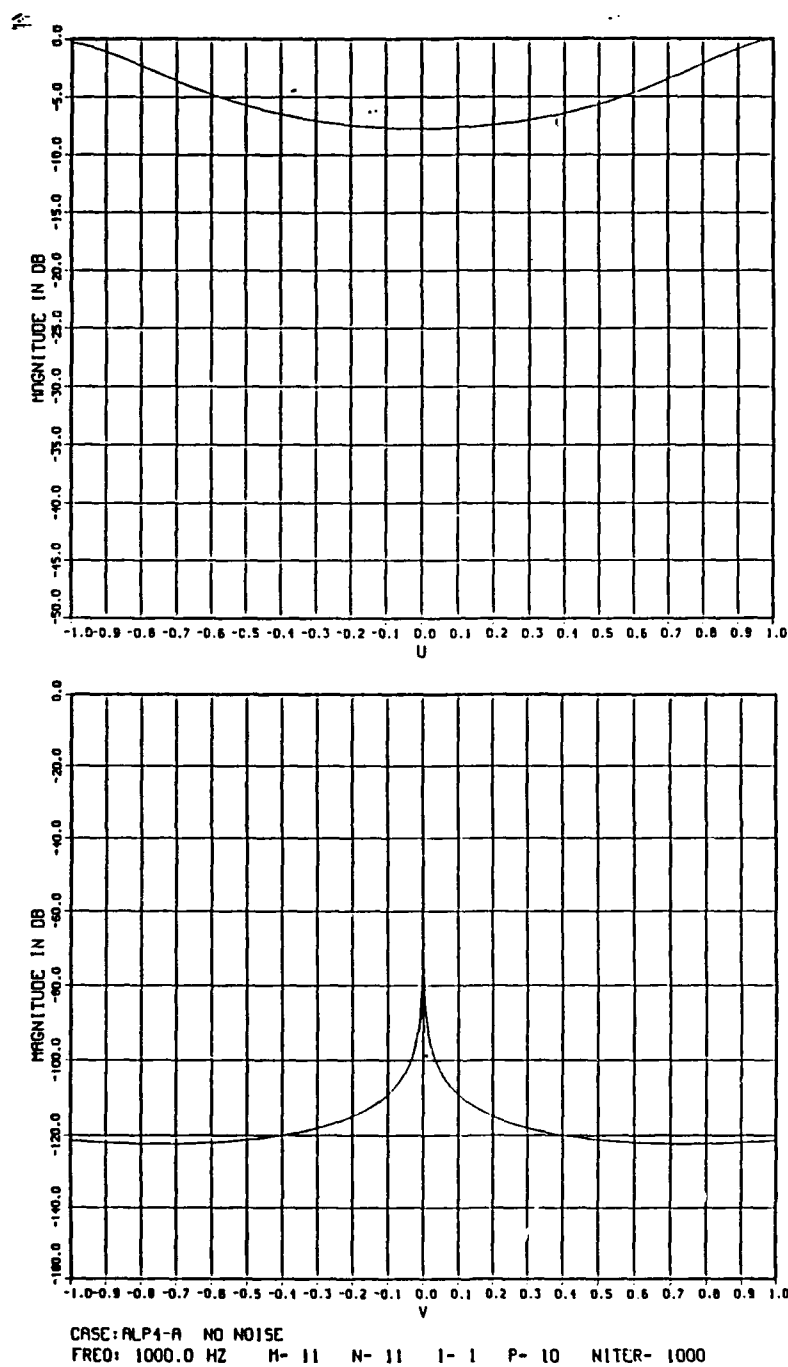
Figure 64.   Estimates of Direction Cosines U0 and V0, Case ALP4-A: No Noise and
q = 1

CASE: ALP4-B  NO NOISE
FREO: 3000.0 HZ    M- 11    N- 11    I- 1    P- 10    NITER- 1000
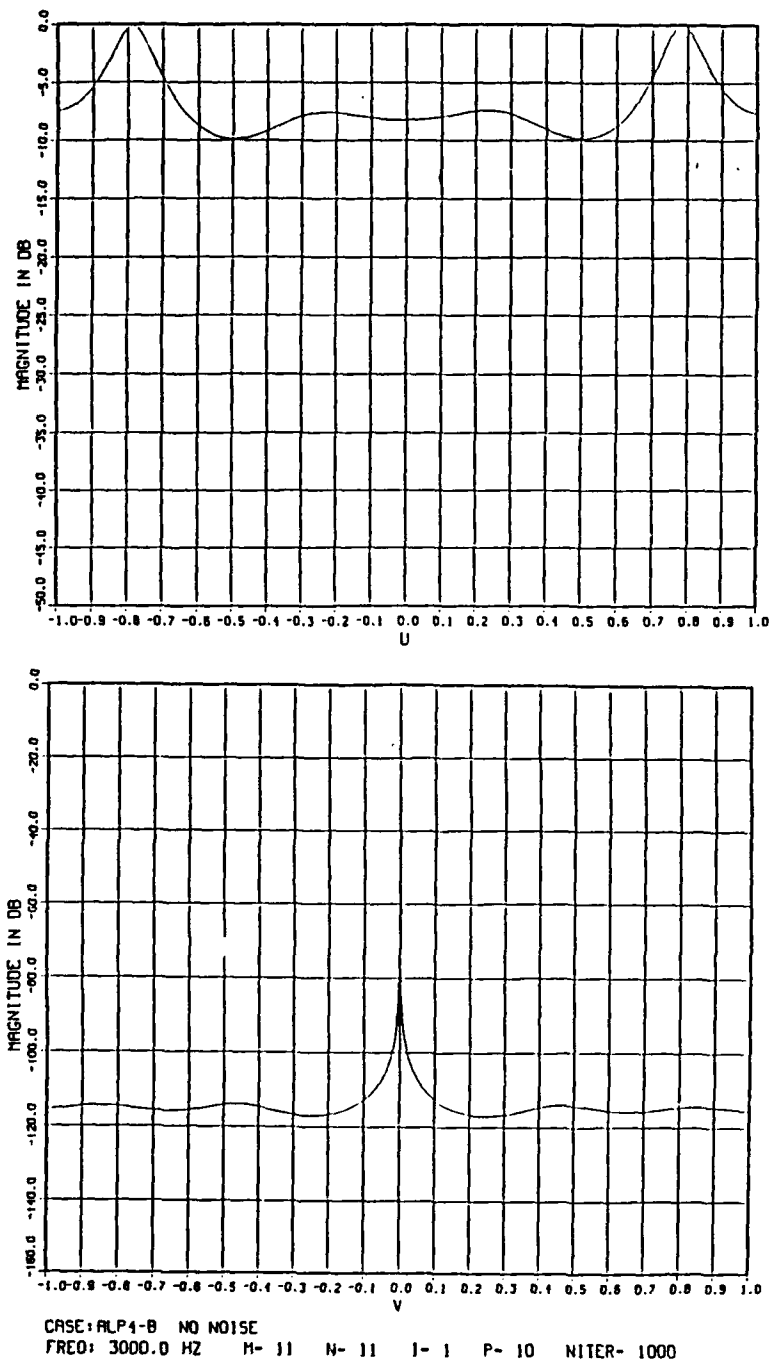
Figure 65.    Estimates of Direction Cosines U0 and V0, Case ALP4-B: No Noise and
q = 3

91
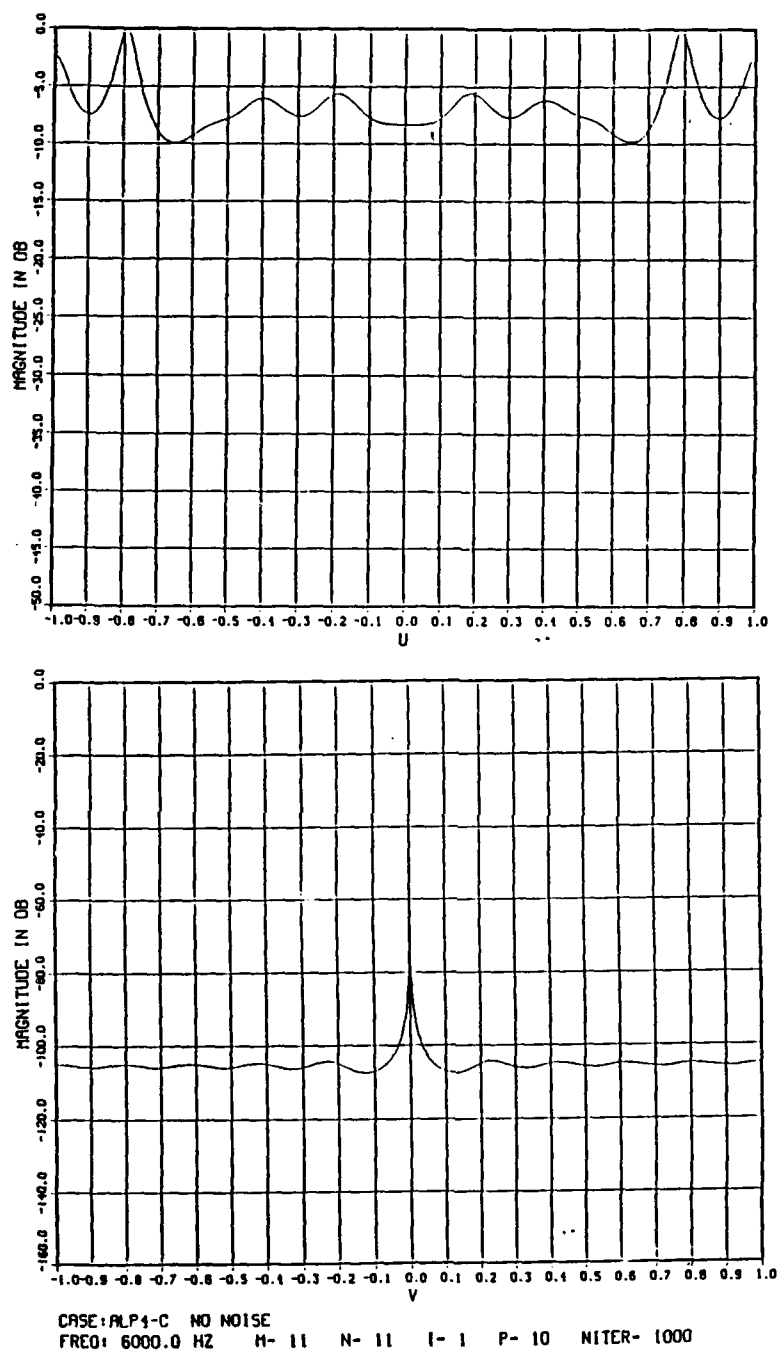
Figure 66.    Estimates of Direction Cosines U0 and V0, Case ALP4-C: No Noise and
q = 6

## E. CASE 5

Case 5 placed three broadband targets at random locations. Target 1 was located at ($\theta_0 = 49^0$, $\psi_0 = 38^0$). Target 2 was located at ($\theta_0 = 5^0$, $\psi_0 = 137^0$). Target 3 was located at ($\theta_0 = 77^0$, $\psi_0 = 307^0$). A total of six harmonics were present in the output electrical signal. The following three subcases were examined:

- Case 5-A: Three targets located at random positions. Targets 1 and 2 have a common spectral line at 1000 Hz.

- Case 5-B: Three targets located at random positions. Targets 1 and 2 share a common spectral line at 3000 Hz.

- Case 5-C: Three targets located at random positions. Targets 1 and 2 share a common spectral line at 6000 Hz.

For these cases, only no noise results were compiled for both algorithms in order to examine the ability of target discrimination when two targets are in random positions and have a common harmonic.

Figures 67, 68 and 69 present estimates of the direction cosines $U_0$ and $V_0$ for each common harmonic, that is, at 1000 Hz for Case ALP5-A, at 3000 Hz for Case ALP5-B and at 6000 Hz for case ALP5-C. Clearly, we can observe that exept for case ALP5-A, the algorithm can discriminate the location of two targets.

Tables 13 through 18 in the Appendix A present numerical data for all the subcases of Case 5 for both algorithms. From these tables we can observe that for all the harmonics, except the common one, both algorithms correctly identified the location of the targets with zero degrees estimation errror. However, for the common harmonic, the LMS algorithm located a false fourth target. On the other hand the ALP algorithm, except for subcase ALP5-A, for the common harmonic, identifies two different estimates of the direction cosines $U_0$ and $V_0$ from the transfer function plots, which results in two different target locations.

93
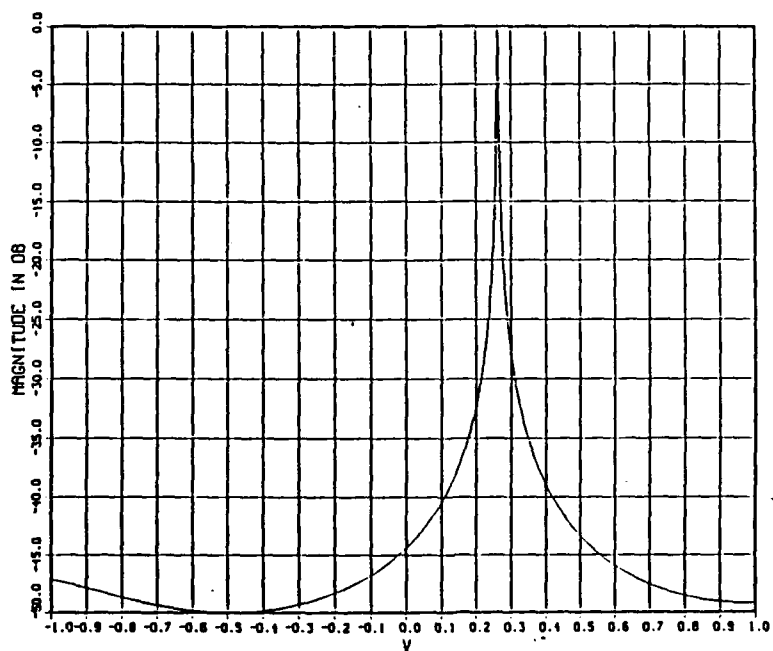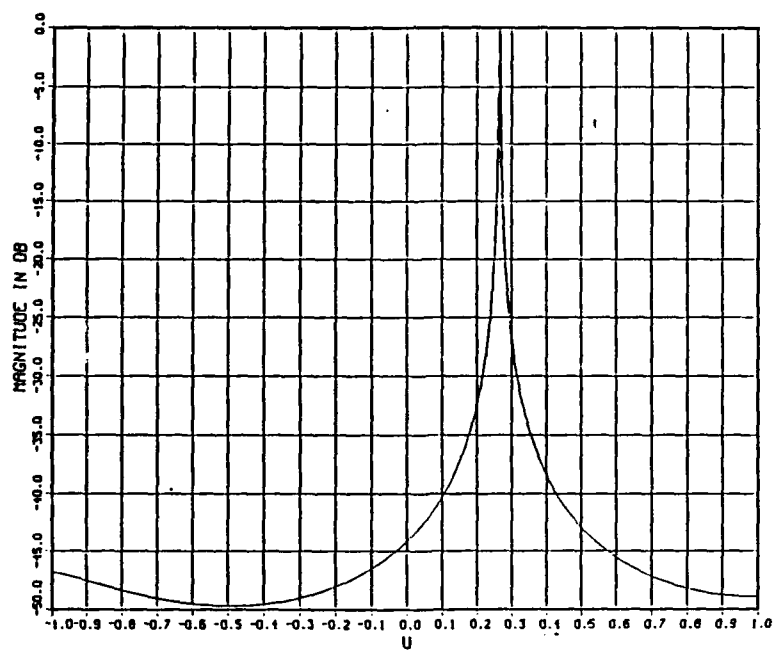
CASE:ALPS-A  NO NOISE
FREQ: 1000.0 HZ    M- 11    N- 11    I- 1    P- 10    NITER- 1000

Figure 67.    Estimates of Direction Cosines U0 and V0, Case ALP5-A: No Noise and
q = 1

94
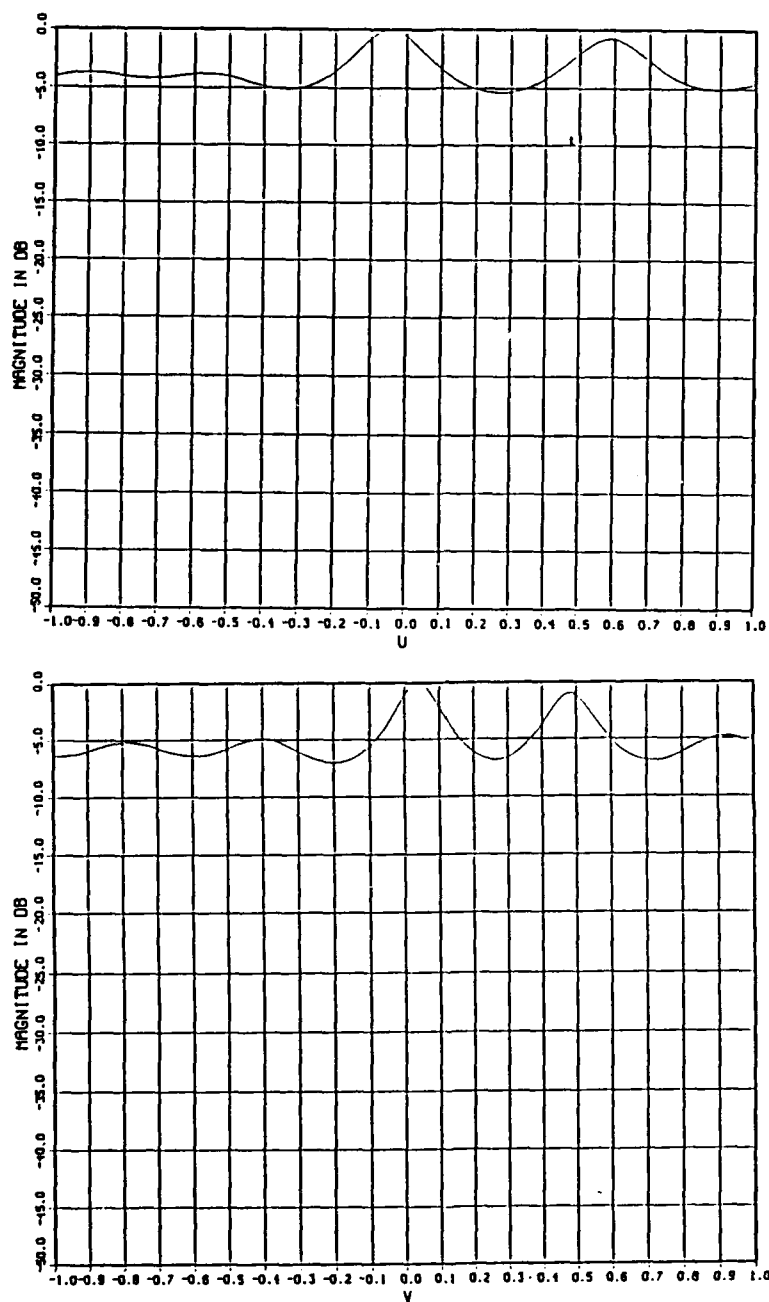
CASE: ALP5-B   NO NOISE
FREQ: 3000.0 HZ      M- 11     N- 11     I- 1     P- 10     NITER- 1000

Figure 68.    Estimates of Direction Cosines U0 and V0, Case ALP5-B: No Noise and
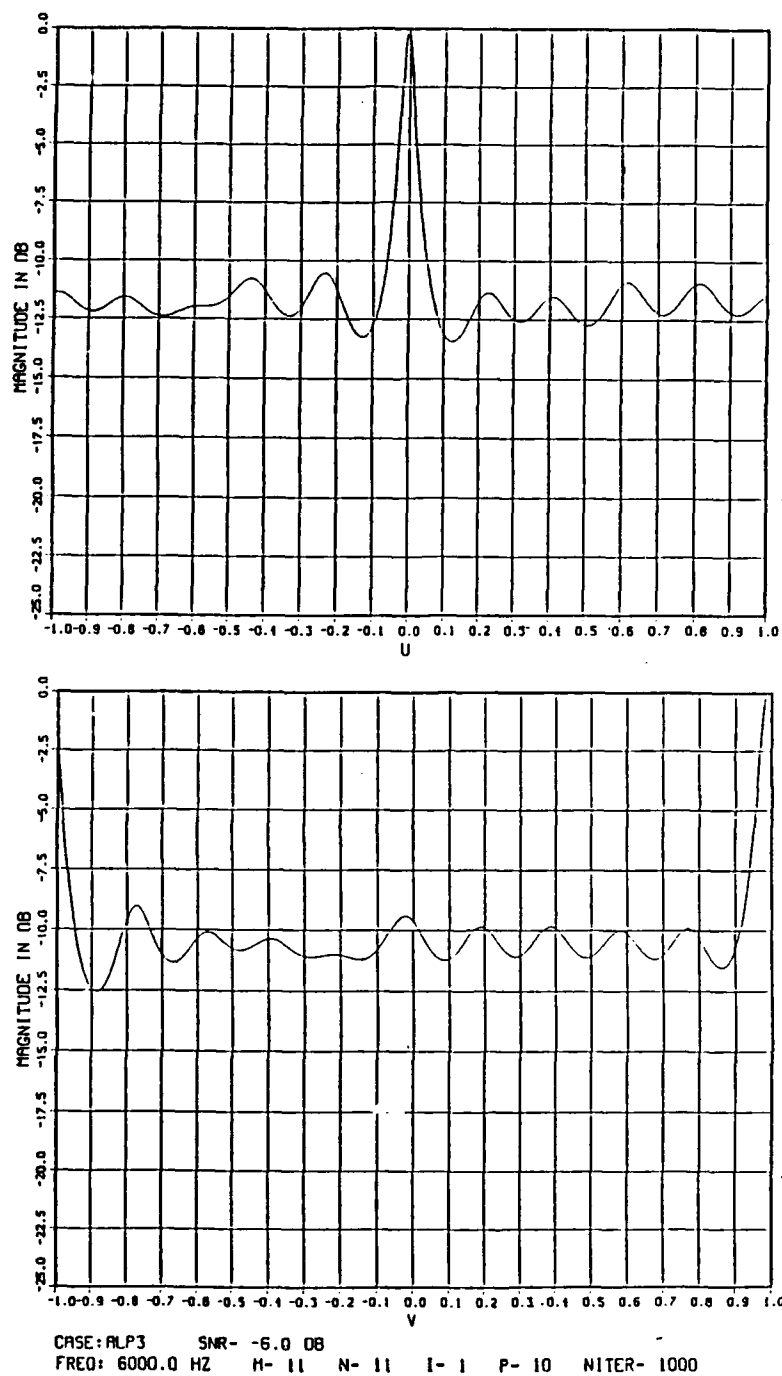             q = 3

CASE: ALP5-C   NO NOISE
FREO: 6000.0 HZ    M- 11    N- 11    I- 1    P- 10   ,NITER- 1000

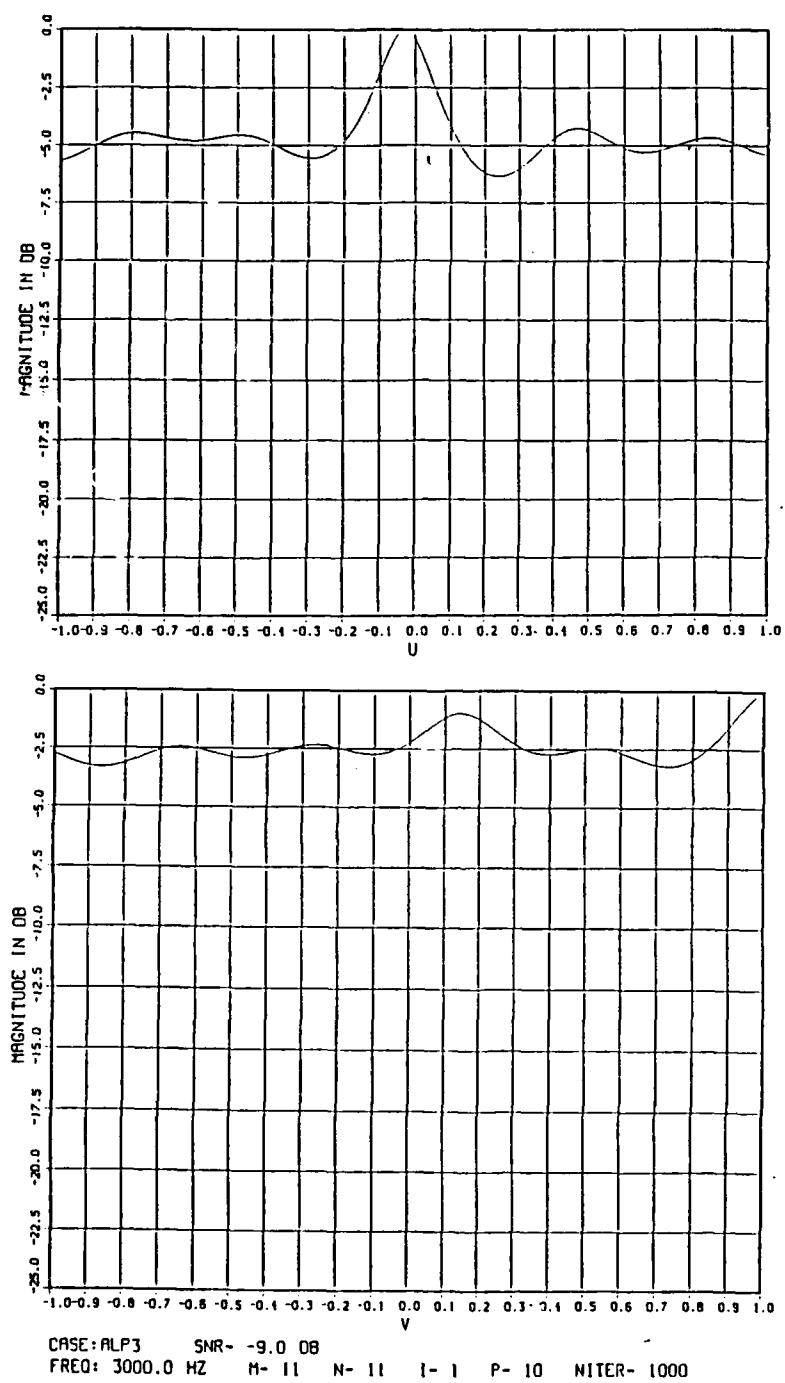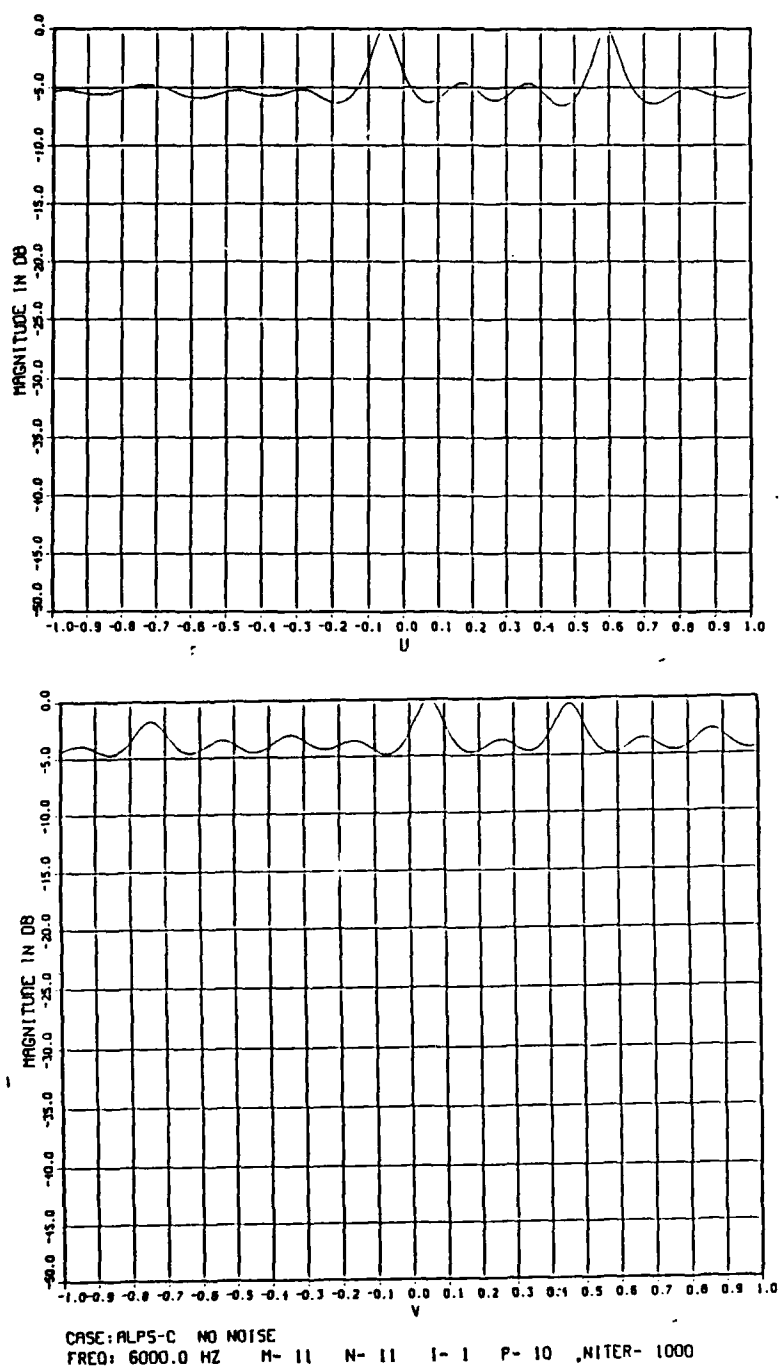**Figure 69.**    Estimates of Direction Cosines U0 and V0, Case ALP5-C: No Noise and
q = 6

96

# IV. CONCLUSIONS AND RECOMMENDATIONS

The goal of this thesis was to evaluate the multiple broadband target localization capability and the full angular coverage capability of two frequency domain adaptive beamforming algorithms. The main advantage of both algorithms is that no a priori knowledge is assumed about the statistics of the received signal, the total number of targets present, where they are located, and the frequency content of the targets.

The two frequency domain adaptive beamforming algorithms evaluated were the modified complex Least-Mean-Square (LMS) algorithm developed by Ziomek and Chan [Ref. 6], and the modified complex Adaptive Linear Prediction-Error (ALP) algorithm which was presented for first time. Chapter 3 presented the results of five test cases which were designed to test both algorithms for several different capabilities. It should also be noted here that the number of time samples taken per element of the array never exceeded 65 time samples, an amount which represents a small number of data points.

Summarizing the simulation results discussed in Chapter 3, we can list the following conclusions:

- In most cases tested, both algorithms can localize multiple broadband targets and they have full angular coverage capability.

- Increasing either the sampling rate or the array size yields better estimates in lower SNR for both algorithms

- ALP generally gives better estimates in lower SNR than LMS

- ALP can, in most of the "no noise" cases, discriminate between two targets that have a common harmonic while LMS cannot

- ALP is more computationally intensive than LMS and requires much more iterations to approach a steady-state error.

- ALP is more flexible than LMS because it can process only a part of the total number of array elements to localize the target

In the course of this investigation, several possible areas for future research presented themselves:

97

- further study of the effects of varying the step-size parameter, $\mu$, in an attempt to decrease the magnitude of the estimation error.

- investigation of parallel processing implementation for the ALP algorithm in order to reduce the computation time.

- investigation of larger array size in lower SNR mainly using the ALP algorithm

- investigation of a noise reduction system prior to processing the output electrical signals.

# APPENDIX A.

This appendix presents the numerical data for all of the test cases. Tables 1 through 6 present numerical data for the three first "noisy" cases, Cases 1 through 3, for both algorithms, while tables 7 through 12 present numerical data from the two "no noise" cases, Case 4 and 5, for both algorithms. The following notation is used in all the tables:

- LMS: When the frequency domain modified complex Least-Mean-Square adaptive beamforming algorithm is used.

- ALP: When the frequency domain modified complex adaptive linear prediction-error filter beamforming algorithm is used

- $\theta_0$ : Depression Angle

- $\psi_0$ : Bearing Angle

- $c_{\theta_0}$ : Average Estimation Error for Depression Angle

- $e_{\psi_0}$ : Average Estimation Error for Bearing Angle

**Table 1.  NUMERICAL DATA CORRESPONDING TO CASE LMS1**

| Harmonic (q) | Location (deg) | | Average Estimation Error (deg) | | |
| --- | --- | --- | --- | --- | --- |
| Case 1: One target located at broadside relative to planar array - six harmonics present in output electrical signal - LMS algorithm is used - 100 iterations | | | | | |
| | $\theta_0$ | $\psi_0$ | SNR | | |
| | | | -3 dB | -6 dB | -9 dB |
| | | | $e_{\theta_0}$ | $e_{\theta_0}$ | $e_{\theta_0}$ |
| 1 | 0 | 270 | -2.169 | -1.789 | -4.382 |
| 2 | 0 | 270 | -0.810 | -1.426 | -2.170 |
| 3 | 0 | 270 | -0.561 | -0.607 | -1.233 |
| 4 | 0 | 270 | -0.360 | -0.760 | -0.649 |
| 5 | 0 | 270 | -0.362 | -0.363 | -0.848 |
| 6 | 0 | 270 | -0.299 | -0.435 | -1.596 |

**Table 2.  NUMERICAL DATA CORRESPONDING TO CASE ALP1**

| Harmonic (q) | Location (deg) | | Average Estimation Error (deg) | | |
| --- | --- | --- | --- | --- | --- |
| Case 1: One target located at broadside relative to planar array - six harmonics present in output electrical signal - ALP algorithm is used - 1000 iterations | | | | | |
| | $\theta_0$ | $\psi_0$ | SNR | | |
| | | | -3 dB | -6 dB | -9 dB |
| | | | $e_{\theta_0}$ | $e_{\theta_0}$ | $e_{\theta_0}$ |
| 1 | 0 | 270 | -3.623 | -4.444 | -6.056 |
| 2 | 0 | 270 | -1.307 | -2.739 | -2.404 |
| 3 | 0 | 270 | -1.325 | -1.831 | -1.993 |
| 4 | 0 | 270 | -1.231 | -1.429 | -1.463 |
| 5 | 0 | 270 | -0.753 | -0.740 | -1.746 |
| 6 | 0 | 270 | -0.471 | -0.665 | -0.951 |

Table 3. NUMERICAL DATA CORRESPONDING TO CASE LMS2

| Case 2: Three targets located at random positions - six harmonics present in output electrical signal - LMS algorithm is used - 100 iterations | | | | | | | | |
|---|---|---|---|---|---|---|---|---|
| Harmonic (q) | Location (deg) | | Average Estimation Error (deg) | | | | | |
| | $\theta_0$ | $\psi_0$ | SNR | | | | | |
| | | | -3 dB | | -6 dB | | -9 dB | |
| | | | $e_{\theta_0}$ | $e_{\psi_0}$ | $e_{\theta_0}$ | $e_{\psi_0}$ | $e_{\theta_0}$ | $e_{\psi_0}$ |
| 1 | 49 | 38 | 0.265 | -0.124 | -0.411 | -0.832 | -0.571 | 0.325 |
| 2 | 5 | 137 | 0.077 | -2.714 | -0.161 | -5.017 | 0.097 | 3.451 |
| 3 | 77 | 307 | 3.037 | -0.108 | 0.351 | -2.625 | 7.991 | 9.333 |
| 4 | 77 | 307 | -10.532 | 1.677 | -5.032 | 0.019 | 3.858 | 26.436 |
| 5 | 5 | 137 | -0.022 | 0.560 | -0.155 | 1.376 | 0.078 | 0.002 |
| 6 | 49 | 38 | 1.081 | -1.531 | -10.852 | 4.382 | -2.355 | -8.784 |

Table 4. NUMERICAL DATA CORRESPONDING TO CASE ALP2

| Case 2: Three targets located at random positions - six harmonics present in output electrical signal - ALP algorithm is used - 1000 iterations | | | | | | | | |
|---|---|---|---|---|---|---|---|---|
| Harmonic (q) | Location (deg) | | Average Estimation Error (deg) | | | | | |
| | $\theta_0$ | $\psi_0$ | SNR | | | | | |
| | | | -3 dB | | -6 dB | | -9 dB | |
| | | | $e_{\theta_0}$ | $e_{\psi_0}$ | $e_{\theta_0}$ | $e_{\psi_0}$ | $e_{\theta_0}$ | $e_{\psi_0}$ |
| 1 | 49 | 38 | -1.470 | 0.098 | -0.826 | 0.380 | 8.243 | -2.443 |
| 2 | 5 | 137 | 0.134 | 6.094 | -1.091 | -8.072 | 0.879 | 1.252 |
| 3 | 77 | 307 | -1.728 | 0.082 | -3.247 | -0.361 | -0.697 | 1.131 |
| 4 | 77 | 307 | -1.968 | 0.526 | -0.964 | 0.218 | -1.763 | -0.035 |
| 5 | 5 | 137 | 0.019 | -0.191 | 0.180 | 1.267 | 0.830 | -6.591 |
| 6 | 49 | 38 | -0.173 | 0.146 | -0.197 | -0.019 | 2.068 | -5.109 |

**Table 5. NUMERICAL DATA CORRESPONDING TO CASE LMS3**

| Harmonic (q) | Location (deg) $\theta_0$ | Location (deg) $\psi_0$ | Average Estimation Error (deg) SNR -3 dB $e_{\theta_0}$ | -3 dB $e_{\psi_0}$ | -6 dB $e_{\theta_0}$ | -6 dB $e_{\psi_0}$ | -9 dB $e_{\theta_0}$ | -9 dB $e_{\psi_0}$ |
|---|---|---|---|---|---|---|---|---|
| 1 | 90 | 90 | 3.355 | -0.055 | 20.000 | 0.545 | 21.186 | 1.023 |
| 2 | 90 | 90 | 33.033 | -0.200 | 40.425 | -0.646 | 27.226 | -0.330 |
| 3 | 90 | 90 | 19.490 | -0.019 | 16.401 | -0.229 | 16.706 | -0.325 |
| 4 | 90 | 90 | 2.247 | 0.006 | 7.365 | 0.287 | 12.025 | -0.139 |
| 5 | 90 | 90 | 2.136 | -0.083 | 1.146 | 0.098 | 14.692 | -18.528 |
| 6 | 90 | 90 | 70.877 | -84.120 | 69.426 | -64.811 | 46.737 | -90.393 |

Case 2: One target located at endfire relative to planar array - six harmonics present in output electrical signal - LMS algorithm is used - 100 iterations

**Table 6. NUMERICAL DATA CORRESPONDING TO CASE ALP3**

| Harmonic (q) | Location (deg) $\theta_0$ | Location (deg) $\psi_0$ | Average Estimation Error (deg) SNR -3 dB $e_{\theta_0}$ | -3 dB $e_{\psi_0}$ | -6 dB $e_{\theta_0}$ | -6 dB $e_{\psi_0}$ | -9 dB $e_{\theta_0}$ | -9 dB $e_{\psi_0}$ |
|---|---|---|---|---|---|---|---|---|
| 1 | 90 | 90 | 3.948 | 0.217 | 7.806 | -0.136 | 6.672 | -0.984 |
| 2 | 90 | 90 | 7.287 | -0.362 | 11.323 | -0.488 | 9.034 | 0.329 |
| 3 | 90 | 90 | 5.342 | -0.107 | 3.732 | -0.370 | 1.935 | -0.767 |
| 4 | 90 | 90 | 2.233 | -0.113 | 2.145 | 0.286 | 7.725 | -0.023 |
| 5 | 90 | 90 | 0.986 | -0.160 | 3.512 | 0.076 | 14.090 | -6.512 |
| 6 | 90 | 90 | 5.229 | -89.997 | 7.051 | -90.029 | 16.548 | -89.088 |

Case 2: One target located at endfire relative to planar array - six harmonics present in output electrical signal - ALP algorithm is used - 1000 iterations

**Table 7.  NUMERICAL DATA CORRESPONDING TO CASE LMS4-A**

| Harmonic (q) | Location (deg) | | Average Estimation Error (deg) | |
|:---:|:---:|:---:|:---:|:---:|
| | $\theta_0$ | $\psi_0$ | $e_{\theta_0}$ | $e_{\psi_0}$ |
| 1 | 45 | 0 | 45.000 | -90.000 |
| 1 | 45 | 180 | 45.000 | 90.000 |
| 2 | 45 | 0 | 0.000 | 0.000 |
| 3 | 33 | 47 | 0.000 | 0.000 |
| 4 | 33 | 47 | 0.000 | 0.000 |
| 5 | 45 | 180 | 0.000 | 0.000 |
| 6 | 33 | 47 | 0.000 | 0.000 |

Case 4a: Three targets two of which are located in the same plane - targets one and two have a common spectral line at 1000 Hz - six harmonics present in output electrical signal - LMS algorithm is used - 100 iterations - no noise

**Table 8.  NUMERICAL DATA CORRESPONDING TO CASE ALP4-A**

| Harmonic (q) | Location (deg) | | Average Estimation Error (deg) | |
|:---:|:---:|:---:|:---:|:---:|
| | $\theta_0$ | $\psi_0$ | $e_{\theta_0}$ | $e_{\psi_0}$ |
| 1 | 45 | 0 | -44.921 | 0.0 |
| 1 | 45 | 180 | -44.921 | 180.000 |
| 2 | 45 | 0 | 0.009 | 0.000 |
| 3 | 33 | 47 | 0.037 | -0.011 |
| 4 | 33 | 47 | 0.037 | -0.011 |
| 5 | 45 | 180 | 0.009 | 0.000 |
| 6 | 33 | 47 | 0.037 | -0.011 |

Case 4a: Three targets two of which are located in the same plane - targets one and two have a common spectral line at 1000 Hz - six harmonics present in output electrical signal - ALP algorithm is used - 1000 iterations - no noise

**Table 9.  NUMERICAL DATA CORRESPONDING TO CASE LMS4-B**

Case 4b: Three targets two of which are located in the same plane - targets one and two have a common spectral line at 3000 Hz - six harmonics present in output electrical signal - LMS algorithm is used - 100 iterations - no noise

| Harmonic (q) | Location (deg) | | Average Estimation Error (deg) | |
|:---:|:---:|:---:|:---:|:---:|
| | $\theta_0$ | $\psi_0$ | $e_{\theta_0}$ | $e_{\psi_0}$ |
| 1 | 33 | 47 | 0.000 | 0.000 |
| 2 | 45 | 0 | 0.000 | 0.000 |
| 3 | 45 | 0 | 45.00 | -90.00 |
| 3 | 45 | 180 | 45.0 | 90.0 |
| 4 | 33 | 47 | 0.000 | 0.000 |
| 5 | 45 | 180 | 0.000 | 0.000 |
| 6 | 33 | 47 | 0.000 | 0.000 |

**Table 10.  NUMERICAL DATA CORRESPONDING TO CASE ALP4-B**

Case 4b: Three targets two of which are located in the same plane - targets one and two have a common spectral line at 3000 Hz - six harmonics present in output electrical signal - ALP algorithm is used - 1000 iterations - no noise

| Harmonic (q) | Location (deg) | | Estimation Error (deg) | |
|:---:|:---:|:---:|:---:|:---:|
| | $\theta_0$ | $\psi_0$ | $e_{\theta_0}$ | $e_{\psi_0}$ |
| 1 | 33 | 47 | 0.037 | -0.011 |
| 2 | 45 | 0 | 0.009 | 0.000 |
| 3 | 45 | 0 | 1.56 | 0.000 |
| 3 | 45 | 180 | 1.56 | 0.000 |
| 4 | 33 | 47 | 0.032 | -0.011 |
| 5 | 45 | 180 | 0.009 | 0.000 |
| 6 | 33 | 47 | 0.037 | -0.011 |

**Table 11. NUMERICAL DATA CORRESPONDING TO CASE LMS4-C**

| Harmonic (q) | Location (deg) | | Average Estimation Error (deg) | |
|---|---|---|---|---|
| | $\theta_0$ | $\psi_0$ | $e_{\theta_0}$ | $e_{\psi_0}$ |
| Case 4c: Three targets two of which are located in the same plane - targets one and two have a common spectral line at 6000 Hz - six harmonics present in output electrical signal - LMS algorithm is used - 100 iterations - no noise | | | | |
| 1 | 33 | 47 | 0.000 | 0.000 |
| 2 | 45 | 0 | 0.000 | 0.000 |
| 3 | 33 | 47 | 0.000 | 0.000 |
| 4 | 33 | 47 | 0.000 | 0.000 |
| 5 | 45 | 180 | 0.000 | 0.000 |
| 6 | 45 | 0 | 45.000 | -90.000 |
| 6 | 45 | 180 | 45.000 | 90.000 |

**Table 12. NUMERICAL DATA CORRESPONDING TO CASE ALP4-C**

| Harmonic (q) | Location (deg) | | Average Estimation Error (deg) | |
|---|---|---|---|---|
| | $\theta_0$ | $\psi_0$ | $e_{\theta_0}$ | $e_{\psi_0}$ |
| Case 4c: Three targets two of which are located in the same plane - targets one and two have a common spectral line at 6000 Hz - six harmonics present in output electrical signal - ALP algorithm is used - 1000 iterations - no noise | | | | |
| 1 | 33 | 47 | 0.037 | -0.011 |
| 2 | 45 | 0 | 0.009 | 0.000 |
| 3 | 33 | 47 | 0.037 | -0.011 |
| 4 | 33 | 47 | 0.037 | -0.011 |
| 5 | 45 | 180 | 0.009 | 0.000 |
| 6 | 45 | 0 | 2.070 | 0.000 |
| 6 | 45 | 180 | 2.070 | 0.000 |

Table 13.   NUMERICAL DATA CORRESPONDING TO CASE LMS5-A

| Harmonic (q) | Location (deg) | | Average Estimation Error (deg) | |
|---|---|---|---|---|
| | $\theta_0$ | $\psi_0$ | $e_{\theta_0}$ | $e_{\psi_0}$ |
| Case 5a: Three targets located at random positions - targets one and two have a common spectral line at 1000 Hz - six harmonics present in output electrical signal - LMS algorithm is used - 100 iterations - no noise | | | | |
| 1 | 49 | 38 | -13.000 | 252.594 |
| 1 | 5 | 137 | -41.000 | -16.406 |
| 2 | 5 | 137 | 0.000 | 0.000 |
| 3 | 77 | 307 | 0.000 | 0.000 |
| 4 | 77 | 307 | 0.000 | 0.000 |
| 5 | 5 | 137 | 0.000 | 0.000 |
| 6 | 49 | 38 | 0.000 | 0.000 |

Table 14.   NUMERICAL DATA CORRESPONDING TO CASE ALP5-A

| Harmonic (q) | Location (deg) | | Average Estimation Error (deg) | |
|---|---|---|---|---|
| | $\theta_0$ | $\psi_0$ | $e_{\theta_0}$ | $e_{\psi_0}$ |
| Case 5a: Three targets located at random positions - targets one and two have a common spectral line at 1000 Hz - six harmonics present in output electrical signal - ALP algorithm is used - 1000 iterations - no noise | | | | |
| 1 | 49 | 38 | 27.121 | -6.674 |
| 1 | 5 | 137 | -16.879 | 92.326 |
| 2 | 5 | 137 | -0.038 | -0.008 |
| 3 | 77 | 307 | 0.094 | 0.012 |
| 4 | 77 | 307 | 0.094 | 0.012 |
| 5 | 5 | 137 | 0.006 | -0.328 |
| 6 | 49 | 38 | 0.094 | 0.012 |

**Table 15. NUMERICAL DATA CORRESPONDING TO CASE LMS5-B**

| Harmonic (q) | Location (deg) | | Average Estimation Error (deg) | |
|:---:|:---:|:---:|:---:|:---:|
| | $\theta_0$ | $\psi_0$ | $e_{\theta_0}$ | $e_{\psi_0}$ |
| | | | | |
Case 5b: Three targets located at random positions - targets one and two have a common spectral line at 3000 Hz - six harmonics present in output electrical signal - LMS algorithm is used - 100 iterations - no noise

| Harmonic (q) | Location (deg) | | Average Estimation Error (deg) | |
|:---:|:---:|:---:|:---:|:---:|
| | $\theta_0$ | $\psi_0$ | $e_{\theta_0}$ | $e_{\psi_0}$ |
| 1 | 77 | 307 | 0.000 | 0.000 |
| 2 | 5 | 137 | 0.000 | 0.000 |
| 3 | 49 | 38 | -13.000 | 252.594 |
| 3 | 5 | 137 | -41.000 | -16.406 |
| 4 | 77 | 307 | 0.000 | 0.000 |
| 5 | 5 | 137 | 0.000 | 0.000 |
| 6 | 49 | 38 | 0.000 | 0.000 |

**Table 16. NUMERICAL DATA CORRESPONDING TO CASE ALP5-B**

Case 5b: Three targets located at random positions - targets one and two have a common spectral line at 3000 Hz - six harmonics present in output electrical signal - ALP algorithm is used - 1000 iterations - no noise

| Harmonic (q) | Location (deg) | | Estimation Error (deg) | |
|:---:|:---:|:---:|:---:|:---:|
| | $\theta_0$ | $\psi_0$ | $e_{\theta_0}$ | $e_{\psi_0}$ |
| 1 | 77 | 307 | 0.094 | 0.012 |
| 2 | 5 | 137 | -0.038 | -0.008 |
| 3 | 49 | 38 | 2.94 | 0.39 |
| 3 | 5 | 137 | 1.505 | -1.992 |
| 4 | 77 | 307 | 0.094 | 0.012 |
| 5 | 5 | 137 | 0.006 | -0.328 |
| 6 | 49 | 38 | 0.094 | 0.012 |

**Table 17. NUMERICAL DATA CORRESPONDING TO CASE LMS5-C**

Case 5c: Three targets located at random positions - targets one and two have a common spectral line at 6000 Hz - six harmonics present in output electrical signal - LMS algorithm is used - 100 iterations - no noise

| Harmonic (q) | Location (deg) | | Average Estimation Error (deg) | |
|---|---|---|---|---|
| | $\theta_0$ | $\psi_0$ | $e_{\theta_0}$ | $e_{\psi_0}$ |
| 1 | 77 | 307 | 0.000 | 0.000 |
| 2 | 5 | 137 | 0.000 | 0.000 |
| 3 | 49 | 38 | 0.000 | 0.000 |
| 4 | 77 | 307 | 0.000 | 0.000 |
| 5 | 5 | 137 | 0.000 | 0.000 |
| 6 | 5 | 137 | -41.000 | -16.406 |
| 6 | 49 | 38 | -13.000 | 252.594 |

**Table 18. NUMERICAL DATA CORRESPONDING TO CASE ALP5-C**

Case 5c: Three targets located at random positions - targets one and two have a common spectral line at 6000 Hz - six harmonics present in output electrical signal - ALP algorithm is used - 1000 iterations - no noise

| Harmonic (q) | Location (deg) | | Average Estimation Error (deg) | |
|---|---|---|---|---|
| | $\theta_0$ | $\psi_0$ | $e_{\theta_0}$ | $e_{\psi_0}$ |
| 1 | 77 | 307 | 0.094 | 0.012 |
| 2 | 5 | 137 | -0.038 | -0.008 |
| 3 | 49 | 38 | 0.094 | 0.012 |
| 4 | 77 | 307 | 0.094 | 0.012 |
| 5 | 5 | 137 | 0.006 | -0.328 |
| 6 | 5 | 137 | 2.615 | -3.84 |
| 6 | 49 | 38 | 0.498 | 2.516 |

# LIST OF REFERENCES

1. Ziomek, L. J. and Behrle, C. D., "Localization of Multiple Broadband Targets Via Frequency Domain Adaptive Beamforming for Planar Arrays," to appear in *The Journal of the Acoustical Society of America* , February or March 1989.

2. Haykin, S., "Radar Array Processing for Angle of Arrival Estimation," in *Array Signal Processing,* ed. S. Haykin, Prentice-Hall, Englewood Cliffs, New Jersey, 1985.

3. Orfanidis, S. J., *Optimum Signal Processing,* Macmillan, New York, 1985.

4. Ziomek, L. J., *Underwater Acoustics - A Linear Systems Theory Approach,* Academic Press, Orlando, Florida, pp. 162-168, 1985.

5. Behrle, C. D., *Computer Simulation Studies of Multiple Broadband Target Localization via Frequency Domain Adaptive Beamforming for Planar Arrays,* Master's Thesis, Naval Postgraduate School, Monterey, California, March 1988.

6. Ziomek, L. J. and Chan, F., "Frequency Domain Adaptive Beamforming for Planar Arrays," *Conference Record Twentieth Asilomar Conference on Signals, Systems, and Computers,* pp. 120-124, Pacific Grove, California, 10-12 November 1986.

# INITIAL DISTRIBUTION LIST

No. Copies

1. Defense Technical Information Center 2
   Cameron Station
   Alexandria, VA 22304-6145

2. Library, Code 0142 2
   Naval Postgraduate School
   Monterey, CA 93943-5002

3. Chairman, Code 62 1
   Department of Electrical and Computer Engineering
   Naval Postgraduate School
   Monterey, CA 93943-5000

4. Professor L. J. Ziomek, Code 62Zm 3
   Department of Electrical and Computer Engineering
   Naval Postgraduate School
   Monterey, CA 93943-5000

5. Professor Murali Tummala, Code 62Tm 1
   Department of Electrical and Computer Engineering
   Naval Postgraduate School
   Monterey, CA 93943-5000

6. LT N. V. Nikitakos, HN 2
   Tripoleos 27 - Piraeus
   GREECE, 18547

7. Dr. Duncan Sheldon (Surface Sonar) 1
   NUSC
   Code 3314
   New London, CT 06320

8. Dr. Rabiner Madan 1
   ONR
   Code 1114
   800 N.Quincy St.
   Arlington, VA 22217-5000